China Geology 4 (2021) 686−719

China Geology

Journal homepage: http://chinageology.cgs.cn
https://www.sciencedirect.com/journal/china-geology

# Geology and mineralization of the Sanshandao supergiant gold deposit (1200 t) in the Jiaodong Peninsula, China: A review

Ming-chun Song[a], Zheng-jiang Ding[a, b], Jun-jin Zhang[c], Ying-xin Song[d], Jun-wei Bo[c], Yu-qun Wang[e], Hong-bo Liu[f], Shi-yong Li[f], Jie Li[g], Rui-xiang Li[a], Bin Wang[a], Xiang-dong Liu[a], Liang-liang Zhang[a], Lei-lei Dong[h], Jian Li[i], Chun-yan He[f]

[a] *Shandong Provincial No.6 Exploration Institute of Geology and Mineral Resources*, *Weihai* 264209, *China*
[b] *Shandong Provincial Bureau of Geology and Mineral Resources*, *Jinan* 250013, *China*
[c] *Shandong Provincial No.3 Exploration Institute of Geology and Mineral Resources*, *Yantai* 264003, *China*
[d] *Shandong Institute of Geological Sciences*, *Jinan* 250013, *China*
[e] *Shandong Provincial Ruihai Mining Limited Company*, *Laizhou* 261400, *China*
[f] *Shandong Institute of Geophysical & Geochemical Exploration*, *Jinan* 250013, *China*
[g] *Hebei Key Laboratory of Strategic Critical Mineral Resources*, *Hebei GEO University*, *Shijiazhuang* 050031, *China*
[h] *School of Civil and Resource Engineering*, *University of Science and Technology Beijing*, *Beijing* 100083, *China*
[i] *School of Resources and Environmental Engineering*, *Shandong University of Technology*, *Zibo* 255000, *China*

ARTICLE INFO

*Article history:*
Received 16 August 2021
Received in revised form 28 November 2021
Accepted 1 December 2021
Available online 8 December 2021

*Keywords:*
Gold deposit
Deep prospecting
Thermal uplifting-extension mineralization
Transformation of mantle properties
Stepped metallogenic model
Mineral exploration engineering
Jiaodong-type gold deposits
Sanshandao
Jiaodong Peninsula
China

ABSTRACT

The Jiaodong Peninsula in Shandong Province, China is the world's third-largest gold metallogenic area, with cumulative proven gold resources exceeding 5000 t. Over the past few years, breakthroughs have been made in deep prospecting at a depth of 500–2000 m, particularly in the Sanshandao area where a huge deep gold orebody was identified. Based on previous studies and the latest prospecting progress achieved by the project team of this study, the following results are summarized. (1) 3D geological modeling results based on deep drilling core data reveal that the Sanshandao gold orefield, which was previously considered to consist of several independent deposits, is a supergiant deposit with gold resources of more than 1200 t (including 470 t under the sea area). The length of the major orebody is nearly 8 km, with a greatest depth of 2312 m below sea level and a maximum length of more than 3 km along their dip direction. (2) Thick gold orebodies in the Sanshandao gold deposit mainly occur in the specific sections of the ore-controlling fault where the fault plane changes from steeply to gently inclined, forming a stepped metallogenic model from shallow to deep level. The reason for this strong structural control on mineralization forms is that when ore-forming fluids migrated along faults, the pressure of fluids greatly fluctuated in fault sections where the fault dip angle changed. Since the solubility of gold in the ore-forming fluid is sensitive to fluid pressure, these sections along the fault plane serve as the target areas for deep prospecting. (3) Thermal uplifting-extensional structures provide thermodynamic conditions, migration pathways, and deposition spaces for gold mineralization. Meanwhile, the changes in mantle properties induced the transformation of the geochemical properties of the lower crust and magmatic rocks. This further led to the reactivation of ore-forming elements, which provided rich materials for gold mineralization. (4) It can be concluded from previous research results that the gold mineralization in the Jiaodong gold deposits occurred at about 120 Ma, which was superimposed by nonferrous metals mineralization at 118–111 Ma. The fluids were dominated by primary mantle water or magmatic water. Metamorphic water occurred in the early stage of the gold mineralization, while the fluid composition was dominated by meteoric water in the late stage. The S, Pb, and Sr isotopic compositions of the ores are similar to those of ore-hosting rocks, indicating that the ore-forming materials mainly derive from crustal materials, with the minor addition of mantle-derived materials. The gold deposits in the Jiaodong Peninsula were formed in an extensional tectonic environment during the transformation of the physical and chemical properties of the lithospheric mantle, which is different from typical orogenic gold deposits. Thus, it is proposed that they are named "Jiaodong-type" gold deposits.



* Corresponding author: *E-mail address*: mingchuns@163.com (Ming-chun Song)

Literary editor: Li-qiong Jia
doi:10.31035/cg2021070
2096-5192/© 2021 China Geology Editorial Office.

## 1. Introduction

The Sanshandao gold deposit is located on the western side of the Jiaodong gold ore concentration area on the

southeastern margin of the North China Craton. With gold reserves of more than 5000 t, and the Jiaodong gold ore concentration area is the world's third-largest gold concentration area after the Witwatersrand Basin in South Africa and the Muruntau area in Uzbekistan. The Sanshandao gold deposit was discovered in 1965 and is the first identified altered rock type gold deposit in fractured zones in China. The deposit has over 60 t of gold resources in 1969, while the overall gold endowment had grown to 118 t above the elevation of −400 m by the end of the last century. The Sanshandao gold deposit was put into production in 1989, and currently, the maximum mining depth has reached 1050 m underground. Meanwhile, it is the first undersea mine in the world. The deep prospecting programs conducted since the 21st century contribute to the discovery of two gold deposits. The first is the Xiling gold deposit with proven gold resources of 383 t, which lies in the deep part of the main orebody of the Sanshandao gold deposit that extends along the dip direction. The second one was discovered under the sea area as the extension of the main orebody along with the trend, with proven gold reservoirs of 470 t. According to statistics from S&P 500, the sea-area gold deposit ranks second among the world's top 10 gold deposits discovered during 2010–2019. Meanwhile, the sea-area gold deposit is also the world's largest gold deposit under the sea area. Deeply drilled cores have revealed that the Xiling and sea area deposits adjacent to the Sanshandao, which were originally considered independent of each other, are interconnected with each other. Therefore, they combine to form a supergiant gold deposit with gold reserves exceeding 1200 t.

Extensive studies have been conducted on the gold deposits in the Sanshandao area and its vicinity (Lü GX and Kong QC, 1993; Lu HZ et al., 1999; Li HM et al., 2003; Wang JC et al., 2003; Li SX et al., 2007; Deng J et al., 2010, 2020a; Song MC et al., 2010a, 2010b, 2012; Niu SY et al.,2019; Jiang XH et al., 2011; Yang LQ et al.,2014; Qiu KF et al.,2014; Sai SX et al.,2014, 2020). Consensus has been roughly reached in many aspects, such as ore-controlling factors, mineralization timing, characteristics of fluid inclusions, stable isotopes, ore-forming stages, and alteration. However, in-depth studies are yet to be carried out on the spatial relationships of the main orebodies discovered in various exploration stages and regions, especially on the mineralization styles and patterns of deep orebodies. Meanwhile, a consensus has not been reached on the genesis of the deposits. For example, previous researchers proposed that the gold deposits are magmatic-hydrothermal ore deposits related to Linglong, Guojialing, or Weideshan granitoids (Wang LG et al.,1998; Li SX et al., 2007; Luo XD et al., 2014; Song MC et al., 2014b, 2015a). Another school of thought classified them as orogenic gold deposits related to the subduction of the paleo-Pacific Plate (Zhou TH and Lu G, 2000; Goldfarb RJ et al., 2001; Deng J et al., 2010), while some argue that the gold deposits are associated with craton destruction (Zhu RX et al., 2015). Based on the summary of the achievements made in gold prospecting in the Sanshandao area, this study investigates the relationships between major gold orebodies in the shallow mining areas previously discovered and those in deep mining areas explored in recent years in detail. Further, this study describes in detail the main features of the gold deposits and their variation in-depth in the Sanshandao area and its vicinity, which constitute a supergiant gold deposit —the supergiant Sanshandao gold deposit (short for Sanshandao gold deposit). Moreover, the authors summarize previous research results and discuss the structural control on the gold mineralization, tectonic background, and genesis model of the deposit. This study is greatly significant for the deep understanding of the metallogenic regularity and formation mechanisms of Jiaodong-type gold deposits and for guiding the deep prospecting of the deposits.

## 2. Regional geological background

The Sanshandao gold deposit is located in the Jiaodong Peninsula, Shandong Province, where the circum-West Pacific metallogenic domain, the Precambrian metallogenic domain, and the Qinling-Qilian-Kunlun metallogenic domain overlap. Multiple tectonic superimpositions, especially the Yanshanian tectono-magmatic activities, led to the Mesozoic explosion of different kinds of mineralization (Hua RM and Mao JW, 1999; Zhai MG et al., 2004). The Jiaodong Peninsula is composed of the ancient metamorphic basement and Mesozoic–Cenozoic continental sedimentary strata and magmatic rocks (Fig. 1). The Jiaobei Terrane to the west of the Jiaodong Peninsula is located on the southeastern margin of the North China Craton. The Weihai Terrane to the east of the Jiaodong Peninsula is a part of the Dabie-Sulu orogenic belt. The sediment and volcanic rocks in Jiaolai Basin to the south of the Jiaodong Peninsula overlay the Jiaobei and Weihai terranes.

### *2.1. Precambrian crystalline basement*

The Precambrian crystalline basement in the Jiaodong Peninsula consists of the Jiaobei and Weihai terranes. The Precambrian crystalline basement of the Jiaobei Terrane consists of the Middle Archean–Neoproterozoic metamorphic rock series. The Mesoarchean–Neoarchean metamorphic rock series is dominated by tonalite-trondhjemite-granodiorite (TTG) gneiss suites. It can be divided into two stages according to isotopic ages, namely the early stage of 2738–2707 Ma and the late stage of 2577–2496 Ma. Besides, there is an age record of about 2.9 Ga (Liu JH et al., 2011; Xie HQ et al., 2013). A small number of Jiaodong rock groups occur in the form of xenoliths in the TTG gneiss suite. They mainly consist of biotite leptynites, amphibolites, and hornblende leptynites interbedded with magnetite quartzites, as well as some visible basic-ultrabasic intrusions such as serpentinized peridotites, meta-pyroxene hornblendes, and metagabbros. The Paleoproterozoic Jingshan and Fenzishan

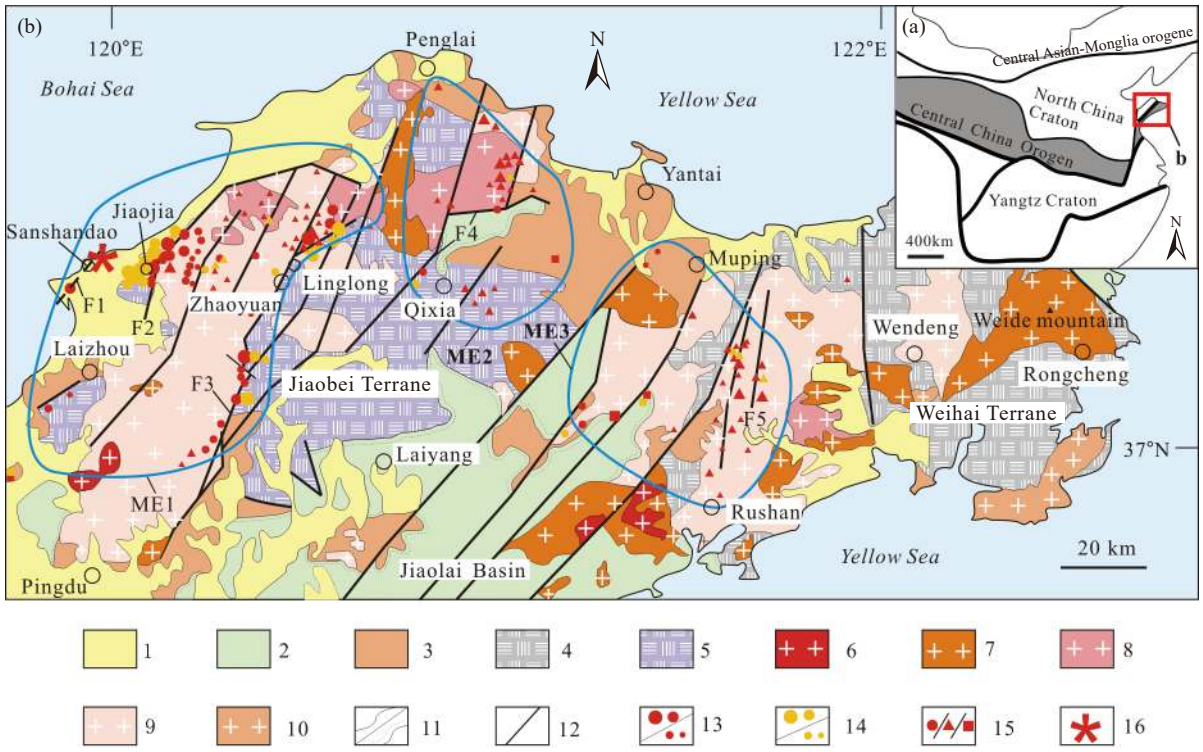


**Fig. 1.** Regional geological sketch map and gold deposit distribution of the Jiaodong Peninsula. 1–Quaternary; 2–Cretaceous; 3–Paleoproterozoic and Neoproterozoic; 4–Neoproterozoic with eclogite granitic gneiss; 5–Archean granite-greenstone belt; 6–Cretaceous Laoshan-type granites; 7–Cretaceous Weideshan-type granites; 8–Cretaceous Guojialing-type granites; 9–Jurassic granitoids; 10–Triassic granitoids; 11–geological conformity/unconformity; 12–fault; 13–shallow gold deposits (very large and large/medium-sized and small); 14–deep gold deposits (very large and large/medium-sized and small); 15–gold deposit of altered rock type/quartz vein type/altered breccia type; 16–supergiant Sanshandao gold deposit. ME1–Jiaoxibei metallogenetic sub-region; ME2–Qipengfu metallogenetic sub-region; ME3–Mouru metallogenetic sub-region; F1–Sanshandao fault; F2–Jiaojia fault; F3–Zhaoping fault; F4–Xilin-Douya fault; F5–Jinniushan fault.

groups, mainly composed of marbles, (graphite-bearing) leptynites, gneiss, and high-alumina schists, possess characteristics similar to those of khondalite series rocks. They are amphibolite-granulite facies metamorphic littoral-neritic sedimentary rock series. The SHRIMP U-Pb age of the youngest detrital zircons in the Jingshan Group is 2175 ± 16 Ma. The metamorphic ages of the Jingshan and Fenzishan groups are about 1.8 –1.7 Ga (Li SZ et al., 2012). The Mesoproterozoic Zhifu Group is mainly composed of quartzites and K-feldspar quartzites interbedded with magnetite layers, and it belongs to the littoral-facies sedimentary rock series of low amphibolite facies. The Neoproterozoic Penglai Group is mainly composed of phyllites, slates, quartzites, crystalline limestones, and marbles, and it is a set of metamorphic littoral-neritic sedimentary rock series of greenschist facies.

The Weihai Terrane is mainly composed of Neoproterozoic granitic gneiss and minor amounts of Paleoproterozoic metamorphic strata, Mesoproterozoic basic-ultrabasic intrusions, and Triassic eclogites. The U-Pb isotopic ages of zircon cores of the Neoproterozoic granitic gneiss are 723 ± 36 Ma, 738 ± 17 Ma, and 744 ± 63 Ma (Tang J et al., 2004). The zircon SHRIMP U-Pb dating of the granitic gneiss shows that the metamorphic basement of the Weihai Terrane is 2400 Ma and experienced metamorphic events at 1800 –1700 Ma and about 200 Ma (Xu ZQ et al., 2006). The age of ultrahigh-pressure metamorphism is 242 –220 Ma and the exhumation age of ultrahigh-pressure metamorphic rocks is 219–202 Ma (Xu ZQ et al., 2006; Liu FL et al., 2003).

### 2.2. Meso-Cenozoic strata and magmatic rocks

Mesozoic strata are mainly distributed in the Jiaolai Basin, which is a Cretaceous continental facies volcanic-sedimentary basin. The Early Cretaceous Laiyang Group in the lower part of the basin is mainly composed of clastic sedimentary rocks such as sandstones, mudstones, and conglomerates of piedmont alluvial facies, fluvial facies, and lacustrine facies. The Early Cretaceous Qingshan Group in the middle part of the basin is an intermediate-basic-acidic volcanic rock suite interbedded with small amounts of sedimentary rocks. The Late Cretaceous Wangshi Group in the upper part of the basin is composed of the clastic rock series, such as the red sandstones, mudstones, and conglomerates of fluvial-lacustrine facies. The isotopic ages of volcanic rocks in the Qingshan Group are 123–98 Ma (Song MC et al., 2009). The Quaternary sediments are widely distributed in modern seashores and river valleys, and Paleogene fluvial-lacustrine sedimentary strata are locally distributed.

The Jiaodong Peninsula experienced intense Mesozoic magmatic activities. Granitoid intrusions in the peninsula mainly include Triassic quartz syenites-syenogranites,

Jurassic monzogranites (Linglong-type granites), Early Cretaceous granodiorites (Guojialing-type granites), Early Cretaceous diorites, Early Cretaceous quartz monzonites-monzogranites (Weideshan-type granites), and Early Cretaceous syenogranites (Laoshan-type granites). Intermediate-basic to acidic vein rocks mainly include lamprophyre dykes, diorite-porphyrite dykes, monzonite dykes, and granite porphyry dykes. Volcanic rocks are mainly an integral part of the Qingshan Group, and small amounts of Cenozoic basalts occur in the western part of the Jiaobei Terrane.

### *2.3. Structures*

The Mesoarchean-Paleoproterozoic rocks in the Jiaobei Terrane underwent three stages of folding and two stages of ductile shearing at 1956–1875 Ma (Li SZ et al., 2012). The Weihai Terrane is characterized by the development of multi-stage and multi-facies ductile shear zones. Faults have widely developed in the Jiaodong Peninsula since the Mesozoic, including the NE-NNE-trending faults, followed by nearly EW-NEE-trending faults. The NE-NNE-trending faults are distributed widely and densely and serve as the major ore-controlling structures in Jiaodong gold deposits. Additionally, EW-trending faults are sporadically exposed, with poor continuity.

### *2.4. Overview of gold resources*

There are more than 200 gold deposits (districts) with proven resources in the Jiaodong Peninsula (Fig. 1), which jointly form the Jiaodong gold province or the Jiaodong gold ore concentration area. According to the spatial distribution of the deposits, the Jiaodong gold province is further divided into three metallogenic sub-regions, namely Jiaoxibei (Laizhou-Zhaoyuan), Qipengfu (Qixia-Penglai-Fushan), and Muru (Muping-Rushan). These three regions consist of six metallogenic belts, namely Sanshandao, Jiaojia, Zhaoping, Qixia-Daliuhang, Taocun, and Muru; and 13 gold orefields, namely Sanshandao, Jiaojia, Lingbei, Anshi, Dazhuangzi, Linglong, Dayingezhuang, Jiudian, Qixia, Daliuhang, Laishan, Pengjiakuang, and Denggezhuang (Song MC et al., 2015b). The styles of gold mineralization in the Jiaodong gold ore concentration area primarily include altered rock type in fractured zones (Jiaojia type), quartz vein type (Linglong type), followed by the sulfide-quartz vein type (Denggezhuang type), and small amounts of other mineralization types.

## 3. Geological background of the northwest Jiaodong Peninsula and Sanshandao ore district

### *3.1. Granitoids related to gold mineralization*

The northwest Jiaodong Peninsula is located on the southeastern side of the Bohai Bay and is adjacent to the famous Tancheng-Lujiang fault zone (which extends into the sea at the Bohai Bay) in the west. It is the most important gold district in the Jiaodong Peninsula, with cumulative proven gold reservoirs of more than 4000 t. The northwest Jiaodong Peninsula is mainly composed of Early Precambrian metamorphic rock series and Jurassic Linglong-type granites, followed by other geological bodies including Jurassic Luanjiahe granites, Cretaceous Guojialing-type granites, Weideshan-type granites, Laoshan-type granites, and various vein dykes. In addition, there are Cretaceous and Quaternary strata in the area (Fig. 2). There is a close spatial-temporal relationship between gold deposits in the northwest Jiaodong Peninsula and Jurassic-Cretaceous magmatic rocks. The ore-hosting magmatic rocks include Linglong-type granites and Guojialing-type granites, which are referred to as ore-hosting geological bodies (Song YX et al., 2017). Meanwhile, the intrusions coeval with the gold mineralization include Weideshan-type granites, Laoshan-type granites, and intermediate-basic vein dykes.

Linglong-type granites are dominated by monzogranites with different textures, structures, or mineral assemblages in terms of lithology (Table 1). The early intrusive bodies mainly include gneissic garnet-bearing monzogranites, while the late intrusive bodies mainly consist of massive light-colored monzogranites. In terms of chemical composition, Linglong-type granites fall in the granite zone in the $SiO_2$ *vs.* $K_2O+Na_2O$ diagram (Fig. 3). With high contents of $Na_2O+K_2O$, low MgO content, and peraluminous characteristics, they are potassic granites and belong to the high-K calc-alkaline rock series (Lin BL et al., 2013). Moreover, they are rich in LREEs and LILEs (Rb, Ba, U, and Sr) and are depleted in HFSEs (Nb, Ta, P, and Ti) (Yang KF et al., 2012). Their $^{87}Sr/^{86}Sr$ ratio, $\varepsilon Nd(t)$, $\varepsilon Hf(t)$ and Sr/Y ratio are 0.711281 –0.712418, 21.6 –19.4, 28.7 –6.2, and 55.07 –214.44, respectively, and their $\varepsilon Hf(t)$ values fall between the crust evaluation curves of 1.9 Ga and 2.5 Ga (Huang T et al., 2014; Yang KF et al., 2012). They show low $\varepsilon Hf(t)$ values, high Sr/Y ratio, and no notable negative europium anomalies, which are similar to those of both adakites (Lin BL et al., 2013; Yang KF et al., 2012) and Neoarchean TTG in the Jiaodong Peninsula (Wu M et al., 2014). Magmas in Linglong-type granites were formed in a relatively high-pressure environment and originated from the partial melting of the thickened lower crust (> 40 km) in North China (Zhang HF et al., 2004; Yang KF et al., 2012). Therefore, Linglong-type granites are S-type granites. The zircon U-Pb isotopic ages of Linglong-type granites are 163–159 Ma (Table 1). There are inherit zircons with ages of 800–700 Ma, 230–200 Ma, 19–18 Ga, and 28–18 Ga (Song MC et al., 2018; Wang B et al., 2021). This indicates that the melting source areas of Linglong-type granites include Neoproterozoic and Triassic materials from the Sulu orogenic belt and Neoarchean –Paleoproterozoic materials from the northern Jiaodong Peninsula.

Guojialing-type granites are mainly composed of monzonitic diorites, quartz monzonites, granodiorites, and monzogranites (Table 1), with porphyroid textures. They are

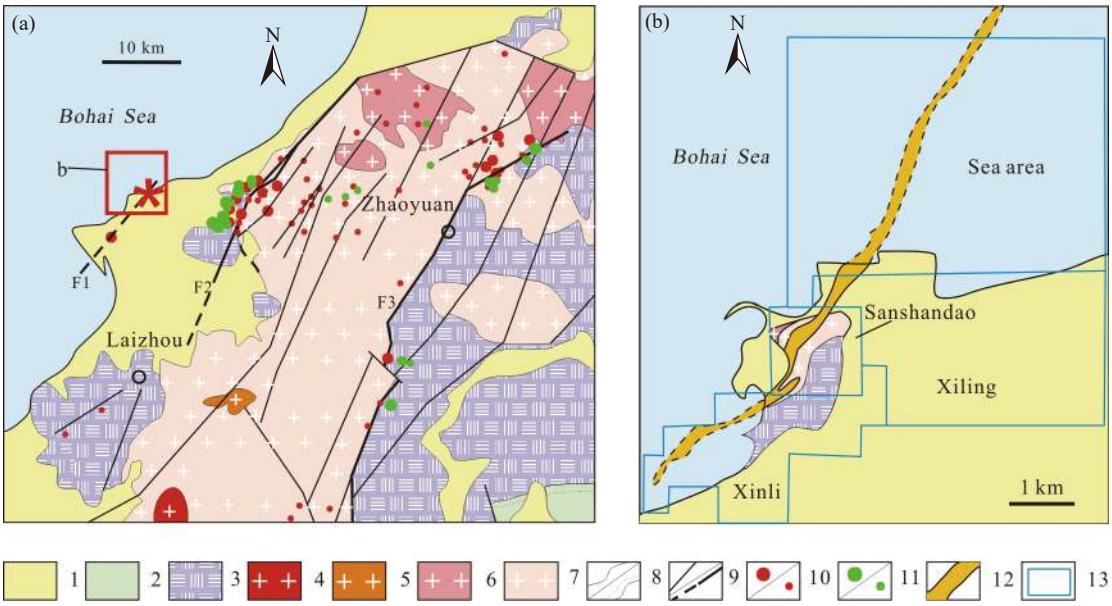


**Fig. 2.** Geological maps of northwest Jiaodong Peninsula (a) and Sanshandao gold deposit (b). 1–Quaternary; 2–Cretaceous; 3–Early Precambrian metamorphic rock series; 4–Cretaceous Laoshan-type granites; 5–Cretaceous Weideshan-type granites; 6–Cretaceous Guojialing-type granites; 7–Jurassic Linglong-type granites; 8–geological conformity/unconformity; 9–fault/main ore-controlling fault; 10–shallow large/medium-small gold deposit; 11–deep large/medium-small gold deposit projected to the surface; 12–alteration zone of Sanshandao fault; 13–ore block boundary. F1–Sanshandao fault; F2–Jiaojia fault; F3–Zhaoping fault.

**Table 1. Characteristics of intrusions related to gold mineralization in the northwest Jiaodong Peninsula.**

| Granitoids | Geological characteristics | Main lithology | Genetic type | Main geochemical characteristics | Isotope ages |
|---|---|---|---|---|---|
| Laoshan-type granites | There is only one Laoshan-type granitic pluton visible—the Dazeshan pluton. It covers an area of about 55 $km^2$ and is in the shape of an ellipse and the NNE strike. The intrusions inside are distributed in the form of irregular zonation | Medium- and medium-coarse-grained monzogranites | A-type granitoids formed from the partial melting of the lower crust in an extensional tectonic setting (Yan QS et al., 2019) | Rich in silicon and alkali and deficient in calcium; belonging to potassic granites, the high-K calc-alkaline rock series, and shoshonite series; rich in LREEs and deficient in HFSEs; showing noticeable negative europium anomalies, and belonging to low-Ba-Sr granites (Goss CS et al., 2010) | 125.0±2.5 Ma, 120±2Ma, 119.9±1.3 Ma (Wang B et al., 2021) |
| Weideshan-type granites | There are two Weideshan-type granitic plutons in and around the area, namely the Nansu and Aishan pluton. The Nansu pluton covers an area of about 15 $km^2$. It is in the shape of an ellipse and strikes NE. The intrusive bodies are distributed in the form of concentric zonation. The Ai Shan pluton is located near the northern side of the eastern part of the study area. It covers an area of about 250 $km^2$ and is present in the form of a nearly SN-trending belt. The intrusive bodies inside are distributed in the form of an irregular belt | The Nansu pluton is dominated by porphyritic, medium-grained hornblende monzogranites. The Aishan pluton is dominated by porphyritic, coarse-medium-grained monzogranites. Other lithology includes medium-grained, medium-coarse-grained, and fine-grained monzogranites, medium-grained and large-porphyritic hornblende monzogranites, medium-fine-grained and porphyritic monzogranites, and medium-fine-grained porphyritic granodiorites | I-type granitoids formed from the mixing of crust-derived acidic magmas of the enriched lithosphere with mantle-derived basic magmas (Song MC et al.,2020a; Yang K et al., 2012) | High total alkali content, low $Na_2O/K_2O$ ratio (0.3–1.1), and low contents of $Fe_2O_3$, MnO, MgO, $TiO_2$, and $P_2O_5$, and is metaluminous. Falling between sodic granites and potassic granites (tending to fall near the former mostly), thus belonging to the high-K calc-alkaline rock series and shoshonite series. Rich in LREEs and LILEs and deficient in HFSEs, with weakly-moderately negative europium anomalies (Goss CS et al., 2010) | 125±3 Ma, 121.3±2.1 Ma, 118± 0.7 Ma, 116.7±1.7 Ma, 116±2 Ma, 114.0±1.2 Ma, 110.5±1.5 Ma (Wang B et al., 2021, Goss CS et al., 2010) |

**Table 1. (*Continued*)**

| Granitoids | Geological characteristics | Main lithology | Genetic type | Main geochemical characteristics | Isotope ages |
|---|---|---|---|---|---|
| Guojialing-type granites | Consist of Shangzhuang, Beijie, Congjia, Qujia, Cangshang, and Xincheng plutons, covering a total area of about 215 $km^2$. Each pluton is in the shape of an ellipse and the nearly EW-NE strike. The intrusive bodies inside are distributed in the form of concentric zonation | Dominated by coarse-medium-grained porphyritic biotite granodiorites, medium-grained hornblende-quartz monzonites, and medium-grained porphyritic hornblende monzonites. Besides, there are medium-grained huge-porphyritic granodiorites and medium-grained porphyritic hornblende-quartz monzonites | I-type granitoids formed form the mixing of lower crust acidic magmas with mantle-derived basic magmas (Jiang P et al., 2016) | Metaluminous, belonging to sodic granites, dominated by the high-K calc-alkaline rock series, with some samples fall into the zone of mugearite series. Rich in CaO, $TFe_2O_3$, MgO, $K_2O$, total alkali, Sr, Ba, LREEs, and LILEs and deficient in Cr, Ni, and HFSEs, without notable europium anomalies, and belonging to high-Ba-Sr granites (Yang KF et al., 2012; Liu Y et al., 2014; Wang ZL et al., 2014a, 2014b; Wang LG et al., 2018; Song YX et al., 2020; Luo XD et al., 2014) | 132.9±2.0 Ma, 132±1 Ma, 131.53±0.86Ma, 131±1 Ma, 130.7±5.1 Ma, 130.3±5.6 Ma, 130.2±8.1Ma, 130±16Ma, 130.0±2.0 Ma, 129.2±9.1Ma, 129±1 Ma, 128.8±2Ma, 128±1 Ma, 127.5±4.6 Ma, 127±2 Ma, 127±1 Ma (Yang KF et al., 2012; Liu Y et al., 2014; Luo XD et al., 2014; Geng K et al., 2015; Deng J et al., 2015b; Cai YC et al., 2018; Feng K et al., 2020) |
| Linglong-type granites | Linglong pluton is the largest outcrop in the area, with an area of about 2183 $km^2$. It strikes NNE and is distributed in a banded shape, and their intrusive bodies are also distributed in a banded shape | Mainly consists of medium-grained biotite monzogranites, medium-coarse-grained monzogranites, and fine-grained weakly-gneissic garnet-containing monzogranites | S-type granitoids formed from the partial melting of the thickened lower crust in North China (Yang KF et al., 2012) | They show high contents of $Na_2O+K_2O$, low content of MgO, and peraluminous characteristics; they are potassic granites and belong to the high-K calc-alkaline rock series; they are rich in LREEs and LILEs and are deficient in HFSEs, and they do not show notable europium anomalies and are high-Ba-Sr granites (Lin BL et al., 2013; Yang KF et al., 2012) | 159±2 Ma, 159±1 Ma, 158.53±0.79 Ma, 157.9±4.1 Ma, and 163.2±9.3 Ma (Wang B et al., 2021; Lin BL et al., 2013; Yang KF et al., 2012) |

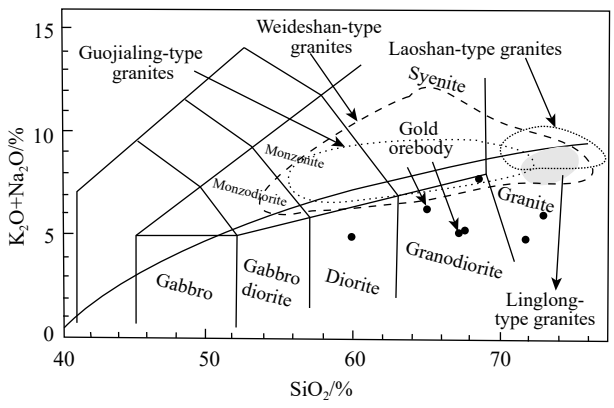


**Fig. 3.** Petrochemical classification diagram of intrusions related to gold mineralization and gold orebodies in the Jiaodong Peninsula (after Song MC et al., 2020a for the ranges of Linglong, Guojialing, Weideshan, and Laoshan-type granites).

monzonite-granite rock series (Fig. 3) and show metaluminous characteristics. They are sodic granites and are dominated by the high-K calc-alkaline rock series, with some samples falling in the zone of shoshonite series. They have high contents of CaO, $TFe_2O_3$, MgO, $K_2O$, total alkali, Sr, Ba, LREEs, and LILEs and are depleted in Cr, Ni, and HFSEs. Their $^{87}Sr/^{86}Sr$ ratio, $\varepsilon Nd(t)$, $\varepsilon Hf(t)$, and Sr/Y ratio are 0.710175–0.71172, from −21.30 to −11.17, from −25.2 to −13.9, and 114 –378, respectively (Yang KF et al., 2012; Wang ZL et al., 2014a, 2014b; Liu Y et al., 2014; Wang LG et al., 2018; Song YX et al., 2020). Their $\varepsilon Hf(t)$ values fall between the crustal evolution curves of 2.5 Ga and 3.0 Ga (Yang KF et al., 2012). According to a previous study (Wang ZL et al., 2014b), the high Ba-Sr contents mainly originated from the partial melting of basement rocks in the northern Jiaodong Peninsula, with the addition of intermediate magmas derived from the partial melting of juvenile basic lower crust formed by the underplating of mantle-derived magmas, which is related to the subduction of the paleo-Pacific plate toward the North China Craton and upwelling of the asthenosphere. The initial $^{206}Pb/^{204}Pb$ and $^{208}Pb/^{204}Pb$ ratios of Guojialing-type granites are 17.047 –17.945 and 37.744 –38.389, respectively, indicating that large quantities of lower crust materials were involved in the diagenesis (Wang ZL et al., 2014a; Song YX et al., 2020). The $\varepsilon Nd(t)$ values of Guojialing-type granites are similar to those of the basic vein rocks in the northwest Jiaodong Peninsula, indicating that the magmas in Guojialing-type granites were derived from the mantle (Yang KF et al., 2012; Liu Y et al., 2014; Wang ZL et

al., 2014a; Wang LG et al., 2018; Luo XD et al., 2014). Guojialing-type granites contain rich Neoarchean and Paleoproterozoic inherited zircons and a small amount of Jurassic inherited zircons but bear no Neoproterozoic and Early Paleozoic inherited zircons (Yang KF et al., 2012). This indicates that the crust-derived materials originated from the basement of the North China Craton (Early Precambrian metamorphic rock series in the Jiaodong Peninsula) and lack the crust materials from the Sulu ultrahigh-pressure metamorphic belt and the Yangtze Craton. Overall, Guojialing-type granites are considered the result of mixing of the lower crust acidic magmas formed from the partial melting of the basement metamorphic rock series in the Jiaodong Peninsula with mantle-derived basic magmas. Meanwhile, it is believed that the formation of magmas is related to the subduction of the paleo-Pacific plate toward the North China Craton and upwelling asthenosphere. The zircon U-Pb isotopic ages vary in the range of 133–127 Ma (Table 1).

Weideshan-type granites are widely distributed in the Jiaodong Peninsula, without noticeable gold mineralization inside the pluton and contact zones. However, they are closely related to copper, lead, zinc, and molybdenum deposits (Ding ZJ et al., 2013; Song MC et al., 2017). They have a complex composition and mainly consist of diorites, quartz monzonites, granodiorites, and monzogranites, with porphyric textures (Table 1). They are chemically classified as monzonitic diorite-granite, with a high total alkali content, a low $Na_2O/K_2O$ ratio (0.3–1.1), low contents of $Fe_2O_3$, MnO, MgO, $TiO_2$, and $P_2O_5$, and metaluminous characteristics (Goss CS et al., 2010). In the petrochemical classification diagram, they mainly fall into the zones between sodic granites and potassic granites (tending to approach the sodic granite zone), thus belonging to the high-K calc-alkaline rock series and shoshonite series. They are rich in LREEs and LILEs and deficient in HFSEs and show weak-moderate negative europium anomalies. They have $\varepsilon Hf(t)$ values of −25.52–−11.55 and strong positive Pb anomalies. Their $T_{DM2}$ model ages are 3096–3434 Ma, indicating that their magma sources are related to the Archean basement and ancient recycled continental crustal materials (Goss CS et al., 2010) and that the magmas originated from the partial melting of recycled continental crustal materials and enriched lithospheric mantle. The zircon U-Pb isotopic age of Weideshan-type granites is 125–110 Ma (Table 1).

Laoshan-type granites are mainly distributed in the ultrahigh-pressure metamorphic belts in the eastern and southern parts of the Jiaodong gold ore concentration area. In terms of spatial distribution, they do not show direct relationships with the mineralization of gold and nonferrous metals. They are monzogranite - syenogranite - alkali-feldspar granite series, while only monzogranites are reported in the northwest Jiaodong Peninsula (Table 1). In the petrochemical classification diagram, they mainly fall into the granite zone (Fig. 3). They are distinctly rich in silica and alkali and deficient in calcium, belonging to potassic granites, the high-K calc-alkaline rock series, and the shoshonite series. Therefore, they have typical characteristics of A-type granites. They show noticeable REE fractionation and significant negative europium anomalies and are rich in LREEs. According to the trace element analysis, Laoshan-type granites show the characteristics of low-Ba-Sr granites with a low Ba content and a high Rb content (Goss CS et al., 2010), and thus they are different from Linglong and Guojialing-type granites with high Ba and Sr contents. Similar to the above-mentioned Linglong, Guojialing, and Weideshan-type granites, Laoshan-type granites are rich in LILEs and depleted in HFSEs, showing negative Ba anomalies, and positive Sr anomalies. They have $\varepsilon Hf(t)$ values of −20.32–−16.53 and $T_{DM2}$ model ages of 3096–3434 Ma. Overall, Laoshan-type granites are A-type granites formed in a regional extensional tectonic setting, and they are the result of Mesozoic lithospheric thinning and craton destruction (Yan QS et al., 2019). The magmas of Laoshan-type granites originated from the partial melting of deep crust, which may be related to the subduction of the paleo-Pacific plate and the recycling of the oceanic crust in subduction zones. The zircon U-Pb isotopic age of Laoshan-type granites is 125–119 Ma (Table 1).

### 3.2. Ore-hosting faults

Jiaodong gold deposits are mainly controlled by NNE- to near SN- trending faults. Large and medium-sized gold deposits in the northwest Jiaodong Peninsula are controlled by the Sanshandao, Jiaojia, and Zhaoping faults and their secondary faults developing on their footwalls. Meanwhile, favorable places for mineralization include the places with sudden changes in fault strike along with the regional trend, the parts with variations in dip angles along the faults, and the places where secondary faults develop.

The Sanshandao fault extends along the Sanshandao-Cangshang-Panjiawuzi area in Laizhou City on the coast of the Bohai Sea, most of which is covered by the Quaternary sediments. The exposed portions of the fault have a length of 12 km, a width of 20–400 m, a general strike of 40°–50°, a dip direction of SE, and a dip angle of 30°–40° (up to 80° locally). It is horizontally S-shaped on the plane and shows irregular morphology (Fig. 4). It controls the Sanshandao (including the Xinli and sea-area ore blocks) and Cangshang large-superlarge altered rock type gold deposits in fractured zones from north to south.

The Jiaojia fault extends from Ziluojijia in Laizhou City in the south to Yaojia in Longkou City in the north. This fault is about 60 km long and 50–500 m wide, with a dip direction of NW and a dip angle of 30°–50° (up to 78° locally). It shows an S shape on the plane, irregular morphology, and noticeable swelling and shrinkage, with many branches parallel to the fault strike or intersecting the Jaiojia fault in the shape of Chinese character “入” on the footwall of the fault. More than 20 gold deposits such as Jiaojia, Xincheng, Hedong, and Hexi are controlled by the Jiaojia fault or its adjacent secondary faults.

The Zhaoping fault is the largest ore-controlling fault exposed in the northwest Jiaodong Peninsula. It starts from

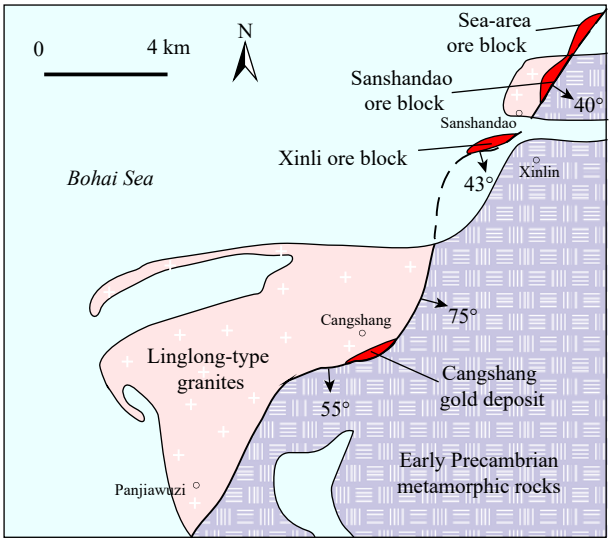


**Fig. 4.** Geological map of bedrocks in the Sanshandao fault.

Songgezhuang in the northern part of Pingdu City in the south and extends northward in the NNE-NE direction to Zhaoyuan City. Afterward, it extends in the NEE direction to the vicinity of Yanjiagou in Longkou City and then pinches out. It is 120 km long in total and 150–200 m wide, with a dip direction of SE-E and a dip angle of 30°–70°. It consists of major faults and a series of secondary faults. Among them, the major fault in the northern of Zhaoyuan City is distributed along the Fushan-Jiuqu Jiangjia area and is called the Jiuqu fault. The northern section of the Zhaoping fault and the secondary faults developing on its footwall control the Linglong gold orefield, the middle section of the Zhaoping fault controls the formation of Dayingezhuang gold orefield, and the southern section of the Zhaoping fault and its secondary faults on the footwall control the Jiudian gold orefield.

### *3.3. Geological characteristics of the Sanshandao ore district*

The Sanshandao ore district is located in a coastal and shallow sea area and consists of Sanshandao, Xinli, Xiling, and sea-area ore blocks (exploration areas; Fig. 2b), which were discovered during different times. This area is mostly covered by Quaternary sediments and seawater, with bedrock outcrops retained only in several areas. The Quaternary sediments have a thickness of several meters to tens of meters, which is up to a maximum of 60 m in the sea area. The bedrock in the gold mine is mainly composed of Jurassic Linglong-type granites and Neoarchean metamorphic rocks (amphibolites and TTG gneisses), and there are numerous vein rocks such as lamprophyres, diabase-porphyries, quartz diorite porphyries, and diorite porphyries. Meanwhile, the Linglong-type granites are intruded by medium-grained porphyritic Guojialing-type granites.

The Sanshandao fault serves as an ore-hosted fault and mainly develops along the contact zones between Linglong-type granites and the Neoarchean metamorphic rock series. It possesses the characteristics of multi-stage activities, including left-lateral transpression before the mineralization, the right-lateral transtension during the mineralization, and the left-lateral transpression after the mineralization (Deng J et al., 2010). In the Xinli ore block, the drilling-controlled fault is 1300 m long and 70–185 m wide, with the fault strike shifting on average from 62° in the south to 38° in the north. The fault has a dip direction of SE and a dip angle of 33°–76° (40°–50° mostly; average: 46°). It extends in a gentle wave pattern in both the strike and the dip direction. The main fracture plane marked by grayish white-grayish black fault gouges continuously develop, and the fault gouges are 0.05–0.50 m thick. In the Sanshandao ore block, the drilling-controlled fault is more than 1000 m long and 50–200 m wide, with an overall strike of 40°, a dip direction of SE, and a dip angle of 35°–45°. It extends in a gentle wave pattern similar to that in the Xinli ore block. Its main fracture plane lies in the upper part of the fractured zone and is covered by 6–40 cm thick fault gouges (Fig. 5a). In the Xiling ore block, the drilling-controlled fault has a length of 2850 m, a fault height of 3215 m, a strike of 35°, and a dip direction of SE, showing a gentle wave pattern along the fault plane. Its dip angle is about 42° in the section at an elevation of above −600 m. It becomes steeper at an elevation of −600–−1000 m, with a dip angle of 70°–80°. Meanwhile, its dip angle is mainly 30°–50° below -1000 m. The fractured zones are 40–400 m wide. White - grayish-black fault gouges continuously develop along its main fracture plane, with a thickness of

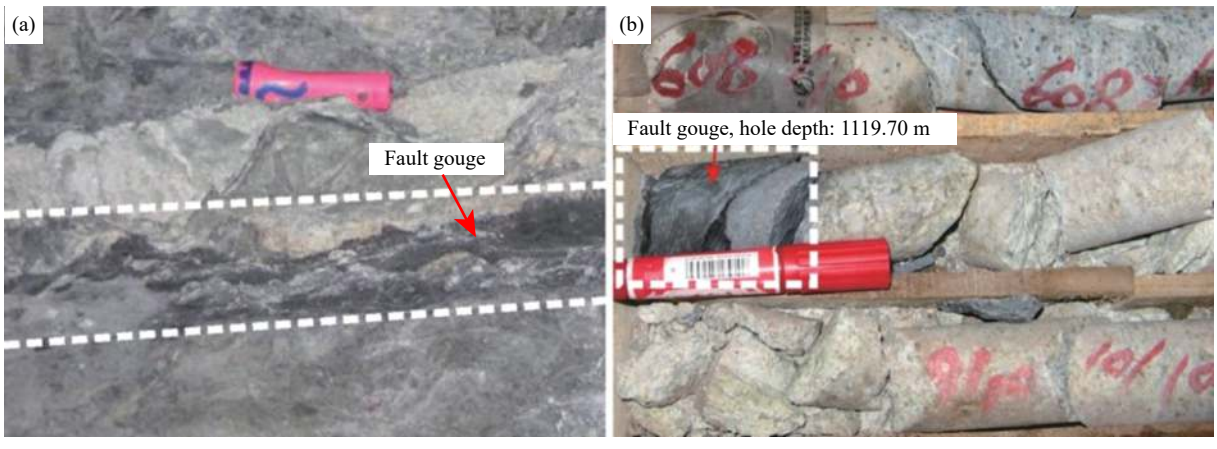


**Fig. 5.** Fault gouges on the main fracture plane in the Sanshandao ore block (a) and sea-area ore block (b) of the Sanshandao gold deposit.

0.02–0.50 m. In the sea-area ore block, the drilling-controlled fault has a length of 4420 m long and a fault height of 2156 m, with a strike of about 35°. It generally extends in a gentle wave pattern, with a dip direction of SE. The dip angles are about 40° in the section at an elevation of above −400 m, 75°–85° at an elevation of −400–−1000 m, and 35°–43° at an elevation of below −1000 m. The main fracture plane marked by grayish white-grayish-black fault gouges continuously develop, the fault gouges are 0.05–0.50 m thick (Fig. 5b), and the fractured zones are 40–400 m wide.

## 4. Alteration and mineralization

### *4.1. Alteration zoning and styles*

#### *4.1.1. Alteration zones*

Alteration zones are controlled by the Sanshandao fault as well, with the scale and zonation consistent with those of fractured zones of the fault. Meanwhile, their alteration intensity and zoning are also consistent with the degree of fragmentation of the wall rocks. The alteration zones are generally 50–200 m wide. Mineralized alteration is visible on both the hanging wall and the footwall of the main fracture plane of the fault. However, the hanging wall shows weak alteration and zoning, with no industrial gold orebodies in general. The mineralized alteration zones along the Sanshandao fault are, from the main fault to the footwall, strongly to weakly sericite-quartz-pyrite altered granites with blurred boundaries. The alteration style is mainly sericite-quartz alteration above the main fault zone, which is not as widespread as that in the footwall overall (Fig. 6).

The alteration zone in the Xinli ore block has a length of 1300 m, a width of 70–185 m, and a controlled height of 1000 m. It has an overall strike of 62°, a dip direction of SE, and a dip angle of 33°–67° (average: 46°). It shows relatively stable morphology overall and extends in a gentle wave pattern, with local abrupt changes in the strike.

There are five alteration zones in the Sanshandao ore block. Among them, the No.1 alteration zone develops along the Sanshandao fault and is the main alteration zone, while other alteration zones are secondary alteration zones underlying the Sanshandao fault. The drilling-controlled section of the No.1 alteration zone is 1700 m long, 50–200 m wide, and 1000 m high. The No.1 alteration zone is wider in the middle part of the ore block and gradually narrows down toward the southern and northern sides, showing arc-shaped morphology on a horizontal plane. The alteration intensity displays symmetrical zoning, with the core dominated by a sericite-quartz-pyrite zone and the two sides (the hanging wall and footwall of the fault) exhibiting sericitolites, sericitolited cataclasites, and sericitized (silicified) cataclastic granites in turn.

The alteration zone in the Xiling ore block has a width of 30 –580 m, which varies greatly at different depths. The maximum controlled height of the alteration zone is up to 3190 m. The strike of the alteration zone is 34° in general. It is about 42° in the southern part of the ore block and changes into about 29° in the north. The changes in the dip angle and alteration zoning of the alteration zone are the same as those of the alternation zone in the sea-area ore block.

The alteration zone between No. 20 and No. 42 exploration lines in the sea-area ore block is 1710 m long along its strike. The width varies greatly at different depths. Specifically, it is 150–260 m above −400 m but reduces to 80 m generally between −400 m and −1000 m. It increases to 300 –400 m at a depth below −1000 m. The maximum controlled height of the alteration zone is 2156 m. The strike and dip angle of the controlled alteration zone is 35° and SE, respectively. The dip angle of the controlled alteration zone varies greatly with the depth. It is about 40° at the depth above −400 m, 75°–85°between −400 m and −1000 m, and 35°–43° at a depth below −1000 m (Fig. 7a). The controlled alteration zone generally shows stable morphology and extends in a gentle wave pattern along its strike and a regular stepped pattern along its dip direction (Fig. 7b). The controlled alteration zone between No. 50 and No. 76 exploration lines has a length of 2040 m in the strike, a width of 234–448 m, and a maximum controlled height of 970 m. It has a strike of 35° overall, a dip direction of SE, and a dip angle of 30°–45°. It shows the noticeable zoning of altered rocks. In detail, a beresitized cataclasite zone exists 0–320 m below the main fracture plane, where alteration and gold mineralization are the most intensive. Outside the beresitized cataclasite zone lie a beresitized granitic cataclasite zone and a beresitized granite zone. In terms of mineralization characteristics, the beresitized cataclasite zone is dominated by disseminated or veinlet-disseminated mineralization, and the beresitized granitic cataclasite zone and beresitized granite zone are dominated by veinlet and stockwork-type mineralization.

#### *4.1.2. Alteration types*

The alteration types in alteration zones of the Sanshandao gold deposit include K-feldspar alteration, quartz-sericite alteration, silicification, carbonation, and chlorite alteration. Among them, the K-feldspar alteration (Fig. 8a, b) has developed at the earliest stage, with a width over 100–200 m. In the main alteration zones, little K-feldspar alteration is observed due to the later superimposition of sericite alteration and silicification, with only a small amount of porphyritic and cloud-like K- feldspar residuals occasionally visible, although it is hard to tell whether they are hydrothermal or magmatic in origin.

The quartz-sericite alteration (Figs. 8c, d) is the major alteration type in the mining area and is closely related to mineralization. It occurs in a wide range and generally develops along the fractured zone of the Sanshandao fault. It is frequently associated with disseminated fine-grained pyrites, with coarse-grained pyrites occasionally visible.

The silicification (Fig. 8e) is mainly present as the replacement of granites by grayish-white quartz. It tends to occur in the form of quartz blocks, in which the content of quartz is over 90%. However, silicification is weak in gold-

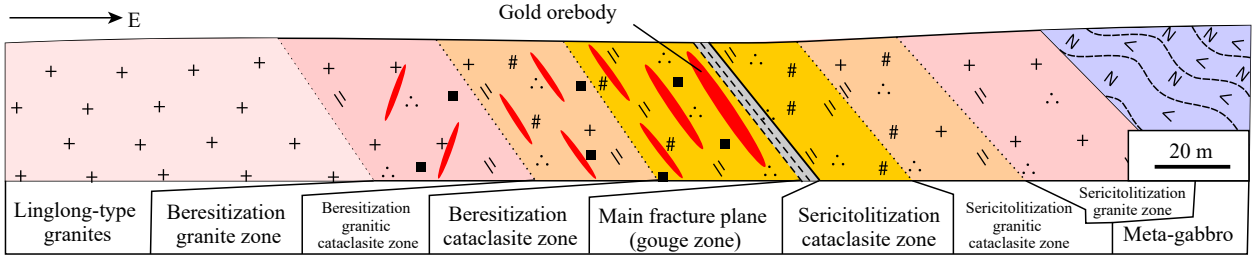


**Fig. 6.** Comprehensive schematic diagram of lithologic zoning of the alteration zones and fractured zones in the Sanshandao fault.

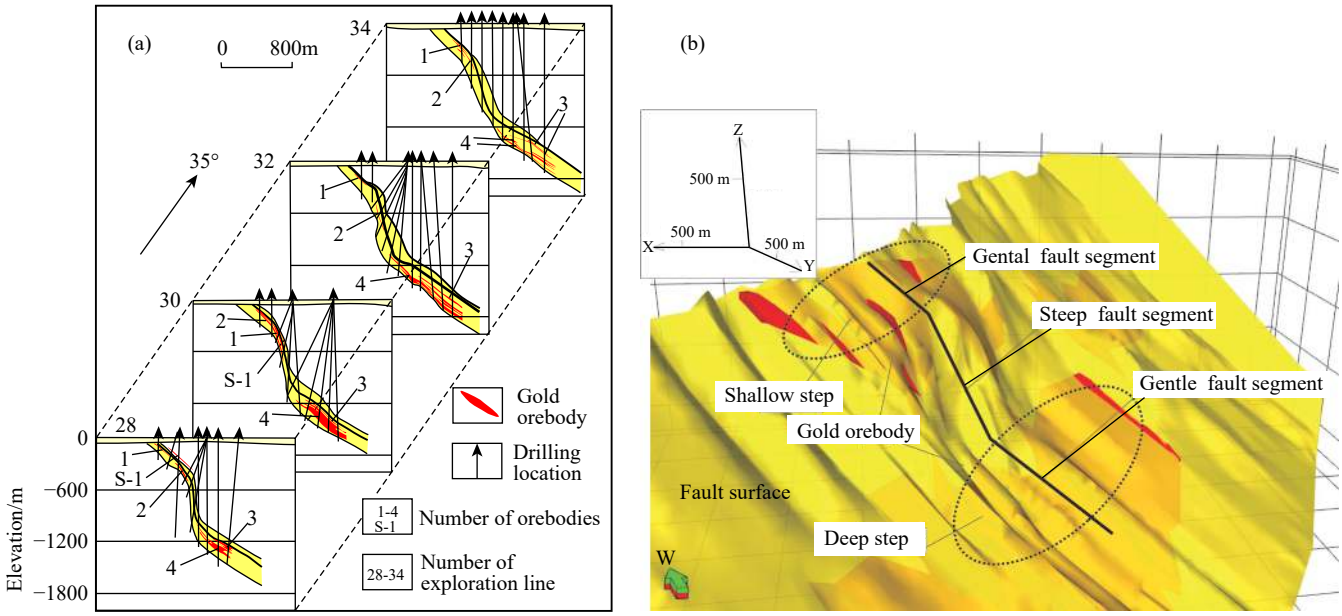


**Fig. 7.** Combined section of exploration lines (a) and 3D view of a fault plane (b) of the sea-area ore block in Sanshandao gold deposit (after Song MC et al., 2015a).

rich beresite orebodies.

Carbonation is an alteration type occurring in the late stage of mineralization, with calcites as the main mineral. Carbonation occurs in two states. One is that carbonation is distributed in quartz-sericite alteration zones in the form of blocks (Fig. 8f) or short veins, with little sulfides such as fine-grained pyrite or sphalerites. The other is that carbonation fills in rock fissures, cleavages, or faults in the form of coarse veins (Fig. 8g). The late state frequently occurs in weakly potassic zones, with coarse-grained pyrites occasionally visible.

The chloritization (Fig. 8h) is a common alteration type. It develops in both surrounding rocks and orebodies. However, it is not as strong as other types of alteration. It mainly develops in cataclasites and is strong on both sides of the main fracture plane. It is present as a non-penetrating alteration, with penetrating alteration occurring in several areas.

### *4.2. Characteristics of orebodies*

The Sanshandao and Xinli gold mines located in the northern section of the Sanshandao fault were discovered in the 1960s and the 1990s, respectively. They have always been regarded as two independent deposits since they were discovered. They are 1 km apart on the ground surface. Since the beginning of this century, gold resources have been successively discovered in the deep parts of the Xinli, Sanshandao, Xiling, and sea-area ore blocks. As revealed by exploration and projects (Song MC et al., 2019), the main gold orebodies in the Xinli, Sanshandao, and sea-area ore blocks, which are independently distributed in shallow parts, are interconnected with each other in deep parts (Fig. 9). They constitute a supergiant deposit with a tonnage aggregation index (the ratio of the tonnage of economic metal in a deposit to average metal content in the crust) of greater than $100\times10^9$, and the cumulative proven gold reservoirs of this supergiant deposit have exceeded 1200 t.

#### *4.2.1. Overall characteristics of orebodies*

There are more than 80 orebodies in the Sanshandao gold deposit. Most of them occur in the beresite on the footwall of the main fracture plane of the Sanshandao fault, and very few of them occur on the hanging wall of fracture planes. The main orebodies are mostly concentrated in the Ⅰ orebody groups, which primarily occur in the alteration zone of beresitized cataclasites on the footwalls of main fracture planes of faults. The main orebodies include the Ⅰ-1 orebody of the Xinli ore block, the Ⅰ-1 and Ⅰ-2 orebodies of the Sanshandao ore block, Ⅰ-1– Ⅰ-7 orebodies of the Xiling ore


**Fig. 8.** Photos of altered rocks in Sanshandao gold deposit (a–h explains see the text).

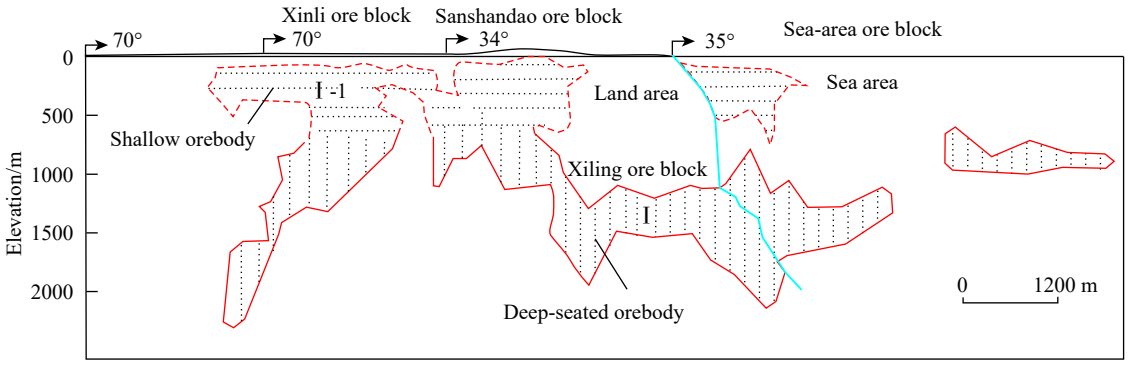


**Fig. 9.** Vertical longitudinal projection of main orebodies in the Sanshandao gold deposit.

block, and the Ⅰ-1– Ⅰ-9 orebodies of the sea-area ore block. The orebodies in the I orebody groups of these ore blocks are connected. As a result, they constitute a giant gold orebody with a total length of 8 km, with a deepest controlled depth of −2312 m, and a maximum controlled height of more than 3 km (Fig. 9). The giant gold orebody is present in the form of a huge vein shape mostly and in a stratoid shape locally. It is distributed in a gentle wave pattern along its strike and dip

direction, with branches and combination as well as swelling and shrinkage. Its attitude is essentially consistent with that of the main fracture plane of the Sanshandao fault, with a strike of 30°–80° (average: 35°), a dip direction of SE, a dip angle of 25°–78° (average: 40°), and it generally inclines towards NE (Fig. 9).

The thickness of single-drilling-controlled orebody is 1.00–122.83 m, with an average of 3.04 m and a coefficient of variation of 112.05%, indicating that the orebodies have stable thickness. There are three parts with thick gold orebodies in the Sanshandao gold deposit. Among them, the shallow parts are mainly located at an elevation of 0–−600 m in the Xinli and Sanshandao ore blocks, while the deep parts mainly lie at an elevation of −1000–−2000 m (Fig. 10a). The single-drilling-controlled gold grade is 1.00–35.32 g/t, with an average of 3.61 g/t and a coefficient of variation of 71.37%, indicating that useful components are evenly distributed in the orebodies. There are three parts with the enrichment of high gold grade in the orebodies. Among them, the shallow parts are located at an elevation of 0 –−500 m in the Xinli and Sanshandao ore blocks, while the deep parts lie at an elevation of −1000 –−2000 m in the Xiling ore block and the sea-area ore block in northern Sanshandao (Fig. 10b). Therefore, the orebody-rich parts highly coincide with the parts with thick orebodies. This indicates that there is a positive correlation between the thickness and gold grade of the orebodies. That is, the thicker the orebodies, the higher the gold grade. The weakly mineralized sections between the shallow parts and the deep parts of orebodies are located at an elevation of −600–−800 m (Fig. 10c).

*4.2.2. Characteristics of main orebodies in each ore block*

The Ⅰ-1 main orebody in the Xinli ore block is controlled by 85 boreholes. It occurs at an elevation of −30 – −710 m, with a maximum controlled length along its strike and dips direction of 1145 m and 900 m, respectively. It has an overall strike of 62°, a dip direction of SE, and a dip angle of 33°–67° (average: 46°). It is present as a huge vein mostly and is stratoid and lensoid in shape locally, and it extends in a gentle wave pattern along the strike and dip direction. Its thickness is 0.48–28.96 m, with an average of 7.42 m and a coefficient of variation of 78.27%, indicating a relatively stable thickness. The gold grade of single-drilling-controlled orebody of the orebody is 1.52–12.53 g/t, with an average of 3.26 g/t and a coefficient of variation of 156.09%, indicating that useful components are unevenly distributed in the orebody.

The I-1 orebody in the Sanshandao ore block occurs at an elevation of −10 – −1950 m, with a maximum controlled length along its strike and dip direction of 1020 m and 1450 m, respectively. It has an overall strike of 35°, a dip direction of SE, and a dip angle of 37°–44°. It is present as irregular veins and is discontinuously distributed along the strike and

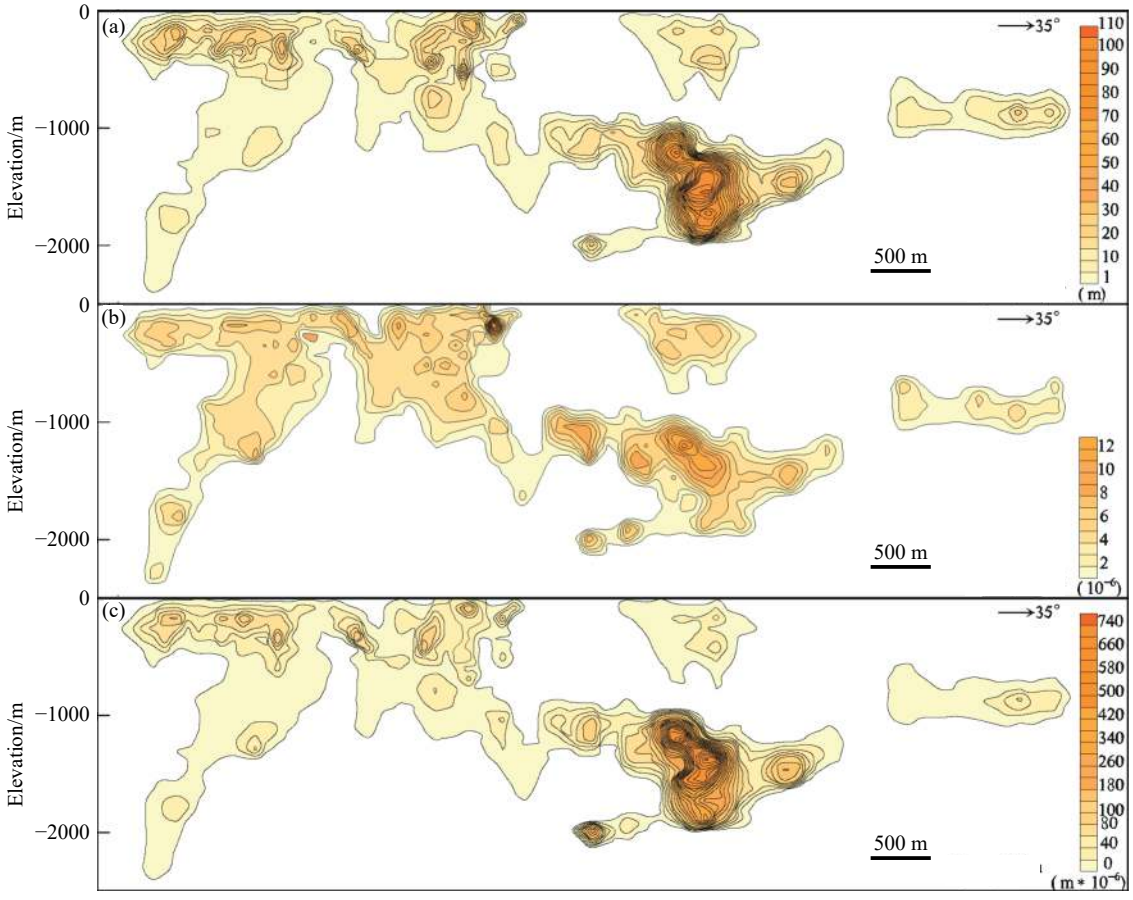


**Fig. 10.** Vertical thickness and grade contour maps of the Sanshandao gold deposit. a –thickness contour map, b –grade contour map, c–grade×thickness contour map.

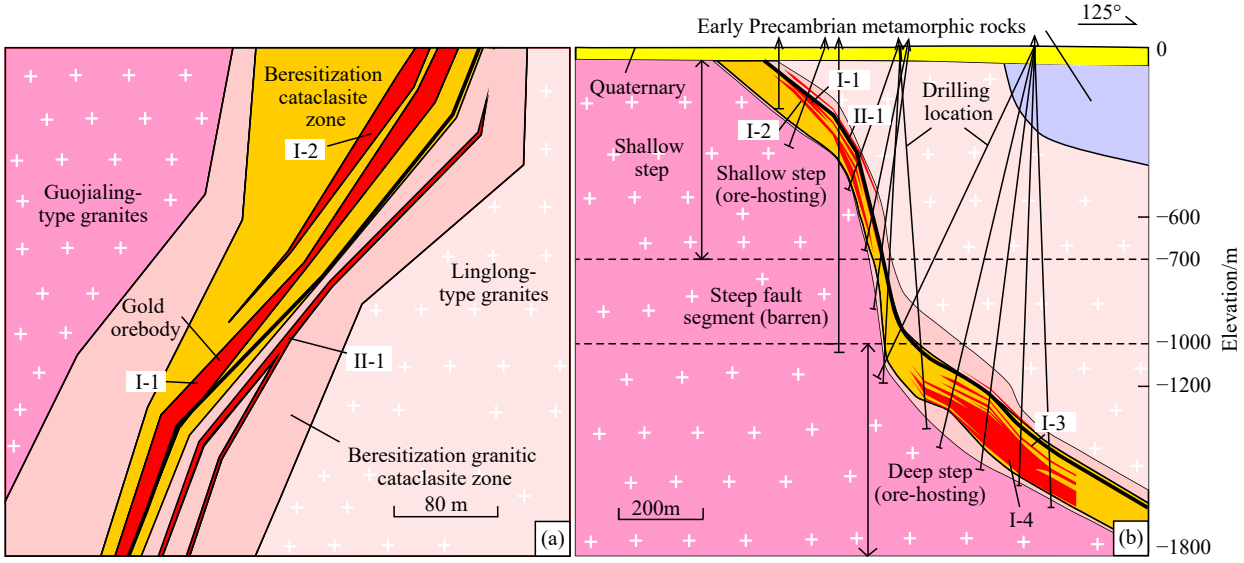


**Fig. 11.** Map showing the horizontal projection of the middle section at an elevation of −400 m (a) and the section of No. 30 exploration line (b) of the sea-area ore block in the Sanshandao gold deposit.

dip direction. It reappears after pinching out in some parts. Its thickness is 0.95–12.08 m, with an average of 6.65 m and a coefficient of variation of 68.9%, indicating a stable thickness. The ore grade of the single-drilling-controlled orebody is 1.74–5.65 g/t, with an average of 3.25 g/t and a coefficient of variation of 70.6%, indicating that useful components are unevenly distributed in the orebody.

The I-2 orebody in the Xiling ore block is controlled by 42 boreholes and occurs at an elevation from −920 to −2250 m. It connects the deep main orebody of the Sanshandao ore block in the south and the deep main orebody of the sea-area ore block in the north (Fig. 9). The drilling-controlled length along the strike and the maximum depth along the dip direction of the orebody is 1940 m and 1500 m, respectively. The controlled orebody is present in the shape of a huge vein as a whole and is stratoid and large-lensoid in shape locally. It has an overall strike of 25°–36°, a dip direction of SE, and a dip angle of 26°–53°. Its thickness ranges from 1.61 m to 97.55 m, with an average of 10.50 m and a coefficient of variation of 123%, indicating a relatively stable thickness. The gold grade of a single sample of the orebody is 0.05–35.19 g/t, with an average of 4.30 g/t and a coefficient of variation of 210%, indicating that the components unevenly change in the orebody.

The sea-area ore block consists of a shallow and a deep orebody group. There are eight gold orebodies in the shallow orebody group. All of them occur on the footwall of the main fracture plane of the Sanshandao fault except for the II-1 orebody, which occurs on the hanging wall of the main fracture plane of the Sanshandao fault (Fig. 11a). There are five gold orebodies in the deep orebody group, and they are nearly parallelly distributed on the footwall of the main fracture plane of the Sanshandao fault. The shallow and deep orebody groups occur in the parts of the Sanshandao fault with relatively gentle dip angles and constitute two ore-hosting steps. The ore-free interval between the shallow and deep orebody groups along the No. 30 exploration line lies at an elevation from −700 to −1000 m (Fig. 11b). The I-4 orebody in the deep orebody group is the main orebody. It is controlled by 29 boreholes and occurs at an elevation from −796 to −1736 m. The drilling-controlled lengths along the strike and the dip direction are 1446 m and 1072 m, respectively. It is present in a large vein shape generally and is stratoid and large-lensoid in shape locally. Meanwhile, it extends in a gentle wave pattern along the strike and dips direction. It has an overall strike of about 35°, a dip direction of SE, and a dip angle of 21°–52° (average: 39°). Its thickness is 1.07–101.86 m, with an average of 30.91 m and a coefficient of variation of 78%, indicating a stable thickness. The gold grade of a single sample of the orebody is 0.05–213.32 g/t, with an average of 5.23 g/t and a coefficient of variation of 202%, indicating that the components are unevenly distributed in the orebody.

*4.2.3. Three-dimensional spatial distribution of orebodies*

According to the three-dimensional geological model of the Sanshandao gold deposit established based on the data of 311 boreholes, the Sanshandao fault is generally in the shape of a dustpan consisting of a steep upper part and a gentle lower section (Fig. 12a), and the main orebodies and thick orebodies are distributed in parts with low dip angles along the fault (Fig. 12b). There are a shallow and a deep orebody group along the fault. Among them, the shallow orebody group is mainly located at an elevation of above −800 m, and it includes 11 gold orebodies, including the Ⅱ-1, Ⅰ-1, Ⅰ-2, Ⅰ-5, Ⅰ-6, Ⅰ-7, Ⅰ-8, and Ⅰ-9 orebodies in the northern sea area and the Ⅰ-1, Ⅰ-2, and Ⅰ-4 orebodies in the Sanshandao ore block. The deep orebody group is located at an elevation of below −1000 m, and it consists of 12 main gold orebodies, including the Ⅰ-3, Ⅰ-4-1, Ⅰ-4-2, Ⅰ-4-3, and Ⅰ-4-4 main gold orebodies in the northern sea area and the Ⅰ-1, Ⅰ-2 (deep), Ⅰ-3, Ⅰ-4, Ⅰ-5, Ⅰ-6, and Ⅰ-7 orebodies in the

Xiling ore block.

Almost 3000 pieces of ore data were evenly extracted from the three-dimensional model after interpolation (2849). According to these data, the orebodies have a large thickness range of 1.00–122.83 m (average: 12.60 m) dominated by 1.00–10.00 m (Fig. 13a). The three-dimensional thickness distribution map (Fig. 14a) shows an area with thick orebodies, indicating that thick orebodies are intensively distributed. Meanwhile, the orebodies show alternating high and low thicknesses along with their strike and dip directions.

According to these data, the ore grade ranges from 1.00 g/t to 35.32 g/t, with an average of 2.43 g/t. The grade data are evenly distributed but slightly vary (Fig. 13b). As shown in the three-dimensional gold grade contour map (Fig. 14b), the gold grades of the orebodies are evenly distributed, with small relative differences. Gold grade tends to be high in areas with thick orebodies, and there is a noticeable positive correlation between the thickness and gold grade of the orebodies.

The value of gold grade × thickness can reflect the enrichment of mineralization. In detail, the higher the values, the richer the mineralization. A total of 2849 values of gold grade × thickness were evenly extracted after interpolation. According to these data, the values of gold grade × thickness fall in the range of 1.00–892.58 m g/t (average: 51.83 m g/t) dominated by 1.00–100 m g/t. The orebody model shows an ore-rich section with the values of gold grade × thickness of greater than 240 m g/t, which are much higher than those of its surrounding areas (Fig. 10c).

### 4.3. Mineralization characteristics

#### 4.3.1. Ore types

The ores in the Sanshandao gold deposit can be divided into the following three natural types according to their mineralization characteristics and their alteration and fragmentation degrees.

(i) Disseminated to veinlet-stockwork beresite type (Fig. 15a, b). The ores are grayish-green -dark gray, and its original rock is mostly granite. They were fractured into fine-grained and uniform cataclasites and then experienced alteration and mineralization later. The ore textures mainly include lepidogranoblastic texture, cataclastic texture, and porphyroclastic texture, along with interstitial and poikilitic textures. In terms of structures, the ores are dominated by fine-grained (pyrite) disseminated structure and densely disseminated structure, as well as veinlet-stockwork structure. The gangue minerals mainly include quartz, sericites, with small amounts of calcites. Meanwhile, the metallic minerals mainly include pyrite and a small amount of chalcopyrite, galena, and sphalerite.

(ii) Veinlet-veined beresitized granitic cataclasite type (Fig. 15c). The ores are grayish-white, gray, and light flesh red and show cataclastic textures and a taxitic structure. Pyrite is fine-grained disseminated and forms veinlet and stockwork

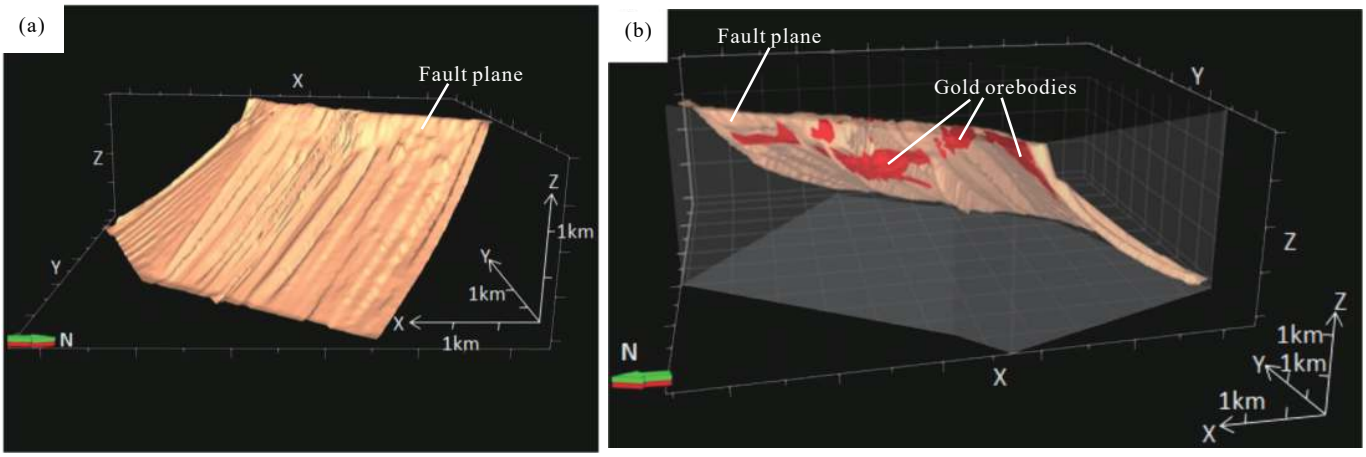


**Fig. 12.** Three-dimensional perspectives of ore-controlling faults (a) and main orebody distribution (b) of the Sanshandao gold deposit.

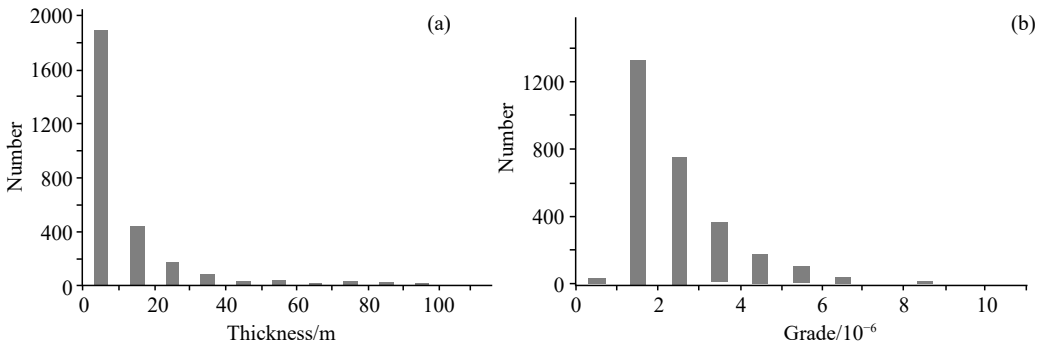


**Fig. 13.** Histograms of the distribution of orebody thickness (a) and gold grade (b) of the Sanshandao gold deposit.

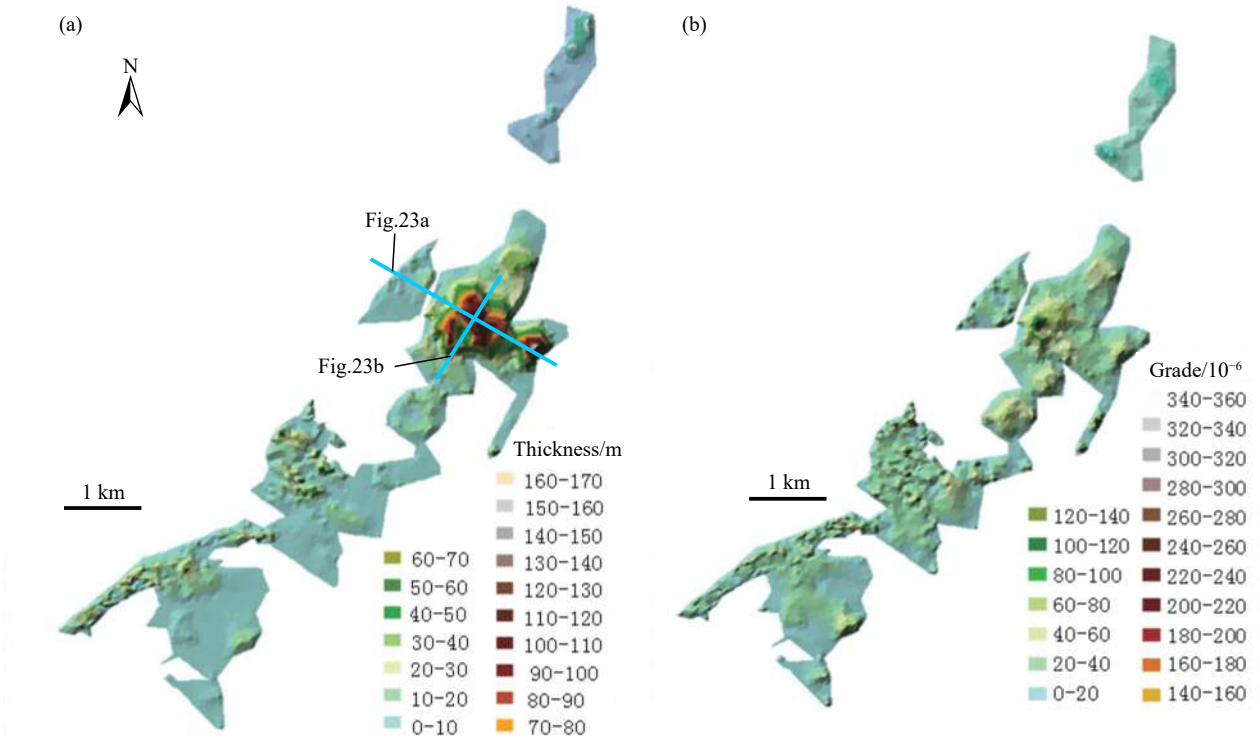


**Fig. 14.** Three-dimensional distribution maps of the thickness (a) and gold grade (b, grade values magnified by 10 times) of orebodies in the Sanshandao gold deposit.

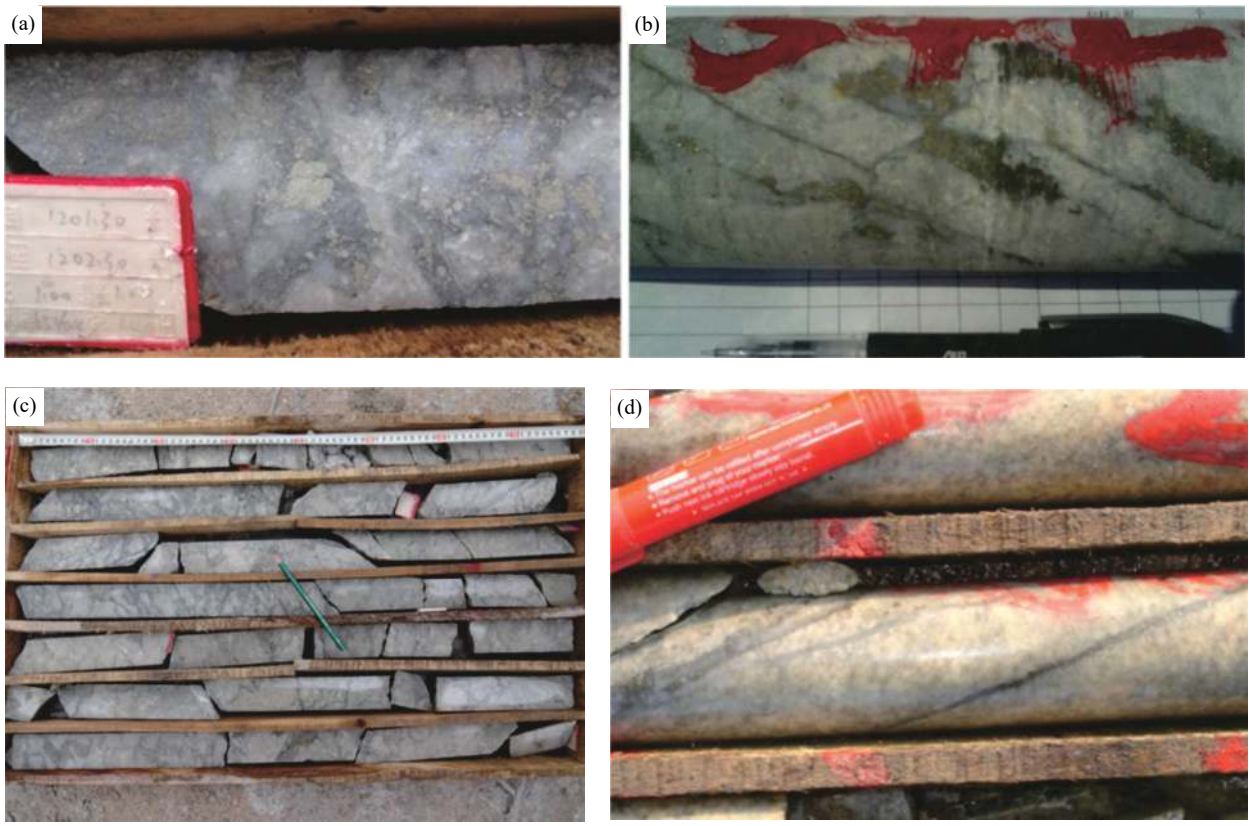


**Fig. 15.** Photos of main gold ore types in the Sanshandao gold deposit. a–disseminated beresite type; b–veinlet-stockwork beresite type; c–veinlet-stockwork beresitized granite cataclasite type; d–veinlet-stockwork potassiumized and beresitized granite type.

distribution together with silicified quartz, forming veinlet disseminated and stockwork structures. The gangue minerals mainly include quartz, feldspar, sericite, and a small amount of calcite. Meanwhile, the metallic minerals include mainly pyrite, with minor chalcopyrite, harrisite, and sphalerite.

(iii) Veinlet-stockwork and veined beresitized and

potassiumized granite type (Fig. 15d). The ores are light flesh red and grayish-white and show blastogranitic textures. Pyrite and gray silicified quartz are distributed in veins and veinlet-stockwork, forming a veined and veinlet-stockwork structure. The gangue minerals include mainly feldspar and quartz, with minor sericite. The metallic minerals are dominated by pyrite, with chalcopyrite occasionally visible.

*4.3.2. Ore mineralogy*

The major metal minerals are pyrite, and the secondary ones are galena, sphalerite, chalcopyrite, arsenopyrite, pyrrhotite, limonite, and magnetite. Primary non-metallic minerals include quartz, sericites, and residual feldspars, and secondary non-metallic minerals are carbonate minerals (e.g., calcites, dolomites, and siderites). Gold minerals in the ores mainly include electrum, followed by native gold and kustelite (Table 2). Among them, pyrite is the main gold-bearing mineral, followed by galena and quartz.

*4.3.3. Chemical composition of ores*

According to the whole-rock analysis results of ore samples (Table 3), the $SiO_2$ content is high (59.82%–72.96%), with an average of 67.54%. Most of the ore samples fall into the zones of granodiorite and granite, and their $K_2O + Na_2O$ content is lower than that of normal granitoid ore-hosting rocks (Fig. 3). The $Fe_2O_3 + FeO$ content is high, and there is a significant positive correlation between it and S (Fig. 16a), with a correlation coefficient of $R = 0.954$ ($R^2 = 0.911$). These indicate that the $Fe_2O_3$+FeO content is mainly correlated with pyrites. Meanwhile, the $K_2O$ content is also high, which is due to the high sericite content.

The primary useful element in the ores is Au, the associated beneficial elements include Ag, S, Cu, Pb, and Zn, and the hazardous element is As. There is a positive

**Table 2. Mineral composition of ores.**

| Relative content | Mineral | | | |
|---|---|---|---|---|
| | Primary minerals | | | |
| | Metallic minerals | | | Non-metallic mineral |
| | Gold and silver minerals | Sulfides | Others | |
| Primary | Electrum | Pyrite | | Quartz, sericite, and residual feldspar |
| Secondary | Kustelite | Sphalerite, galena, chalcopyrite, arsenopyrite, and pyrrhotite | Magnetite, limonite, and pyrolusite | Calcite, dolomite, and muscovite |
| Small amounts | Native gold | Chalcocite, bornite, tennantite, and freibergite | Hematite, pyrolusite, and bismuthite | Biotite, hornblende, zircon, epidote, apatite, rutile, and barite |

**Table 3. Composition of major elements (%) and trace elements ($10^{-6}$ for Au, Ag, As, Sb, and Bi; $10^{-9}$ for Hg, and % for others).**

| Sample No. | 13SHQ01 | 13SHQ02 | 13SHQ03 | 13SHQ04 | 13SHQ05 | 13SHQ06 | 13SHQ07 |
|---|---|---|---|---|---|---|---|
| $SiO_2$ | 59.82 | 68.65 | 67.45 | 71.82 | 64.93 | 67.18 | 72.96 |
| $Al_2O_3$ | 10.06 | 15.19 | 12.96 | 12.82 | 11.78 | 13.2 | 12.51 |
| $Fe_2O_3$ | 10.44 | 0.83 | 0.93 | 3.15 | 5.23 | 0.31 | 3.78 |
| FeO | 1.93 | 1.14 | 4.04 | 1.75 | 1.8 | 1.54 | 0.36 |
| $P_2O_5$ | 0.02 | 0.03 | 0.03 | 0.03 | 0.03 | 0.04 | 0.03 |
| $K_2O$ | 3.99 | 5.01 | 4.82 | 4.5 | 4.25 | 4.39 | 5.52 |
| $Na_2O$ | 1.07 | 2.67 | 0.48 | 0.4 | 2.07 | 0.84 | 0.49 |
| MgO | 0.44 | 0.53 | 0.75 | 0.58 | 0.41 | 0.69 | 0.56 |
| CaO | 0.62 | 2.02 | 2.22 | 0.57 | 1.16 | 3.41 | 0.3 |
| $TiO_2$ | 0.1 | 0.12 | 0.14 | 0.12 | 0.09 | 0.14 | 0.1 |
| MnO | 0.03 | 0.06 | 0.46 | 0.03 | 0.08 | 0.09 | 0.06 |
| LOI | 9.6 | 2.82 | 5.02 | 3.82 | 5.16 | 4.28 | 2.94 |
| Tatal | 98.12 | 99.07 | 99.3 | 99.59 | 96.99 | 96.11 | 99.61 |
| Au | 10.92 | 3.88 | 0.95 | 3.74 | 1.25 | 3.4 | 1.5 |
| Ag | 36 | 3.8 | 5.8 | 3.2 | 49.5 | 47 | 8.8 |
| Cu | 0.4 | 0.006 | 0.012 | 0.044 | 0.022 | 0.18 | 0.01 |
| Pb | 1.24 | 0.046 | 0.18 | 0.012 | 2.04 | 3.4 | 0.16 |
| Zn | 0.16 | 0.012 | 0.16 | 0.008 | 0.69 | 0.14 | 0.012 |
| Mo | <0.004 | <0.004 | <0.004 | <0.004 | <0.004 | <0.004 | <0.004 |
| Co | 0.001 | 0.001 | 0.001 | 0.001 | 0.001 | 0.001 | 0.001 |
| Ni | 0.014 | 0.012 | 0.01 | 0.014 | 0.011 | 0.013 | 0.02 |
| S | 9.3 | 0.48 | 0.74 | 2.59 | 4.98 | 0.75 | 0.94 |
| As | 625 | 29.4 | 36.2 | 51.2 | 211.4 | 3.2 | 3.3 |
| Sb | 12.81 | 0.32 | 0.86 | 0.42 | 24.16 | 24.6 | 0.18 |
| Bi | 12.8 | 0.3 | 3.04 | 10.66 | 0.57 | 0.07 | 11.73 |
| Hg | 10 | 7 | 8.8 | 7.8 | 28 | 7.9 | 6.8 |

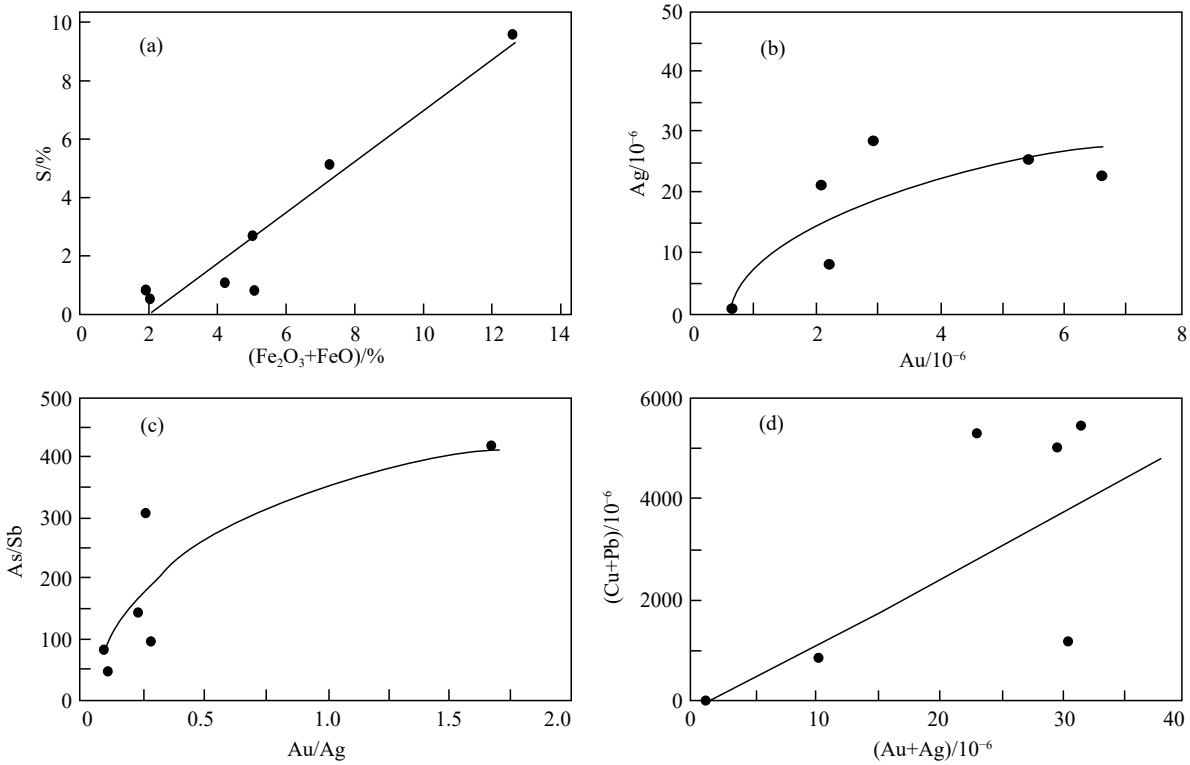


**Fig. 16.** Curves showing relationships of ($Fe_2O_3$+FeO) *vs*. S (a), Au *vs*. Ag (b), Au/Ag *vs*. As/Sb (c), and (Au+Ag) *vs*. (Cu+Pb) (d) of ores.

correlation between Au and Ag (Fig. 16b), with a correlation coefficient of $R$ = 0.7971 ($R^2$ = 0.6354). There is also a positive correlation between Au/Ag and As/Sb, with a correlation coefficient of $R$ = 0.8768 ($R^2$ = 0.7688) (Fig. 16c), which reflects that As-bearing minerals such as arsenopyrites are correlated with gold minerals. There is also a certain correlation between Au+Ag and Cu+Pb (Fig. 16d), with a correlation coefficient of $R$ = 0.9204 ($R^2$ = 0.8471), which reflects the relationships of gold and silver minerals with polymetallic sulfides such as chalcopyrites and galenas. The content of hazardous element As is high, with an average of $137.1\times 10^{-6}$ ($3.2\times10^{-6}$–$625.0\times10^{-6}$).

According to the analytical results of combined samples, the average grades of associated components silver, sulfur, and lead are $6.4\times10^{-6}$ ($0.5\times10^{-6}$–$130.0\times10^{-6}$), 2.78% (0.27%–11.59%), and 0.39% (0.001%–4.40%), respectively, which reach the standards for comprehensive utilization. Meanwhile, the contents of copper and zinc are 0.0222% (0.001% –0.280%) and 0.0799% (0.001% –3.020%), respectively, which are below the standards for comprehensive utilization.

*4.3.4. Textures and structure of ores*

The ore structures mainly include the disseminated structure, followed by stockwork, brecciated, and veinlet structures. The disseminated structure mainly refers to that metal sulfides such as pyrite, chalcopyrite, galena, and sphalerite, which are densely or sparsely distributed in gangue minerals. The stockwork structure refers to that polymetallic sulfides are present in a veinlet form and they fill the fissure network of beresite. The brecciated structure is developed as follows. Some ores are brecciated after fracturing, and they are cemented by quartz or polymetallic sulfides. The veinlet structure (Fig. 18d) refers to that metal sulfides such as pyrite, chalcopyrite, galena, and sphalerite are distributed in altered rocks such as beresite and quartz veins in the form of veinlets with different vein magnitudes.

The ore texture is mainly lepidogranoblastic texture, followed by cataclastic, porphyroclastic, granular, and metasomatic textures. Besides, a small number of ores have emulsion texture. The lepidogranoblastic texture (Fig. 17a) is mainly composed of fine-grained granular minerals (i.e., feldspar, quartz, and calcite) and flaky sericite, all of which are closely arranged. The cataclastic texture (Fig. 17b) is developed from the fracturing of minerals in original rocks, which results in irregularly shaped particles. As for the porphyroclastic texture, the porphyroclasts are angular in shape and randomly distributed, and they suffer metasomatic replacement by quartz and sericite, showing unclear boundaries partially. The granulitic texture consists of angular granular minerals, which suffer metasomatic replacement by sericite and quartz into pseudomorph minerals and show unclear or no boundaries mostly. The metasomatic texture is developed by the interpenetration replacement of early metal sulfide minerals by late metal sulfide minerals, such as the metasomatic replacement of pyrites by arsenopyrites and galena (Fig. 17c) and the interpenetration replacement of quartz by chalcopyrite. As for the emulsion texture, chalcopyrite formed from dissolution is distributed in galena, thus forming the emulsion texture.

*4.3.5. Mineral characteristics of ores*

(i) Metallic minerals

Pyrite. Pyrite is not only the main metal mineral in the

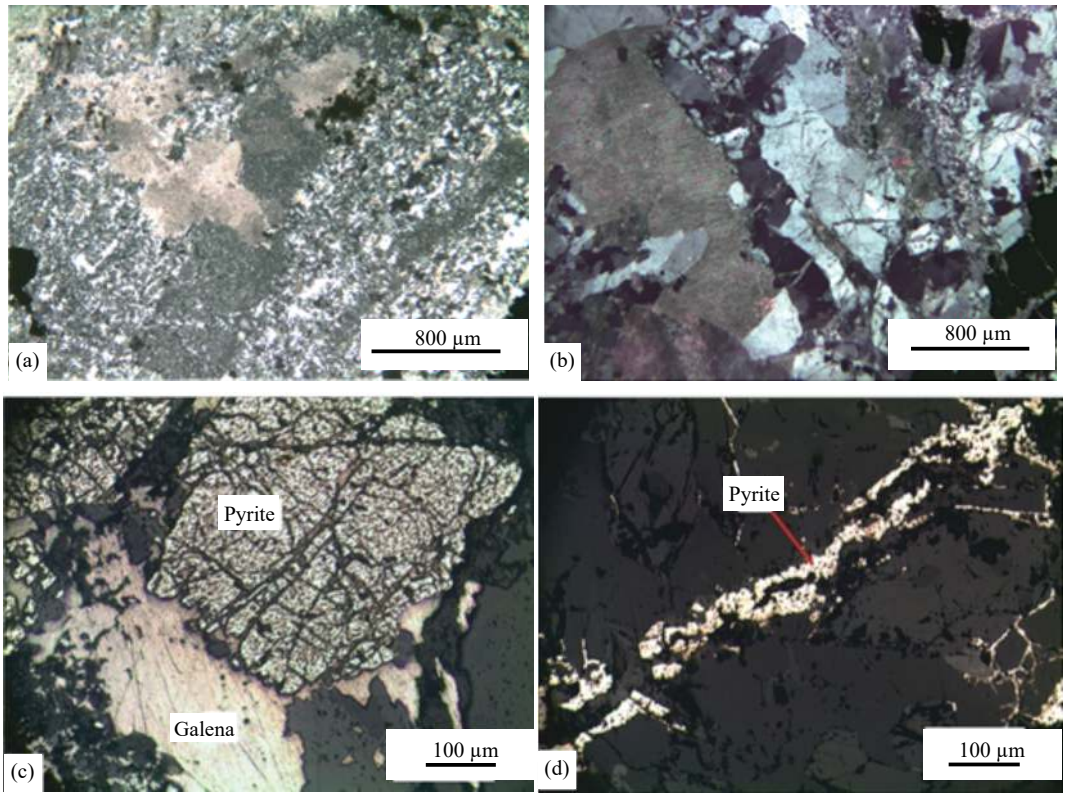


**Fig. 17.** Granular lepidoblastic texture (a), cataclastic texture (b), metasomatic texture (c), and veinlet texture (d) of ores.

ores but also the most important gold-bearing mineral. Its content accounts for more than 90% of the total metallic mineral in the ore. It is xenomorphic-semi-xenomorphic granular and irregularly granular in shape mostly and is distributed in a disseminated or veinlet pattern. Its particle size is mainly 0.01–2 mm. Generally, the gold grade is high in parts rich in fine-grained pyrites. It can be classified into early and late generations. The early generation pyrite is irregularly granulitic, with a small amount of cubic euhedral crystals distributed in quartz and sericite. Owing to later hydrothermal transformation and stress, it is often crushed by extrusion, shows crack development, and is replaced by minerals such as late fine-grained pyrite and arsenopyrite or filled by the late generation of pyrite. Coarse-grained pyrite often contains chalcopyrite and pyrrhotite or is interspersed with galena and chalcopyrite veinlets at the stage of gold-bearing polymetallic sulfides. The late generation fine-grained pyrite, together with chalcopyrite, galena, and tennantite, is distributed in quartz, and the early generation of pyrite in veinlet and stockwork patterns.

Arsenopyrite. Arsenopyrite is one of the major gold-bearing minerals, its content is second only to pyrite, but its content varies greatly in different sections. It generally has automorphic or semi-automorphic granulitic textures, with a grain size of 0.005 –1 mm. It is distributed in non-metallic minerals or early pyrite and metasomatized early pyrite. It tends to contain minerals such as chalcopyrite, pyrrhotite, and galena. Besides, it bears sphalerite inclusions locally.

Galena. Galena mainly has a particle size of 0.005 –0.3 mm. It frequently occurs in pyrite and non-metallic minerals in veinlet and disseminated patterns or produces metasomatized pyrite and tennantite. It commonly coexists with electrums and is distributed in pyrite fissures in a veined pattern. It is also visible that the galena is distributed in a veined pattern alone or together with tennantite and chalcopyrite in the form of xenomorphic crystals.

Sphalerite. Sphalerite is distributed among gangue mineral grains in a xenomorphic granular form or distributed in pyrite fissures in vein aggregates. Besides, a small amount of it, together with chalcopyrite, is distributed among gangue mineral grains in a xenomorphic microparticle shape.

Chalcopyrite. Chalcopyrite is frequently wrapped in pyrite in xenomorphic or irregular forms, fills pyrite fissures or non-metallic mineral fissures in veined or stockwork forms, or coexists with galena. It is commonly dissolved in sphalerite in the form of emulsion. Sometimes, it is distributed in sericitolite alone in a disseminated form.

(ii) Non-metallic minerals

Quartz. Quartz is the most important non-metallic mineral in the Sanshandao gold deposit and can be divided into primary and secondary types. The primary quartz is automorphic or semi-automorphic in shape, with large grain size. It is mostly distributed in the form of aggregates, lumps, and veins-veinlets. The secondary quartz is xenomorphic crystals with a small grain size or occurs in a sub-rounded shape. It often appears in aggregate with sericite. It is of hydrothermal alteration origin, is closely related to gold mineralization, and contains a small amount of intergranular gold.

Sericite. Sericite is also the major non-metallic mineral in

the ore, which is a fine-grained aggregate. It is mainly the product of metasomatic potassium feldspar and plagioclase. Meanwhile, it is a hydrothermal alteration mineral and is frequently associated with fine-grained quartz and disseminated pyrite.

Calcite. Calcite in the ores is scattered in a xenomorphic granular form, with some aggregates distributed in a veined pattern.

(iii) Gold minerals

The gold minerals in the Sanshandao gold deposit include native gold and electrum. Native gold is golden yellow - bright golden yellow, while electrum is light milky yellow with poor polishability. According to the quantitative test results of 139 gold-mineral grains obtained through electron microprobe analysis (EPMA), the chemical components of the gold minerals mainly include Au and Ag, as well as trace elements such as Fe, Cu, Cr, S, Co, Zn, Ni, As, Sb, Bi, Te, and Sb. From shallow to the deep parts of the Sanshandao gold deposit, Au tends to be enriched, Ag tends to be depleted, and all impurity elements tend to be depleted except for Fe, which tends to be enriched (Fig. 18a).

According to the statistics of 39 gold-mineral grains, the gold minerals in the Sanshandao gold deposit mainly include electrum (78.57%), followed by native gold (19.29%), and kustelite (2.14%). Meanwhile, the highest and lowest fineness of the gold minerals is 923 and 372, respectively, with an average of 704. Compared with shallow gold minerals (9.43%), deep gold minerals do not contain kustelite and have a higher content of native gold (29.03%) (Fig. 18b) and a much higher fineness.

According to the statistics of 729 gold-mineral grains, the contents of coarse-grained, medium-grained, fine-grained, micro-fine-sized gold in the deposit are 1.94%, 9.04%, 48.43%, and 44.59%, respectively, and thus the gold minerals are dominated by fine-grained and micro-fine-sized gold. Compared to shallow gold minerals, deep gold minerals have notably increased grain size. In detail, the content of coarse-grained gold increases from 0.91% to 3.15%, the content of medium-grained gold increases from 6.02% to 11.24%, the content of fine-grained gold increases from 42.15% to 54.38%, and the content of micro-fine-sized gold decreases from 50.91% to 31.24% (Fig. 18c).

According to the statistics of 891 gold-mineral grains, gold minerals in the deposit are mainly in a granular form (Fig. 19a), with granular gold minerals accounting for 73.78%, followed by needle-like, foliaceous, and branch-like gold minerals (Fig. 19b), which account for 26.22%. Compared to shallow gold minerals, deep gold minerals have a lower content of granular gold minerals and higher contents of other forms of gold minerals such as branch-like and line-like gold minerals and tend to have diverse morphologies.

According to the statistics of 1329 gold-mineral grains, gold minerals in the deposit can be divided into the crack, intergranular, and inclusion types based on their occurrence states. They are dominated by the former two types, which account for 41.56% and 33.59%, respectively. The gold minerals in shallow parts of the deposit are dominated by the crack type (64.91%) and the intergranular type (20.57%), while those in deep parts of the deposit mainly include the intergranular type (60.22%) and the inclusion type (23.82%)

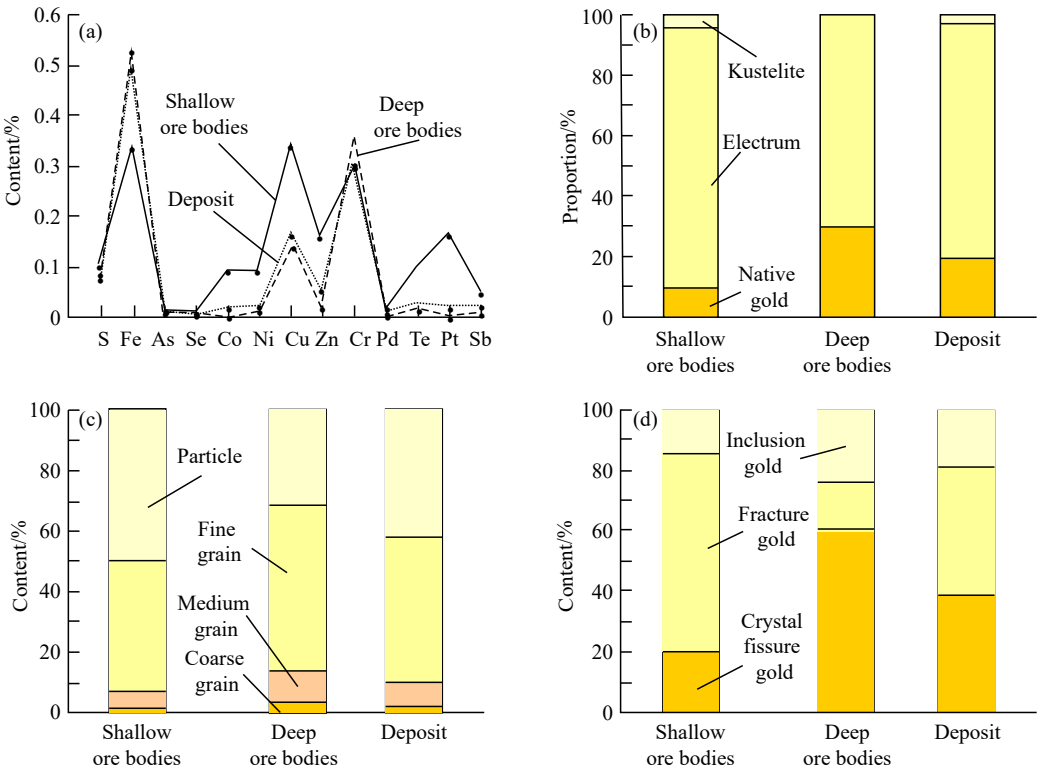


**Fig. 18.** Diagrams showing characteristics of gold minerals in the Sanshandao gold deposit. a–line chart of trace element contents in gold minerals; b–histogram of gold mineral contents; c–histogram of grain size of gold minerals; d–histogram of occurrence state of gold minerals.

(Fig. 18d).

### 4.4. Ore-forming stages

It can be concluded that mineralized altered minerals were formed in four ore-forming stages from the above-mentioned mineral composition of ores, the mineral paragenesis, crosscutting relationships among minerals, and the textures and structures of ore (Table 4).

(i) Sericitolite stage: The early stage of mineralization. Sericitolites were formed from hydrothermal metasomatism at this stage, and the mineral assemblage formed is quartz + sericite.

(ii) Gold-quartz-pyrite-arsenopyrite stage: The middle stage of mineralization. At this stage, fine-grained xenomorphic pyrite and arsenopyrite were formed and replaced or filled early pyrite. It is the main ore-forming stage of gold, at which gold minerals mainly included electrum and native gold wrapped in pyrite or distributed in the pores and fissures of pyrite and arsenopyrite. The mineral assemblage formed at this stage is pyrite + arsenopyrite + pyrrhotite + quartz + electrum + native gold.

(iii) Gold - quartz - polymetallic sulfide stage: The middle-late stage of mineralization. At this stage, polymetallic sulfides were fine-grained in shape and were distributed in veinlet and disseminated forms. Owing to the intense filling and metasomatism among minerals, gold (silver) minerals formed at this stage mainly include electrum and kustelite, which are distributed in the fissures of pyrite, galena, and quartz. Therefore, this stage is the late ore-forming stage of gold. The mineral assemblage formed at this stage is pyrite + chalcopyrite + galena + sphalerite + tennantite + freibergite + quartz + electrum + kustelite.

(iv) Quartz-carbonate stage: The end stage of mineralization. At this stage, carbonate minerals such as quartz and calcites were mostly interspersed with ores in the form of veins, with no gold mineralization occurring.

### 4.5. Resources of the Sanshandao gold deposit

The Sanshandao gold deposit is mainly controlled by intensive drillings. The controlled resources, proven resources, probable mineral reserves, and proven mineral reserves have been explored in different ore blocks individually, with drilling spacing used including (200–240) m× (240–300) m, (100–120) m× (120–160) m, and (20–40) m× (20 –60) m (strike × dip direction). The cumulative resources of gold ores and gold of all ore blocks are

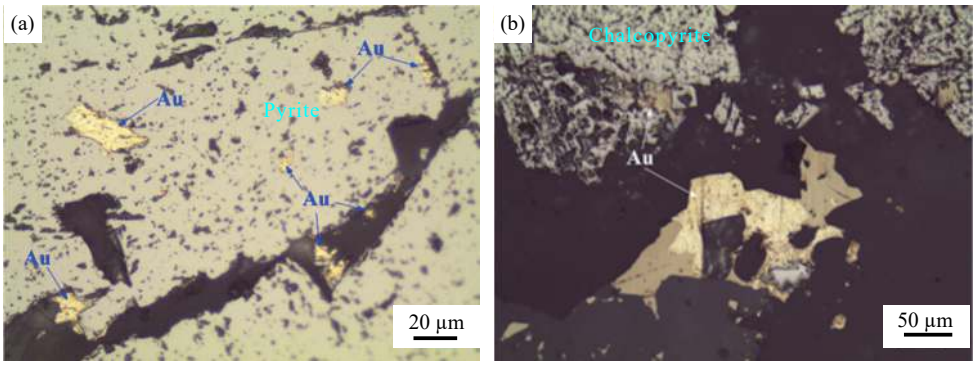


**Fig. 19.** Gold minerals are distributed in pyrite pores and among pyrite and gangue mineral grains in an angular granular or flaky form (a), and chalcopyrites and gangue minerals in a branch-like form (b).

**Table 4. Ore-forming stages and mineral formation sequence of the Sanshandao gold deposit**

| Ore-forming stage | I | II | III | IV |
|---|---|---|---|---|
| Minerals | Sericitolite stage | Gold-quartz-pyrite-arsenopyrite stage | Gold-quartz-polymetallic sulfide stage | Quartz-carbonate stage |
| Quartz | ——— | ——— | ——— | ——— |
| Sericite | ——— | ——— | ——— | |
| K-feldspar | ——— | | | |
| Pyrite | | ——— | ——— | |
| Arsenopyrite | | ——— | | |
| Pyrrhotine | | ——— | | |
| Galena | | | ——— | |
| Sphalerite | | | ——— | |
| Chalcopyrite | | | ——— | |
| Tennantite | | | ——— | |
| Freibergite | | | ——— | |
| Native gold | | ——— | | |
| Electrum | | ——— | ——— | |
| Kustelite | | | ——— | |
| Calcite | | | | ——— |

333.65×10$^6$ t and 1240679 kg, respectively, with an average orebody thickness of 7.93 m and an average ore grade of 3.72 g/t. Among them, 81.50×10$^6$ t of gold ores and 238503 kg of gold are obtained from shallow orebodies, with an average orebody thickness of 8.10 m and an average ore grade of 2.93 g/t. Meanwhile, 252.14×10$^6$ t of gold ores and 1002176 kg of gold are obtained from deep orebodies, with an average orebody thickness of 7.90 m and an average ore grade of 3.98 g/t. The resources ratio, ore grade ratio, and orebody thickness ratio between deep and shallow orebodies are 4.20, 1.36, and 0.97, respectively. Therefore, the scale and enrichment degree of deep orebodies are both greater than those of shallow orebodies.

## 5. Discussion

### 5.1. Metallogenic epoch

There were many disputes about the metallogenic epoch of the Jiaodong gold deposits in the past. Early researchers thought that the Jiaodong gold deposits were formed during the Archean or the Proterozoic. Later, multi-stage mineralization was proposed, that is, Archean, Proterozoic, and the Mesozoic were all the important metallogenic epochs (Li SX et al., 2007). In addition, some studies held that there are three metallogenic events at 150 Ma, 120–110 Ma, and 100 –110 Ma (Ding ZJ et al., 2015). At present, most researchers agree that the Jiaodong gold deposits were mainly formed in the Early Cretaceous and concentrated in a short period of about 120 Ma (Yang LQ et al., 2014; Zhu RX et al., 2015; Fan HR et al., 2016).

According to the test results of the Sanshandao gold deposit, the sericite Rb-Sr isochron age and the sericite $^{40}$Ar-$^{39}$Ar isochron age are 117.6 ± 3.0 Ma (Hu FF et al., 2013) and 118.56 ± 1.37 Ma (Yang ZY et al., 2020), respectively. As revealed by the test results of the Cangshang gold deposit in the southern part of the Sanshandao fault, the sericite $^{40}$Ar-$^{39}$Ar isochron age is 121.1 ± 0.5 Ma (Zhang XO et al., 2003), and the fluid inclusions Rb-Sr isochron age is 113.5 ± 0.6 Ma (Chen YJ et al., 2004).

In recent years, Deng J et al. (2020b) have selected hydrothermal monazites with a symbiotic relationship with natural gold, pyrite, and sericite to carry out in-situ U-Pb dating. The SHRIMP U-Pb ages of the Jiaojia and Linglong gold deposits in the western part of the Jiaodong Peninsula are 121.8 ± 3.6 Ma and 120.0 ± 4.6 Ma, respectively, and the LA-ICP-MS U-Pb ages are 119.8 ± 2.1 Ma and 119.1 ± 1.4 Ma, respectively. The LA-ICP-MS monazite U-Pb ages dated by other researchers are 120.5 ± 1.7 Ma (the Daliuhang gold deposit in Penglai City), 120.0 ± 1.4 Ma (the Xiadian gold deposit in Zhaoyuan City), and 120.0 ± 3.1 Ma (the Hushan gold deposit in Qixia City) (Ma WD et al., 2017; Yang KF et al., 2018; Feng K et al., 2020). All these dated ages fall in the range of 121.8–119.1 Ma.

The $^{40}$Ar-$^{39}$Ar ages of the Sanshandao and Cangshang gold deposits are consistent with the monazite U-Pb ages of the gold deposits in the western Jiaodong Peninsula. This paper holds that the $^{40}$Ar-$^{39}$Ar age represents the main metallogenic age of the Sanshandao gold deposit, that is, the deposit was formed at about 120 Ma. The Rb-Sr isochron ages are consistent with the early age of Weideshan-type granites and the isotopic ages of silver and nonferrous metal deposits in the Jiaodong Peninsula (118–111 Ma; Song MC et al., 2017), which indicates the time of magmatic-metallogenic events or the age of gold - quartz - polymetallic sulfide stage after the main gold ore-forming stage of the gold deposit.

### 5.2. Sources of ore-forming fluids and minerals

#### 5.2.1. Nature of ore-forming fluids

Many studies have been conducted on the ore-forming fluids in the Sanshandao gold deposit (Guo CY, 2009; Jiang XH et al., 2011; Deng J et al., 2015a; Wen BJ et al., 2016; Liu YZ et al., 2019), obtaining the following understanding. The ore-forming fluids belong to a medium-low-temperature, low-salinity, and reducing $H_2O$-$CO_2$-NaCl ± $CH_4$ hydrothermal system. The inclusions are generally small, mainly ranging from 3μm to10 μm. They are mainly of three types, pure $CO_2$, $CO_2$-$H_2O$, and pure water inclusions. Besides, multiphase fluid inclusions containing daughter minerals such as NaCl are also visible. The $V_{CO2}$ + $L_{CO2}$ inclusions include $V_{CO2}$ + $L_{H2O}$ two-phase and $V_{CO2}$ + $L_{CO2}$ + $L_{H2O}$ three-phase inclusions at room temperature. According to the proportion of vapor phase and liquid phase, the two-phase inclusions can be divided into vapor-rich [V/(V+L)> 50%] and liquid-rich [L/(V+L)> 50%] subtypes. The pure water inclusions consist of the liquid-phase and vapor-phase types, with the latter accounting for 5%–30% of the total pure water inclusions. The fluid inclusions formed during the early mineralization contain vapor-phase components $CO_2$ and $H_2O$, with no $CH_4$ and $N_2$ being detected. In comparison, rich $CH_4$ (Liu YZ et al., 2019) and the presence of $N_2$ (Jiang XH et al., 2011) have been detected in the $CO_2$-$H_2O$ inclusions formed in the main ore-forming stage. In the liquid phase, the cations mainly include $Na^+$ and $K^+$, followed by $Mg^{2+}$ and $Ca^{2+}$, and the anions mainly include $SO_4^{2-}$ and $Cl^-$, as well as low content of $F^-$ (Guo CY, 2009).

The homogenization temperatures of the fluid inclusions fall in the range of 101°C –400°C, and those at the first, second-third, and fourth ore-forming stages are 239°C–400°C, 207°C –336°C, and 101°C –269°C, respectively. The fluid pressure and salinity at the main ore-forming stage were about 90–175 MPa and 2.06%–17.57% $NaCl_{eqv}$, respectively. The fluid density is about 0.61–1.11 g/cm$^3$ (Wen BJ et al., 2016; Liu YZ et al., 2019). From the early to the late ore-forming stage, the temperature and pressure significantly dropped, while the salinity was relatively higher at the main ore-forming stage (Yang LQ et al., 2014), indicating that the decrease in temperature and pressure is one reason for the gold mineralization.

#### 5.2.2. Sources of ore-forming fluids

The hydrogen-oxygen isotopic components of the gold deposit are widely distributed (Table 5). Some samples fall in

**Table 5. Hydrogen and oxygen isotopic compositions of fluid inclusions in the Sanshandao gold deposit.**

| Ore block | Mineral | $\delta^{18}O_{V\text{-}SMOW}$ /‰ | $\delta^{18}O_{H2O\text{-}SMOW}$ /‰ | Homogenization temperature/°C | $\delta D_{v\text{-}SMOW}$/‰ | Data source |
|---|---|---|---|---|---|---|
| Sanshandao | Quartz | 13.3, 13.6, 13.9, 12.6、13.5, 13.5, 12.8, 12.8, 13.5, 13.9 | 5.3, 5.6, 7.9, 1.9, 4.3, 1.8, 2.7, 6.1, 7.4, 7.8 | 272, 272, 328, 217, 245, 200, 227, 306, 322, 323 | −100, −95, −85, −84, −89, −116, −94, −85, −79, −86 | Guo CY, 2009 |
| | | 8.1, 11.8, 11.9, 10.7, 9.9, 8.9, 9.1 | 3.1, 2.8, 2.9, 5.1, 7.5, 6.5, 4.1 | 282, 182, 178, 266, 327, 320, 283 | −58.3, −60.4, −77.6, −59, −61.7, −53.6, −66 | Jiang XH et al., 2011 |
| | | 14.7, 14.2, 15.1, 14.5, 12.5 | 5.7, 5.2, 6.1, 5.5, 3.5 | 250, 250, 250, 250, 250 | −72, −71, −39, −72, −92 | Wang YW, 1993 |
| | | 12.5, 12.8 | 0.96, 1.26 | | −92, −72 | Luo ZK and Miao LC, 2001 |
| | Sericite | 10.7, 11.7, 12.0, 9.7, 10.9, 11.0 | 7.55, 8.55, 8.85, 6.55, 7.75, 7.85 | 250, 250, 250, 250, 250, 250 | −52, −48, −52, −53, −50, −67 | Mao JW et al., 2008 |
| | Pyrite | | −12.6, −11.8, −9.6, −6, −7.9, −11.2, −10.9 | | −111, −103, −119, −86, −121, −105, −110 | Guo CY, 2009 |
| Xinli | Quartz | 14.0, 13.7, 13.5, 13.1, 14.7, 15.2, 13.4, 9.9, 14.1, 10.4, 11.0 | 7.1, 6.8, 7.5, 2.8, 4.3, 8.7, 5.1, 2.3, 6.5, 0.7, 4.1 | 300, 300, 326, 224, 222, 311, 265, 280, 282, 234, 301 | −95, −91, −91, −101, −83, −90, −91, −98, −88, −76, −80 | |
| | Pyrite | | −5.8, −8.1, −14.7, −8.6, −11.8 | | −121, −118, −129, −90, −118 | |

the zones of primary magmatic water, metamorphic water, and typical orogenic gold deposits. In comparison, large numbers of the samples fall between primary magma water (or primary mantle water and metamorphic water) and meteoric precipitation and between the mixed trend of chemical precipitation water and that of organic water (Fig. 20). The fluid inclusions in different minerals greatly differ in hydrogen-oxygen isotopic characteristics. In detail, the hydrogen-oxygen isotopic compositions in fluid inclusions of quartz mainly fall near zones of primary magmatic water and primary mantle water, those of sericites mainly fall in the zone representing metamorphic water, and those of pyrites mainly fall near the Mesozoic meteoric water and formation water in the Jiaodong Peninsula. Quartz existed throughout the pre-ore and the ore-forming stage, sericites were formed from mineralized alteration at the ore-forming stage, and pyrites were formed at the main ore-forming stage and thereafter. Given these, it is considered that the ore-forming fluids before gold mineralization were dominated by primary mantle water or magmatic water, and metamorphic water appeared in the early stage of gold mineralization. With the progress of mineralization, meteoric water entered the fluids, and the late ore-forming fluids were dominated by meteoric water.

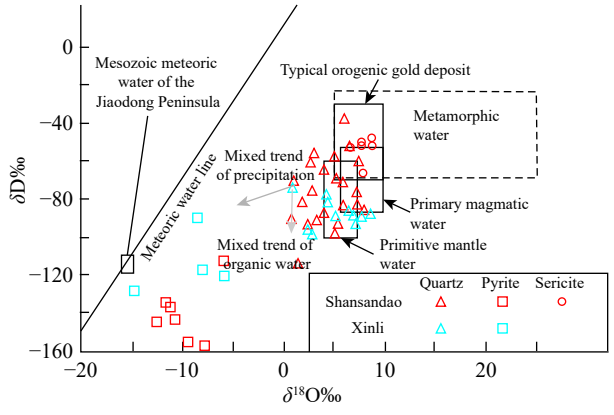


**Fig. 20.** $\delta$D *vs.* $\delta^{18}$O diagram of ore-forming fluids in the Sanshandao gold deposit (after Taylor HP, 1974; Sheppard SMF,1986 for the base map).

The $^{3}He/^{4}He$ ratio of fluid inclusions in pyrite is 0.043–2.94 Ra (Han ZY et al., 2019; Wen BJ et al., 2016), which is between the crustal value (0.01–0.05 Ra) and the mantle value (6–9 Ra) (Stuart FM, 1995; Burnard PG, 1999), indicating the characteristics of crust-mantle mixing composition. Mantle-derived He content was calculated to be 0.37%–2.51% (Han ZY et al., 2019) using the formula:

mantle-derived He (%) = [(R–Rc)/(Rm–Rc)]×100,

where Rc end-member value = $2\times10^{-8}$ and Rm end-member value = $1.1\times10^{-5}$ (Han ZY et al., 2019).

This indicates that He in the Sanshandao gold deposit mainly comes from the crust and a small amount of mantle source. Meanwhile, the $^{40}Ar/^{36}Ar$ values range from 488.00 to 5926.44, and the He-Ar isotopic composition of the fluids falls between the crust source and mantle source areas on the relevant diagrams (Han ZY et al., 2019; Wen BJ et al., 2016). As indicated by these He-Ar isotopic characteristics, the ore-forming fluids were mainly sourced from the crust and were mixed with varying volumes of deep mantle-derived fluids, and then meteoric water entered the ore-forming fluids during the rise of the fluids.

The carbon isotopic data of calcites, siderites, ankerites, and quartz formed in the late ore-forming stage show that the $\delta^{13}C_{PDB}$ values fall in the range of−6.6‰ – −1.9‰ (Table 6), which is close to the $\delta^{13}C$ values of igneous/magmatic system (−30‰ – −3‰) and the $\delta^{13}C$ values of carbon reservoirs of the mantle (−7‰ – −5‰; Hoefs J, 1997). This indicates that the carbon in the ore-forming fluids comes from the magmatic system or the mantle.

### *5.2.3. Sources of ore-forming materials*

(i) Sulfur isotopes. The Sanshandao gold deposit is enriched in $\delta^{34}S$, with the $\delta^{34}S$ values falling in the range from +7.1‰ – +12.8‰ (from +10.1‰ to +12.8‰ mostly; Table 7),

**Table 6. Carbon isotopic analysis results of fluid inclusions in the Sanshandao gold deposit.**

| Ore block | minerals | $\delta^{13}C_{PDB}$/‰ | $\delta^{18}O_{PDB}$/‰ | $\delta^{18}O_{SMOW}$/‰ | Data source |
|---|---|---|---|---|---|
| Xinli | quartz | −3.7, −4.2, −3.1, −2.9 | | | Guo CY, 2009 |
| Sanshandao | quartz | −6.6, −2.1, −1.9, −2.1, −2.4, 3.4 | | | |
| | ankerites | −5.9 | | 13.8 | Jiang XH et al., 2011 |
| | calcites | −6.6 | | 12.4 | |
| Sea-area | siderites | −5.0, −4.5, −5.6, −5.1, −5.8, −4.9 | −15.8, −18.2, −15.3, −16.5, −15.4, −16.0 | 14.6, 12.1, 15.1, 13.9, 15.1, 14.4 | Ding ZJ et al., 2018① |

**Table 7. $\delta^{34}S$ value of the Sanshandao gold deposit.**

| Ore block | Mineral | Analytical result of $\delta^{34}S_{V\text{-}CDT}$ /‰ | Data source |
|---|---|---|---|
| Sanshandao | Pyrite | 8.5, 10.5, 8.4, 10.4, 9.3, 9.2, 8 | Jiang XH et al., 2011 |
| | | 12.0, 12.0, 11.7, 11.9, 11.5 | Mao JW et al., 2008 |
| | | 12.6, 12.5, 12.1, 11.8, 11.6, 11.1, 11.2 | Li SX et al., 2007 |
| | Chalcopyrite | 11.5, 10.1, 10.7, 10.5 | Deng J et al., 2010 |
| | Galena | 7.9 | |
| | Sphalerite | 11.4, 11.1 | |
| Sea-area | Pyrite | 9.6, 12.8, 10.3, 12.6, 11.2, 11.2, 8.3, 10.1, 7.1, 12.1, 9.7, 12.3, 8.5, 9.9, 11.3 | Ding ZJ et al., 2018 (refer to Table 6) |
| Xinli | Pyrite | 9.87, 10.85, 11.51 | Wang JT et al., 2005 |

which deviates from meteorite sulfur positively, and the sulfur isotopes are highly homogeneous. The $\delta^{34}S$ values are in the order of pyrites < sphalerites < galenas in the deposit, indicating that sulfur isotopic fractionation roughly reached equilibrium during the mineralization. The $\delta^{34}S$ values of the Sanshandao gold deposit overlap with those of relevant geological bodies to a high extent (Fig. 21), indicating that the deposit inherited sulfur isotopes from the relevant geological bodies (Yang LQ et al., 2014). Related geological bodies include Early Precambrian metamorphic rocks, Guojialing-type granites, intermediate-basic vein rocks, Linglong-type granites, and Weideshan-type granites, of which the $\delta^{34}S$ values gradually increase. According to statistics, the peak $\delta^{34}S$ value of the Sanshandao gold deposit is higher than the average $\delta^{34}S$ value of relevant geological bodies and is closer to the Jurassic crust-derived Luanjiahe granitic pluton (belonging to Linglong-type granite), reflecting that the crust-derived materials contribute significantly to sulfur sources.

(ii) Lead isotopes. The Pb isotopic compositions of five samples from the Sanshandao gold deposit slightly vary, with the $^{206}Pb/^{204}Pb$, $^{207}Pb/^{204}Pb$, and $^{208}Pb/^{204}Pb$ ratios of 17.167 –17.464, 15.235 –15.766, and 37.269 –38.763, respectively (Table 8). The characteristic values of source areas of Pb isotopes in the deposit are as follows. The $\mu$ value (7.5) is lower than the normal $\mu$ value of the crust (9.58) and close to the $\mu$ value of the mantle (7.3 –8.0). The $\omega$ value (33.32) is lower than that of the crust (36.50), and the Th/U value (4.38) is higher than the normal Th/U value of the crust (3.8), indicating that the ore-forming materials are partially mantle-derived. In the tectonic setting discrimination diagram (Fig. 22) proposed by Zartman RE and Dou BR (1981), the samples fall into the lower crust and are consistent with the falling scope of Pb from the Jiaodong gold deposits, both indicating the characteristics of Pb isotope in the lower crust. Overall, Pb in the Sanshandao gold deposit was mainly sourced from the lower crust, with a small amount originating from the mantle.

(iii) Strontium isotopes. The initial $^{87}Sr/^{86}Sr$ ratio of calcites in the Sanshandao gold deposit is 0.710657–0.711542 (Deng J et al., 2015a), which is higher than 0.710 and overlaps with the $^{87}Sr/^{86}Sr$ ratio ranges of Linglong-type granites, Guojialing-type granites, and mafic dykes formed during the ore-forming stage to a high extent (Yang LQ et al., 2014). This indicates crust-derived characteristics. Therefore, the ore-forming materials may directly come from Linglong and Guojialing-type granites, and some ore-forming materials may be provided by mafic dykes or their magmatic source areas during the metallogenic period.

### *5.3. Ore-controlling mechanisms of faults and metallogenic model*

#### *5.3.1. The control of faults on gold mineralization*

(i) The shielding effect of fault gouges on gold mineralization

The Sanshandao gold deposit has high-number and large-scale orebodies, most of which occur on the footwall of the main fracture plane of the Sanshandao fault and are distributed in parallel to the main fracture plane. The main orebodies generally occur in the beresitized cataclasite and beresitized granitic cataclasite near the main fracture plane, while the secondary orebodies occur in the beresitized granitic cataclasites and beresitized granite that are slightly far away from the main fracture plane. In addition, the steep quartz-vein-type orebodies that obliquely cross the main fracture plane and the main orebodies occur in the weakly altered

①Ding ZJ, Zhang JJ, Bo JW, Li GH, Wei XF. 2018. Research report on structural type and ore-controlling regularity of the shallow-sea area of Sanshandao fault zone, Shandong Province. Yantai, Shandong Provincial No.3 Exploration Institute of Geology and Mineral Resources.

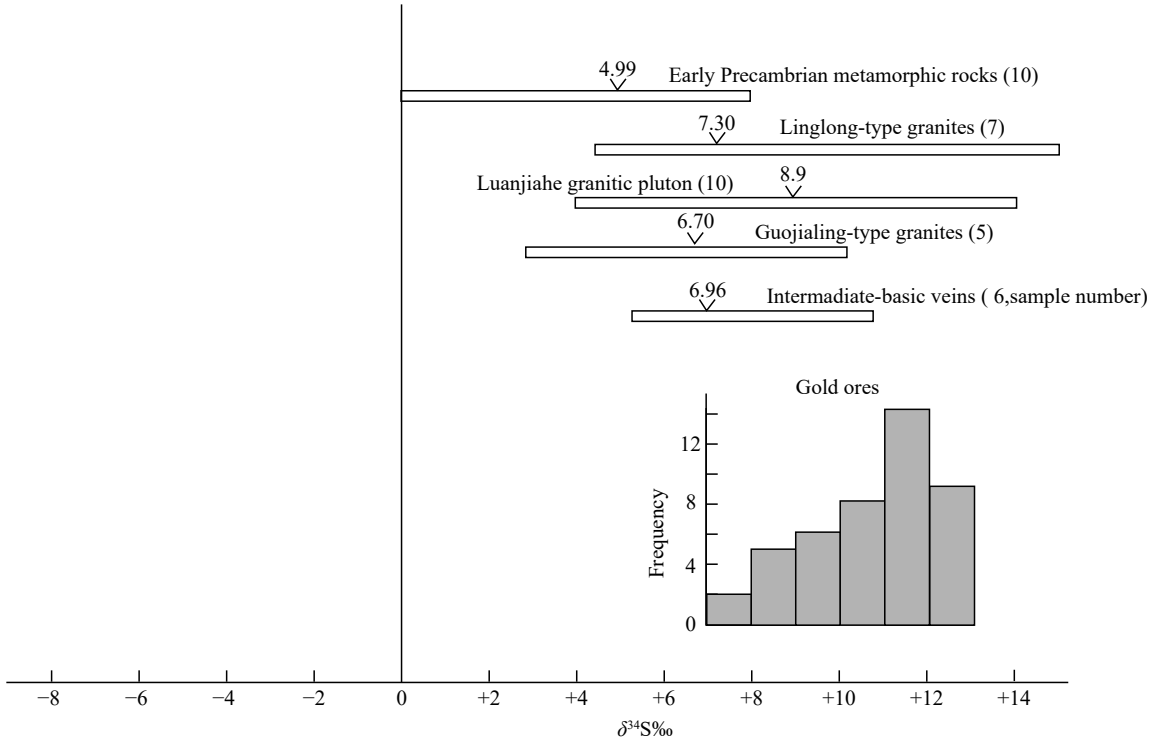


**Fig. 21.** Sulfur isotopic compositions of ores and geological bodies related to gold mineralization in the Sanshandao gold deposit (after Li JJ, 2006 for geological bodies related to gold mineralization).

**Table 8. Pb isotopic components of ores in the Sanshandao gold deposit (after Wang YW, 1988; Li SX et al., 2007).**

| No. | $^{206}Pb/^{204}Pb$ | $^{207}Pb/^{204}Pb$ | $^{208}Pb/^{204}Pb$ | $\mu$ | $\omega$ | Th/U |
|---|---|---|---|---|---|---|
| 1 | 17.353 | 15.518 | 38.072 | 7.55 | 33.32 | 4.38 |
| 2 | 17.191 | 15.473 | 37.867 | | | |
| 3 | 17.290 | 15.400 | 37.740 | | | |
| 4 | 17.464 | 15.766 | 38.763 | | | |
| 5 | 17.167 | 15.235 | 37.269 | | | |
| Avg. | 17.293 | 15.478 | 37.942 | | | |

granites far away from the main fracture plane. Although sericitized alteration occurs on the hanging wall of the fault, the pyritization on the hanging wall is noticeably weaker than that on the footwall, and only small-scale gold orebodies are locally visible. Fault gouges with a thickness of about 0.05–0.50 m occur continuously and stably along the main fracture plane of the fault. They are mainly composed of clay minerals such as kaolinite and montmorillonite, with no gold mineralization and alteration. The enrichment degree of gold mineralization is positively correlated with the thickness of the fault gouges, and the gold grade tends to be high in parts with thick fault gouges (Guo CY, 2009). The fact that sericitized alteration occurs on both the hanging wall and the footwalls of the fault while gold orebodies mainly occur on the footwall implies that the fault gouges imposed no impact at the sericitolite stage in the early ore-forming stage but blocked and shielded the migration of ore-bearing fluid in the main ore-forming stage. The grayish-black fault gouges in the Jiaojia fault were previously dated to be 131.05–123.53 Ma (Song MC et al., 2010a), which is slightly older than the gold mineralization, also proving that the gold mineralization has

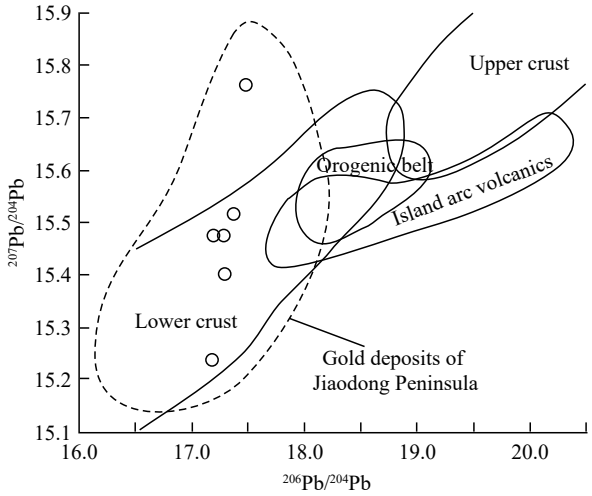


**Fig. 22.** Tectonic setting discrimination diagram of Pb isotopes in ores in the Sanshandao gold deposit (after Zartman RE and Dou BR, 1981). Note: the reference ranges of Jiaodong gold deposits are from Yang LQ et al., 2014.

not penetrated upward through fault gouges. The reasons for fault gouges controlling the distribution of the Sanshandao gold deposit are as follows. On one hand, the clay minerals dominant in the fault gouges have a dense structure and poor permeability; thus it is difficult for ore-bearing fluid to penetrate the fault gouge zone. On the other hand, as the major component of the hanging wall of the fault, the Early Precambrian metamorphic rock series has experienced long-term deformation-induced reformation, weathering and denudation, and penetration of meteoric water, which combined with a low-temperature form a circulation system

of the oxidizing aqueous solution. Meanwhile, the Mesozoic granites that constitute the footwall of the fault have an age close to the gold mineralization and have a high temperature, forming a circulation system of reducing aqueous solution. The junctions of the above two aqueous solution circulation systems serve as parts favorable for the accumulation and precipitation of ore-bearing fluids.

(ii) The effect of the changes in fault occurrence on gold mineralization

The Jiaodong gold deposits are controlled by faults. Massive studies were previously conducted focusing on the relationships between faults and gold mineralization and the ore-controlling regularity of faults, obtaining some understanding such as gold orebodies occurring at the turning parts of faults and fault junctions, pitching regularity of the orebodies along faults, and gold deposits controlling at broom-like structures and the composite parts of NNE-NE-trending faults and EW-trending basement structures, as well as noticing that the Cangshang and Xinli gold deposits in the Sanshandao fault zone both occur in the parts of the NNE-trending fault turning to NE-trending fault and its NE-trending section, respectively (Li HJ, 2002; Li SX et al., 2004; Song MC et al., 2015b; Deng J et al., 2019; Wang SR et al., 2020). Based on deep prospecting results, researchers have proposed some important new understanding of the relationships between the Sanshandao fault and gold deposits, as stated below. It is considered that gold orebodies are mainly enriched in the fault parts with a transition between steep-gentle dip angles and fault sections with gentle dip angles, thus forming a stepped distribution pattern (Song MC et al., 2015b). In the Xinli ore block, the changes in the strike and dip angle of faults control the fluid accumulation and the formation of ore-rich pillars (Yang L et al., 2018). In the Sanshandao ore block, the deposit is distributed in the parts where the Sanshandao fault turns from the NE trending to the NEE-trending, ore zones become wider and gentler and pitch northward, and high-grade ore zones occur in the fault parts with gentle dip angles (Zhang L et al., 2020a).

As stated above, the shallow and deep orebody groups in the sea-area ore block are both distributed in fault sections with a gentle dip angle, thus forming a stepped metallogenic model. The first orebody step in the shallow part is at an elevation of above −800 m, where the dip angle of orebodies is 25°–50°. The second orebody step in the deep part lies at an elevation of below −1000 m, where the dip angle of orebodies is 35° –40°. Weak mineralization or even no ore occurs between the first and second steps, where the dip angle of the Sanshandao fault is 75°–85° and the vertical distance is about 200 m. For the deep orebody-rich parts in the sea-area ore block, fault dip angles and the values of grade × thickness of orebodies were extracted every 20 m along the sections of the dip direction and strike of the ore-controlling fault (Fig. 14) according to the established three-dimensional geological model of deposits. Based on these data, the relationships of the fault dip angle versus the value of grade × thickness of orebodies were plotted (Fig. 23). As shown in the diagram showing the relationship obtained based on the section along the dip direction of the fault (Fig. 23a), the fault dip angle roughly changes in five sections from shallow to deep parts, and the details are as follows. Section I is between the seabed and an elevation of −420 m, where the dip angle sharply changes from low to high and the slope increases from 36.24° to 61.96°, with a slope difference of 25.72°. In this section, the value of grade × thickness of orebodies ranges from 1.00 m g/t to 32.66 m g/t, indicating medium ore-discovery effects. Section II is between −420 m and an −800 m in elevation. It is a structurally steep section with a slope of 70.75°–80.78°, and it is an ore-free section. Section III is between −800 m and −1000 m in elevation, where the slope decreases from 77.23° to 42.47°, with a difference of 34.76°. Therefore, it is a section with a steep-to-gentle transition of the fault dip angle. As the slope gradually decreases, the value of grade× thickness of orebodies gradually increases, and it is up to 305.65 m g/t when the slope decreases to the minimum. Section IV is between −1000 m and −1800 m in elevation. In this section, the slope is 39.47°–52.86°, and it is low overall and slightly fluctuates. Therefore, this section is gentle and is also an orebody-rich section, where the value of grade × thickness of orebodies is 79.72–552.28 m g/t, with an average of 322.48 m g/t. Section V is between −1800 m and −1960 m in elevation, where the slope tends to significantly increase and reaches 51.31° at an elevation of −1960 m. It is an ore-

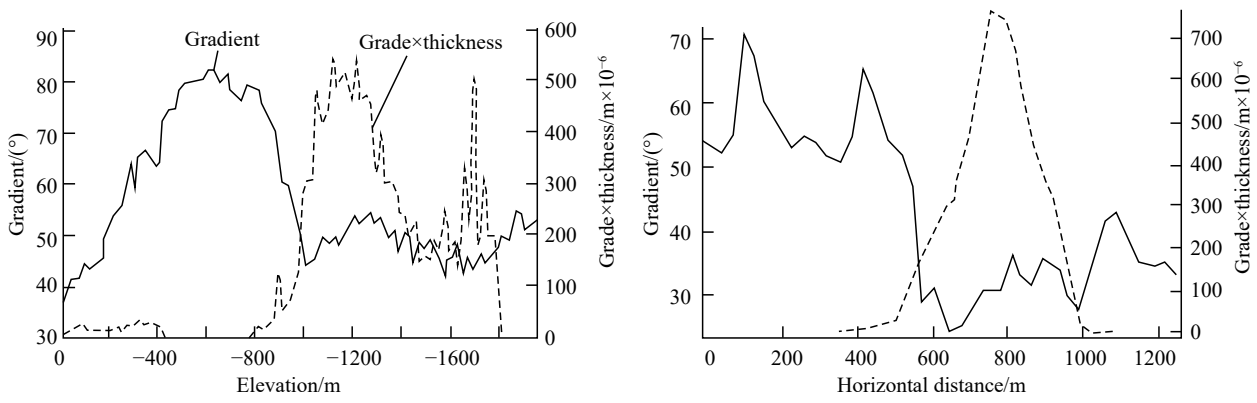


**Fig. 23.** Diagrams showing the relationships between the fault dip angle *vs.* the value of grade×thickness of orebodies along with the fault dip direction (a) and along the fault strike (b) in sea-area ore block of the Sanshandao gold deposit.

free section. On the relationship diagram obtained based on the section along the fault strike (Fig. 23b), the fault dip angle also noticeably changes, and areas with high values of grade × thickness of orebodies coincide with the areas with a distinct steep-to-gentle transition of the fault dip angle. The above sections along the two directions show that the changes in the fault dip angle have noticeable impacts on mineralization, and the enrichment degree of gold mineralization is high in the sections with a sharp steep-to-gentle transition of the fault dip angle. This relationship between the Sanshandao fault and orebodies strongly supports the stepped distribution model of deep gold orebodies (Song MC et al., 2012).

The controlling effect of the changes in the fault dip angle on the gold mineralization is related to the pressure change in the process of fluid flow. The research shows that water/rock reactions, fluid immiscibility, and fluid mixing are the main mechanisms leading to gold precipitation in the Jiaodong gold deposits (Zhang L et al., 2020b), and pressure fluctuation is the main reason for fluid immiscibility (Yang LQ et al., 2016). When fluids flow through a fault section with a sharp change of fault dip angle, the pressure fluctuation of the fluids increases significantly, resulting in fluid immiscibility, which provides favorable conditions for gold precipitation. When migrating in a fault section with a steep dip angle, ore-forming fluids migrate rapidly from the deep area with high stress to the shallow area with low stress. In this case, the fluids are not liable to be deposited and mineralized. When the fluids flow through a fault section with a steep-to-gentle transition of the fault dip angle and then migrate toward a fault section with a gentle fault dip angle, the pressure sharply drops, the flow rate significantly reduces. In this case, fluid immiscibility tends to occur, resulting in gold precipitation and mineralization. Therefore, gold mineralization mainly occurs in fault sections with a changing or relatively gentle fault dip angle.

*5.3.2. Tectonic setting of gold mineralization*

The massive gold mineralization in the Jiaodong Peninsula occurred under the background of the North China Craton destruction and lithospheric thinning, which is closely related to the spatio-temporal relationship of extensional structures (Qiu YM et al., 2002; Mao JW et al., 2008; Deng J et al., 2015b; Li L et al., 2015; Song MC et al., 2015b; Yang QY and Santosh M, 2015). Since the Late Mesozoic, the eastern part of the North China Craton has experienced large-scale lithospheric destruction characterized by lithospheric thinning, forming large-scale extensional structures represented by faulted basins, detachment faults, and metamorphic core complex (Zhang YQ et al., 2004; Ratschbacher et al., 2000; Liu JL et al., 2006; Wang T et al., 2007). Late Mesozoic extensional structures are widely developed in the Jiaodong Peninsula. Among them, the Jiaolai Basin is an extensional superimposed basin featuring northern fault and southern stratigraphic overlap between the North China Craton and the Sulu Orogenic Belt. A very thick volcanic sedimentary rock series were deposited in the basin. Among them, the volcanic interbeds in the Laiyang Group in the lower part of the basin yield isotopic ages of 129.7 ± 1.7 Ma and 129.4 ± 2.3 Ma (Zhang YQ et al., 2008), the volcanic rocks in the Qingshan Group in the central part of the basin yield an isotopic age range from 123.6 ± 3.1 Ma to 98 ± 1 Ma (Qiu JS et al., 2001; Ling WL et al., 2007; Zhang YQ et al.,2008; Liu S et al., 2009; Kuang YS et al., 2012), and the volcanic interbeds in the Wangshi Group in the upper part of the basin yield an isotopic age of 73.2 ± 0.3 Ma (Yan J et al., 2005). In addition to the parallel unconformity between the Qingshan and Laiyang groups, and the angular unconformity between the Wangshi and Qingshan groups, the basin was in a continuous extensional state during 130–73 Ma. Latitic volcanic rocks and bimodal volcanic rocks are developed in the Qingshan Group, indicating a strong crustal extension process. Meanwhile, the geochemical characteristics of these volcanic rocks indicate that the rocks were formed in a back-arc extensional active continental margin environment (Liu S et al., 2009; Kuang YS et al., 2012). Metamorphic core complexes in the Jiaodong Peninsula include Linglong, Queshan, and Kunyushan (Yang JZ et al., 2000; Charles et al., 2011), of which the cores consist of Jurassic Linglong-type granites, the inside contains a small amount of Guojialing or Weideshan-type granites, and the edges are surrounded by Early Precambrian metamorphic rocks or Mesozoic sedimentary strata. The detachment faults in the Jiaodong Peninsula include boundary faults of metamorphic core complexes, Mesozoic basin-margin faults, and late bedding slip faults in the Early Precambrian basement. As revealed by the S-wave velocity structure obtained through the ambient noise tomography of short-period dense seismic array profiles (Yu GP et al., 2020), the faults in the northwest Jiaodong Peninsular all show low dip angles and, meanwhile, the basement/shallow seismic discontinuities with high-velocity anomalies on the hanging walls and footwalls of the faults represented by the Sanshandao and Zhaoping faults with a dip direction of SE show remarkable dislocation. All these indicate that the faults in the northwest Jiaodong Peninsular are large-scale extensional detachment faults. Charles et al. (2013) proposed that the extensional structural characteristics in the Jiaodong Peninsular are consistent with the wide rift model.

The mineralization of the Jiaodong gold deposits exactly occurs during the above-mentioned extensional tectonic activity, and the metallogenic epoch is consistent with the isotopic age of the volcanic rocks in the Qingshan Group at the peak of the extensional tectonic activity. All these indicate that the Jiaodong gold deposits were formed in an extensional tectonic setting. The study of extensional structures in East China and its adjacent areas shows that the extensional structures evolved in two stages, namely 140 –125 Ma, at which the original extensional detachment structures were initially formed in the middle-lower crust, and 125–110 Ma, at which the detachment structures experienced rapid uplifting and exhumation (Yang Q et al., 2019). The extensional activity mainly resulted from the roll-back of the subducted

paleo-Pacific plate, which led to the collapse of the early thickened crust (Davis GA et al., 2001; Yang JH et al., 2007) and also induced back-arc tension or intraplate extension. Therefore, it can be inferred that the Jiaodong gold deposits were formed during the quick uplift and exhumation of detachment structures, which is attributable to the back-arc tension or intraplate extension induced by the roll-back of the paleo-Pacific plate.

The Jiaodong-type gold deposits that were formed in an extensional tectonic setting are different from internationally known gold deposits. Some researchers classified the Jiaodong gold deposits as orogenic gold deposits (Zhou TH and Lu G, 2000; Qiu YM et al., 2002; Goldfarb RJ et al., 2001; Chen YJ et al., 2004), while others pointed out that the Jiaodong gold deposits are distinctly different from typical orogenic gold deposits (Goldfarb RJ et al., 2014; Deng J et al., 2015a; Li L et al., 2015; Zhu RX et al., 2015). For example, Zhu RX et al. (2015) classified the Jiaodong gold deposits as decratonic gold deposits and considered that the essential difference between them and orogenic gold deposits lies in the extensional tectonic setting of the Jiaodong gold deposits. Li L et al. (2015) defined the Jiaodong-type gold deposits as the gold deposits that were formed in an extensional lithospheric tectonic setting and are distributed along the margins, inner ancient suture zones, or microplate junction zones of an activated craton. The comprehensive analysis shows that the Jiaodong-type gold deposits are significantly different from orogenic gold deposits. Typical orogenic gold deposits in foreign countries are primarily related to the setting of continental-margin accretion induced by the subduction of oceanic crust and were formed from the tectonic-magmatic thermal event at 20–200 Ma after regional metamorphism (Goldfarb RJ et al., 2001). They show the zonings of Au-As, Au-As-Te, and Au-Sb from hypogene to hypergene zones. However, the Jiaodong-type gold deposits are quite different. They were formed in the extensional intracontinental lithospheric setting with continental-arc to back-arc extension (Song MC et al., 2015a; Li L et al., 2015), the gold mineralization occurred about 1.9 Ga later than the regional metamorphism, and the associated beneficial components mainly include Au, Ag, Cu, Pb, and Zn. Therefore, this paper believes that it is suitable to refer to all gold deposits formed in the Late Mesozoic extensional tectonic setting in the Jiaodong Peninsular represented by the Sanshandao gold deposit as Jiaodong-type gold deposits.

*5.3.3. Metallogenic model and process*

The genetic model of the Jiaodong gold deposits (including the Sanshandao gold deposit) has always been the focus of geologists, and the understanding of it has been constantly deepened and developed. The Jiaodong gold deposits were considered the gold deposits of the greenstone belt type in the early stage (Yang MZ and Lü GX, 1996; Shen BF et al., 1997). Afterward, they were long regarded as magmatic-hydrothermal gold deposits related to Late Mesozoic granitoid intrusions in the geological exploration of gold deposits in the Jiaodong Peninsular (Li SX et al., 2007). Early in this century, they were classified as orogenic gold deposits by some researchers (Zhou TH and Lu G, 2000; Goldfarb RJ et al., 2001; Qiu YM et al., 2002; Chen YJ et al., 2004; Jiang SY et al., 2009) and the gold mineralization model of the devolatilization of a subducted slab was proposed (Goldfarb RJ and Santosh M, 2014; Groves DI and Santosh M, 2016). In recent years, they were widely considered to be different from typical orogenic gold deposits in terms of the metallogenic tectonic setting, great differences between the metallogenic epoch and the metamorphic period of wall rocks, and mineralized alteration characteristics and were correspondingly divided into Jiaodong-type gold deposits, extensional gold deposits, and decratonic gold deposits (Zhai MG et al., 2004; Li L et al., 2015; Zhu RX et al., 2015).

According to a relevant study, the geochemical properties of rocks in the Jiaodong Peninsular were significantly different before and after the gold mineralization during the Late Mesozoic. Meanwhile, the ancient enriched lithospheric mantle was replaced with the depleted oceanic lithosphere (Wu FY et al., 2000), which was reflected in the significant changes in the geochemical characteristics of magmatic rocks. As revealed by the studies on the intermediate-basic intrusions in the Luxi district and volcanic rocks in the Jiaolai Basin, the mantle peridotite xenolith in Early Cretaceous and Late Cretaceous mantle-derived magmatic rocks have different mineral chemical and geochemical characteristics (Dai FQ et al., 2019). Specifically, for the mantle peridotite xenolith in Early Cretaceous mantle-derived magmatic rocks, their geochemical characteristics are similar to those of island arc basalts and they show the features of the ancient lithospheric mantle (Xu WL et al., 2003). In contrast, for the mantle peridotite xenolith in the Late Cretaceous mantle-derived magmatic rocks, their geochemical characteristics are similar to those of oceanic island basalts and they show the features of the new depleted lithospheric mantle (Yan J et al., 2005; Liu JM et al., 2004). Meanwhile, the Cretaceous basic dykes developing in the Jiaodong gold ore concentration area also show different geochemical characteristics. The early basic dykes have typical geochemical characteristics of island arc basalts and were formed from the partial melting of the ancient enriched lithospheric mantle that suffered metasomatic replacement by fluid-rich melts. In contrast, the late basic dykes have the geochemical characteristics of oceanic island basalts and may have been sourced from the partial melting of the lithospheric mantle with mantle convection (Ma L et al., 2014; Deng J et al., 2019). Late Mesozoic granitoids in the Jiaodong Peninsular also show important changes in geochemical characteristics, and their changing trends from the Late Jurassic Linglong-type granites to the Guojialing-type granites of the early stage of the Early Cretaceous and the Weideshan- and Laoshan-type granites of the middle stage of the Early Cretaceous are stated as follows. They are shifted from high-K calc-alkaline series to shoshonite series and from peraluminous to metaluminous

rocks in terms of petrochemical composition. Their trace element characteristics are shifted from high Ba and Sr to low Ba and Sr, and from high Sr and low Y to low Sr and high Y. Their REEs characteristics are shifted from no or weakly positive europium anomalies to significantly negative europium anomalies. In terms of zircon types, they are shifted from rocks bearing many ancient residual zircons and ultrahigh-pressure metamorphic zircons to rocks bearing no ultrahigh-pressure metamorphic zircons and to rocks bearing no ancient residual zircons. In terms of granite types, they change from S-type to I-A-type granitoids and from adakitic to arc granites. Furthermore, their diagenetic setting is shifted from a compressional to an extensional setting. Among these granites, Guojialing-type granites have transitional characteristics. Their contents of Ba, Sr, and Y are similar to those of Linglong-type granites and have the characteristics of adakites. However, the mantle-derived diorite xenoliths and Sr-Nd isotopic characteristics of the rocks are closer to those of Weideshan- and Laoshan-type granites. The Jiaodong gold deposits were exactly formed after the diagenesis of Guojialing-type granites, which is contemporary with the early magmatic activities of Weideshan-type and Laoshan-type granites. This indicates that the transformation of mantle properties and the changes in the geochemical composition of magmas in the Jiaodong Peninsular serve as important factors in the gold mineralization in the area.

Late Mesozoic extensional structures and the transformation of mantle properties jointly constitute the important metallogenic setting of the Jiaodong-type gold deposits. Based on this, the authors put forward the thermal uplifting-extensional metallogenic model of the Jiaodong-type gold deposits (Song MC et al., 2014a, 2015b). During the Late Jurassic, affected by the post-collision compression between the North China Craton and the Yangtze Craton and the subduction of the paleo-Pacific plate or Izanagi plate toward the Asia continent, the Jiaodong Peninsula suffered strong compressional intraplate deformation and crustal thickening (Zhang YQ et al., 2007). This led to the activation of the lower crust and the large-scale remelting of continental crust. As a result, Linglong-type granites were formed. The Cretaceous is an important transformation period for the structural evolution of plates (Wu GY, 2006). During this period, the lithosphere and crust in the North China Craton intensely thinned (Zhai MG et al., 2005) and the Early Cretaceous destruction of the North China Craton reached its peak (Wu FY et al., 2005), which were accompanied by strong tectonism, magmatic activities, metallogenic explosion, and the formation of large basins. Consequently, various extensional structures developed (Wang T et al., 2007; Lin W et al., 2013). The dynamic mechanisms of large-scale regional extensional structures are related to the intraplate or back-arc extension induced by the westward subduction of the paleo-Pacific plate and the collapse of the crust thickened early, which resulted from the roll-back of the subducted plate (Davis GA et al., 2001; Zhu G et al., 2011). In the Jiaodong Peninsula, the subduction and roll-back of the paleo-Pacific plate resulted in lithospheric thinning, asthenospheric upwelling, crust-mantle interactions, and large-scale magmatic activities and extensional tectonism (Fig. 24a). Consequently, a thermal uplifting-extensional structural system was formed (Song MC et al., 2018). In this process, the enriched mantle was transformed into a depleted mantle, and the magmatic rocks were shifted from the adakitic type to the island arc and oceanic island types, resulting in the activation and exchange of crust-mantle elements. Au elements were enriched at the peak of lithospheric thinning and when arc granites completely replaced adakitic granites, which provided abundant ore-forming materials for the gold mineralization. Meanwhile, magmatism provides necessary thermodynamic conditions for gold migration. Owing to the back-arc extension or intraplate extension caused by the roll-back of the subducted paleo-Pacific plate, the Jiaodong Peninsula suffered intense extension and quick crustal uplifting, resulting in large-scale interlayer gliding in the crust. The induced detachment faults developing along weak structural surfaces such as the interfaces between Jurassic Linglong granites and Early Precambrian metamorphic rocks provided a favorable space for the migration and accumulation of ore-forming fluids. Due to the shielding of the fault gouge of the detachment fault, the ore-forming materials are mainly enriched in the footwall of the fault (Fig. 24b). Owing to inhomogeneous crustal structures, the detachment faults show a stepped pattern of alternate steep-gentle dip angles. Deep gold orebodies primarily occur in fault plane parts with a gentle fault dip angle or a steep-gentle transition of the fault dip angle, and thus a stepped metallogenic model was formed (Fig. 25). The tectonic space in the main detachment fault zones was occupied by cataclasite. In this case, ore-forming fluids slowly flowed along loose rock strata, and gradually precipitated and formed altered rock type gold deposits via water-rock metasomatism. Owing to the quick uplifting of the crust and the propping of deep arc granites (Weideshan- and Laoshan-type granites), a large number of tensile fractures obliquely crossing the main detachment faults or featuring a steep dip angle were generated among the adakitic granites (Linglong- and Guojialing-type granites) that were formed earlier on the footwall of the main detachment fault. Then ore-forming fluids filled these faults via the action of pumping, and thus quartz-vein-type gold deposits were formed. The thermal uplifting-extensional and stepped metallogenic models of the Jiaodong-type gold deposits provide direction for the deep prospecting of gold deposits.

## 6. Conclusions

(i) Multiple adjacent deposits in the Sanshandao area, Jiaodong Peninsula that were previously thought to be independent of each other constitute a supergiant deposit with gold reserves of more than 1200 t (including 470 t Under the Bohai sea area). The main orebodies in the supergiant deposit have a total length of nearly 8 km, a deepest controlled

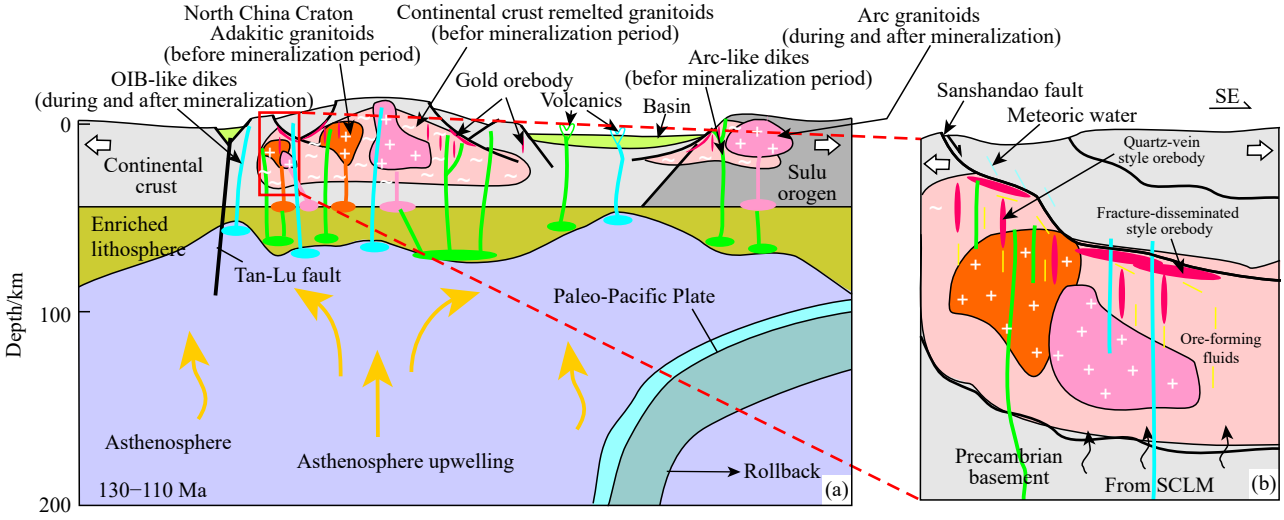


**Fig. 24.** Thermal uplifting-extensional metallogenic model for the Jiaodong-type gold deposits (a) and the Sanshandao gold deposit (b).

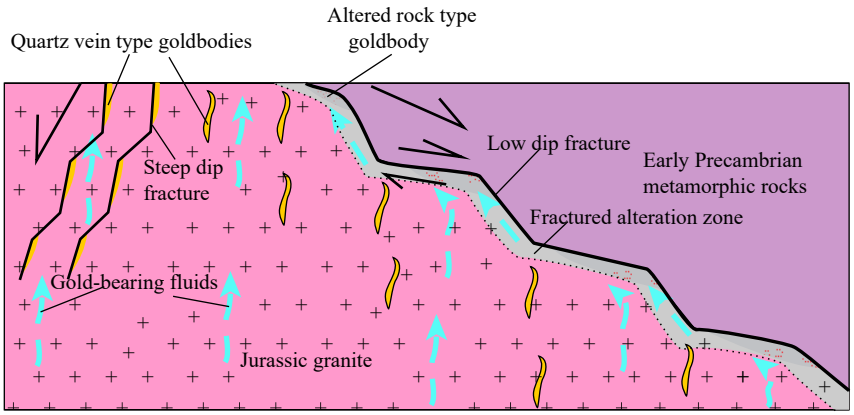


**Fig. 25.** Stepped metallogenic model of Jiaodong-type gold deposits (Song MC et al., 2020b).

elevation of −2312 m, and a maximum controlled length along their dip direction of greater than 3 km.

(ii) The Jiaodong gold deposits were formed at about 120 Ma and experienced the superposition of polymetallic metallogenic events at 118–111 Ma. The ore-forming fluids are the medium-low-temperature, low-salinity, and reducing $H_2O$-$CO_2$-NaCl±$CH_4$ hydrothermal system. Before gold mineralization, the fluids were mainly primary mantle water or magmatic water, metamorphic water appeared in the early stage of mineralization, and meteoric water dominated in the late stage of mineralization. The He-Ar isotopes and C isotopes of the ore-forming fluids reflect the addition of mantle-derived fluids addition. The isotopic characteristics of S, Pb, and Sr of ores are similar to those of ore-hosting rocks, indicating that the ore-forming materials mainly include crust-derived materials and minor amounts of mantle-derived materials.

(iii) The orebodies of the supergiant Sanshandao gold deposit mainly occur on the footwall of the Sanshandao fault and the fault sections with a steep-to-gentle transition of the fault dip angle, thus forming a stepped metallogenic model. Fault gouges developing along the Sanshandao fault blocked the gold orebodies onto the footwall of the main fault plane. Owing to the fluctuations in the fluid pressure caused by the changes in the fault dip angle, gold in the fluids was liable to accumulate and be mineralized in the gentle sections with a steep-to-gentle transition of the fault dip angle.

(iv) The Jiaodong gold deposits were formed in the background consisting of extensional structures and the transformation of mantle properties. Therefore, they are different from internationally known gold deposit types such as typical orogenic gold deposits and are referred to as Jiaodong-type gold deposits. The thermal uplifting-extensional structures provide thermal dynamic conditions and fluid migration and enrichment space for the gold mineralization. Furthermore, the changes in mantle properties lead to the transformation of the geochemical properties of the lower crust and magmatic rocks. This further led to the activation and exchange of elements, which provided rich materials for gold mineralization. The gold orebodies are distributed in a stepped pattern along ore-controlling faults.

## CRediT authorship contribution statement

Ming-chun Song and Zheng-jiang Ding conceived and designed the ideas. Jun-jin Zhang, Ying-xin Song, Jun-wei

Bo, Yu-qun Wang, Hong-bo Liu, Shi-yong Li, Jie Li, and Rui-xiang Li participated in field investigation. Bin Wang, Xiang-dong Liu, and Liang-liang Zhang performed the data processing. Lei-lei Dong, Jian Li, and Chun-yan He reviewed and edited the draft.

## Declaration of competing interest

The authors declare that they have no competing interests.

## Acknowledgment

Professor Jun Deng and Researcher Zhi-cheng Lv reviewed the entire manuscript and proposed valuable comments. Researcher Zi-guo Hao suggested preparing this paper. The authors hereby would like to extend their sincere gratitude to all of them. Meanwhile, this paper was funded by the NSFC-Shandong Joint Fund Program entitled *Control Mechanisms of Faults on Deep Gold Deposits in Jiaodong Peninsula* (U2006201).

## References

Burnard PG, Hu R, Turner G, Mantle. 1999. Mantle, crustal and atmospheric noble gases in Ailaoshan Gold deposits, Yunnan Province, China. Geochimica et Cosmochimica Acta, 63, 1595–1604. doi: 10.1016/S0016-7037(99)00108-8.

Cai YC, Fan HR, Santosh M, Hu FF, Yang KF. 2018. Decratonic gold mineralization: Evidence from the Shangzhuang gold deposit, eastern North China Craton. Gondwana Research, 54, 1–22. doi: 10.1016/j.gr.2017.09.009.

Charles N, Gumiaux C, Augier R, Yan C, Zhu R, Wei L. 2011. Metamorphic core complexes vs. synkinematic plutons in continental extension setting: Insights from key structures (Shandong Province, Eastern China). Journal of Asian Earth Sciences, 40, 261–278. doi: 10.1016/j.jseaes.2010.07.006.

Charles N, Augier R, Gumiaux C, Monié P, Chen Y, Faure M, Zhu RX. 2013. Timing, duration and role of magmatism in wide rift systems: Insights from the Jiaodong Peninsula (China, East Asia). Gondwana Research, 24, 412–428. doi: 10.1016/j.gr.2012.10.011.

Chen YJ, Franco P, Lai Y, Li C. 2004. Metallogenic time and tectonic setting of the Jiaodong Gold Province Eastern China. Acta Petrologica Sinica, 20(4), 907–922 (in Chinese with English abstract). doi: 10.3969/j.issn.1000-0569.2004.04.013.

Dai FQ, Zhao ZF, Zheng YF, Sun GC. 2019. The geochemical nature of mantle sources for two types of cretaceous basaltic rocks from Luxi and Jiaodong in east-Central China. Lithos, 344–345, 409–424. doi: 10.1016/j.lithos.2019.07.007.

Daivis GA, Zheng YD, Wang C, Darby BJ, Zhang CH, Gehrels GE. 2001. Mesozoic tectonic evolution of the Yanshan fold and thrust belt, with emphasis on Hebei and Liaoning provinces, northern China. In:Hendrix MS and Davis GA(eds. ). Paleozoic and Mesozoic Tectonic Evolution of Central and Asia:From Continental Assembly to Intracontonental Deformation. Geological Society of American Memoir, 194, 171–197.

Deng J, Chen YM, Liu Q, Yang LQ. 2010. The Gold Metallogenic System and Mineral Resources Exploration of Sanshandao Fault Zone, Shandong Province. Beijing, Geological Publishing House, 1–371 (in Chinese).

Deng J, Liu XF, Wang QF, Pan RG. 2015a. Origin of the Jiaodong-type Xinli gold deposit, Jiaodong Peninsula, China: Constraints from fluid inclusion and C-D-O-S-Sr isotope compositions. Ore Geology Reviews, 65, 674–686. doi: 10.1016/j.oregeorev.2014.04.018.

Deng J, Wang CM, Bagas L, Carranza EJM, Lu YJ. 2015b. Cretaceous–Cenozoic tectonic history of the Jiaojia Fault and gold mineralization in the Jiaodong Peninsula, China: Constraints from zircon U-Pb, illite K-Ar, and apatite fission track thermochronometry. Mineral Deposita, 50, 987–1006. doi: 10.1007/s00126-015-0584-1.

Deng J, Yang LQ, Li HR, Groves DI, Santosh M, Wang ZL, Sai SX, Wang SR. 2019. Regional structural control on the distribution of world-class gold deposits: An overview from the Giant Jiaodong Gold Province, China. Geological Journal, 54, 378–391. doi: 10.1002/gj.3186.

Deng J, Yang LQ, Groves DI, Zhang L, Wang QF. 2020a. An integrated mineral system model for the gold deposits of the giant Jiaodong province, eastern China. Earth-Science Reviews, 208(2), 103274. doi: 10.1016/j.earscirev.2020.103274.

Deng J, Qiu KF, Wang QF, Goldfarb R, Yang LQ, Wei J, Geng JZ, Ma Y. 2020b. In situ dating of hydrothermal monazite and implications for the geodynamic controls on ore formation in the Jiaodong gold Province, eastern China. Economic Geology, 115(3), 671–685. doi: 10.5382/econgeo.4711.

Ding ZJ, Sun FY, Liu FL, Liu JH, Liu DH, Zhang PJ, Du SX, Li B. 2013. U-Pb dating of zircons from the Weideshan molybdenum copper polymetallic deposits in Jiaodong Peninsula, China, and its geological significance. Acta Petrologica Sinica, 29(2), 607–618 (in Chinese with English abstract). doi: 10.3724/SP.J.1008.2010.00937.

Ding ZJ, Sun FY, Liu FL, Liu JH, Peng QM, Ji P, Li BL, Zhang PJ. 2015. Mesozoic geodynamic evolution and metallogenic series of major metal deposits in Jiaodong Peninsula, China. Acta Petrologica Sinica, 31(10), 3045–3080 (in Chinese with English abstract).

Fan HR, Feng K, Li XH, Hu FF, Yang KF. 2016. Mesozoic gold mineralization in the Jiaodong and Korean peninsulas. Acta Petrologica Sinica, 32(10), 3225–3238 (in Chinese with English abstract).

Feng K, Fan HR, Groves DI, Yang KF, Hu FF, Liu X, Cai YC. 2020. Geochronological and sulfur isotopic evidence for the genesis of the post-magmatic, deeply sourced, and anomalously gold-rich Daliuhang orogenic deposit, Jiaodong, China. Mineral Deposita, 55, 293–308. doi: 10.1007/s00126-019-00882-8.

Geng K, Wang RJ, Li HK, Shan W, Li DP. 2015. Zircon SHRIMP age of diorite-porphyrite in Beijie gold deposit from the northwest Jiaodong area and its geological implications. Acta Geologica Sinica, 89(6), 1099–1107 (in Chinese with English abstract).

Goldfarb RJ, Groves DI, Gardoll S. 2001. Orogenic gold and geologic time: A global synthesis. Ore Geology Reviews, 18(1), 1–75. doi: 10.1016/S0169-1368(01)00016-6.

Goldfarb RJ, Santosh M. 2014. The dilemma of the Jiaodong gold deposits: Are they unique? Geoscience Frontiers, 5(2), 139–153. doi: 10.1016/j.gsf.2013.11.001.

Goss S, Wilde S, Wu FY, Yang JH. 2010. The age, isotopic signature and significance of the youngest Mesozoic granitoids in the Jiaodong Terrene, Shandong Province, North China Craton. Lithos, 120(3–4), 309–326. doi: 10.1016/j.lithos.2010.08.019.

Groves DI, Santosh M. 2016. The giant Jiaodong gold province: The key to a unified model for orogenic gold deposits. Geoscience Frontiers, 7(3), 409–417. doi: 10.1016/j.gsf.2015.08.002.

Guo CY. 2009. The Gold Metallogenic System of Tectonic-Magma-Fluid for Gold Metallogenic Belt of the Sanshandao-Cangshang in Jiaodong Peninsula. Beijing, China University of Geosciences, PhD Dissertation (in Chinese with English abstract).

Han ZY, Yu XW, Li SJ, Tian JX, Wang ZL, Yu XJ, Wang LG. 2019. He-Ar isotopic tracing of pyrite from ore-forming fluids of the Sanshandao Au deposit, Jiaodong area. Acta Geologica Sinica (English Edition), 93(6), 1797–1807. doi: 10.1111/1755-6724.14335.

Hua RM, Mao JW, Li XB. 1999. A preliminary study of large-scale metallogenesis and large clusters of mineral deposits. Mineral Deposits, 18(4), 291–299 (in Chinese with English abstract). doi: 10.3969/j.issn.0258-7106.1999.04.001.

Hoefs J. 1997. Stable Isotope Geochemistry: 4th. Edition. Berlin, Springer Verlag, 1–20.

Huang T, Yang LQ, Liu XD, Li HL, Zhang BL, Wang JG, Zhao YF, Zhang N. 2014. Crustal evolution of the Jiaobei terrane: Evidence from U-Pb ages trace element compositions and Hf isotopes of inherited zircons of the Linglong biotite granite. Acta Petrologica Sinica, 30(9), 2574–2594 (in Chinese with English abstract).

Hu FF, Fan HR, Jiang XH, Li XC, Yang KF, Mernagh T. 2013. Fluid inclusions at different depths in the Sanshandao gold deposit, Jiaodong Peninsula, China. Geofluids, 13(4), 528–541. doi: 10.1111/gfl.12065.

Jiang P, Yang KF, Fan HR, Liu X, Cai YC, Yang YH. 2016. Titanite-scale insights into multi-stage magma mixing in Early Cretaceous of NW Jiaodong terrane, North China Craton. Lithos, 258 –259, 197–214. doi: 10.1016/j.lithos.2016.04.028.

Jiang SY, Dai BZ, Jiang YH, Zhao HX, Hou ML. 2009. Jiaodong and Xiaoqinling: Two orogenic gold provinces formed in different tectonic settings. Acta Petrologica Sinica, 25(11), 2727–2738 (in Chinese with English abstract).

Jiang XH, Fan HR, Hu FF, Yang KF, Lan TG, Zheng XL, Jin NX. 2011. Comparative studies on fluid inclusion in different depths and ore genesis of the Sanshandao gold deposit, Jiaodong Peninsula. Acta Petrological Sinica, 27(5), 1327–1340 (in Chinese with English abstract).

Kuang YS, Pang CJ, Luo ZY, Hong LB, Zhong YT, Qiu HN, Xu YG. 2012. $^{40}$Ar-$^{39}$Ar geochronology and geochemistry of mafic rocks from Qingshan Group, Jiaodong area: Implication for the destruction of the North China Craton. Acta Petrologica Sinica, 28(4), 1073–1091 (in Chinese with English abstract).

Li HJ. 2002. Ore-forming rule of endogenetic gold deposit in north of Jiaodong area. Geology of Shandong, 18(3/4), 72–77 (in Chinese with English abstract).

Li HM, Mao JW, Shen YC, Liu TB, Zhang LC. 2003. Ar-Ar ages of K-feldspar and quartz from Dongji gold deposit, Northwest Jiaodong, and their significance. Mineral Deposits, 22(1), 72–77 (in Chinese with English abstract).

Li JJ. 2006. Metallogeny and Prospecting Direction of Main Metallogenic Belts in North China Block. Tianjin:Tianjin Science and Technology Press, 297–312.

Li L, Santosh M, Li SR. 2015. The 'Jiaodong type' gold deposits: Characteristics, origin and prospecting. Ore Geology Reviews, 65, 589–611. doi: 10.1016/j.oregeorev.2014.06.021.

Li SZ, Zhao GC, Santosh M, Liu X, Dai LM, Suo YH, Tam PY, Song MC, Wang PC. 2012. Structural evolution of the southern segment of the Jiao-Liao-Ji belt, north China Craton. Precambrian Research, 200–203, 59–73. doi: 10.1016/j.precamres.2012.01.007.

Li SX, Liu CC, An YH. 2007. Geology of Gold Deposits in the Shandong Peninsula. Beijing, Geological Publishing House (in Chinese).

Lin BL, Li BL. 2013. Geochemistry, U-Pb dating, Lu-Hf isotopic analysis and geological significance of Linglong granite in Jiaodong Peninsula. Journal of Chengdu University of Technology (Science & Technology Edition), 40(2), 147–160 (in Chinese with English abstract). doi: 10.3969/j.issn.1671-9727.2013.02.06.

Lin W, Wang J, Liu F, Ji WB, Wang QC. 2013. Late Mesozoic extension structures on the North China Craton and adjacent regions and its geodynamics. Acta Petrologica Sinica, 29(5), 1791–1810 (in Chinese with English abstract).

Ling WL, Xie XJ, Liu XM, Cheng JP. 2007. Zircon U-Pb dating on the Mesozoic volcanic suite from the Qingshan Group stratotype section in eastern Shandong Province and its tectonic significance. Science China Earth Sciences, 50(6), 813–824. doi: 10.1007/s11430-007-2065-6.

Liu FL, Xu ZQ, Song B. 2003. Determination of UHP and retrograde metamorphic ages of the Sulu Terrane: Evidence from SHRIMP U-Pb dating on zircons of gneissic rocks. Acta Geologica Sinica, 2003,77(2), 229–237 (in Chinese with English abstract). doi: 10.3321/j.issn:0001-5717.2003.02.011.

Liu JM, Zhang HF, Sun JG, Ye J. 2004. Geochemical research on C-O and Sr-Nd isotopes of mantle-derived rocks from Shandong Province, China. Science in China (Ser. D, Earth Sciences), 47(2), 171–180. doi: 10.3321/j.issn:1006–9267.2003.10.002.

Liu JH, Liu FL, Liu PH, Wang F, Ding ZJ. 2011. Polyphase magmatic and metamorphic events from Early Precambrian metamorphic basement in Jiaobei area: Evidence from the zircon U-Pb dating of TTG and granitic gneisses. Acta Petrological Sinica, 27(4), 943–960 (in Chinese with English abstract).

Liu JL, Guan HM, Ji M, Hu L. 2006. Late Mesozoic metamorphic core complexes: New constraints on lithosphere thinning in North China. Progress in Natural Science, 16(6), 633–638. doi: 10.1080/10020070612330045.

Liu S, Hu RZ, Gao S, Feng CX, Yu BB, Qi Y, Wang T, Feng GY, Coulson IM. 2009. Zircon U-Pb age, geochemistry and Sr-Nd-Pb isotopic compositions of adakitic volcanic rocks from Jiaodong, Shandong Province, eastern China: Constraints on Petrogenesis and implications. Journal of Asian Earth Sciences, 35, 445–458. doi: 10.1016/j.jseaes.2009.02.008.

Liu YZ, Yang LQ, Wang SR, Liu XD, Wang H, Li DP, Wei PF, Cheng W Chen BY. 2019. Origin and evolution of ore-forming fluid and gold-deposition processes at the Sanshandao gold deposit, Jiaodong Peninsula, eastern China. Minerals, 9(3), 189. doi: 10.3390/min9030189.

Liu Y, Deng J, Wang ZL, Zhang L, Zhang C, Liu XD, Zheng XL, Wang XD. 2014. Zircon U-Pb age Lu-Hf isotopes and petrogeochemistry of the monzogranites from Xincheng gold deposit northwestern Jiaodong Peninsula China. Acta Petrologica Sinica, 30(9), 2559–2573 (in Chinese with English abstract).

Lu HZ, Guy A, Li YS, Wei JX, Chen NN, Zhang GP, Yuan WC, Chen XL, Long HB. 1999. The relation between deformation types and gold mineralization in the Linglong-Jiaojia district, Shandong Province, China. Acta Geologica Sinica, 73(2), 174–188 (in Chinese with English abstract). doi: 10.1088/0256-307X/15/11/025.

Luo XD, Yang XY, Duan LA, Sun WD. 2014. Geochemical and geochronological study of the gold-related Guojialing pluton and Shangzhuang pluton in Jiaobei block. Acta Geological Sinica, 88(10), 1874–1888 (in Chinese with English abstract). doi: 10.3969/j.issn.0001-5717.2014.10.008.

Luo ZK, Miao LC. 2001. Granitoids and Gold Deposits of the Zhaolai Area in the Jiaodong Peninsula. Beijing, Metallurgical Industry Press, 1–157 (in Chinese).

Lü GX, Kong QC. 1993, Geological Characteristics of the Linglong–Jiaojia Type Gold Deposits in Jiaodong Peninsula. Beijing, Science Press, 1–253 (in Chinese).

Ma L, Jiang SY, Hou ML, Dai BZ, Jiang YH, Yang T, Zhao KD, Pu W, Zhu ZY, Xu B. 2014. Geochemistry of Early Cretaceous calc-alkaline lamprophyres in the Jiaodong Peninsula: Implication for lithospheric evolution of the eastern North China Craton. Gondwana Research, 25(2), 859–872. doi: 10.1016/j.gr.2013.05.012.

Ma WD, Fan, HR, Yang YH, Liu X, Pirajno F, Yang KF. 2017. Geochronological framework of the Xiadian gold deposit in the Jiaodong province, China: Implications for the timing of gold mineralization. Ore Geology Reviews, 86, 196–211. doi: 10.1016/j.oregeorev.2017.02.016.

Mao JW, Wang YT, Li HM, Pirajno F, Zhang CQ, Wang RT. 2008. The relationship of mantle-derived fluids to gold metallogenesis in the

Jiaodong Peninsula: Evidence from D-O-C-H isotope systematics. Ore Geology Reviews, 33, 361–381. doi: 10.1016/j.oregeorev.2007.01.003.

Niu SY, Chen C, Zhang JZ, Wang FX, Sun FX. 2019. The thermal and dynamic process of core→mantle→crust and the metallogenesis of Guojiadian mantle branch in northwestern Jiaodong. Minerals, 9(4), 249. doi: 10.3390/min9040249.

Qiu JS, Wang DZ, Luo QH, Liu H. 2001. $^{40}$Ar-$^{39}$Ar dating for volcanic rocks of Qingshan Formation in Jiaolai Basin, eastern Shandong Province: A case study of the Fenlingshan volcanic apparatus in Wulian County. Geological Journal of China Universities, 7(3), 351–355 (in Chinese with English abstract).

Qiu KF, Goldfarb RJ, Deng J, Yu HC, Gou ZY, Ding ZJ, Wang ZK, Li DP. 2020. Gold Deposits of the Jiaodong Peninsula, Eastern China. SEG Special Publications, 23.

Qiu YM, Groves ID, McNaughton GN, Wang LG, Zhou TH. 2002. Nature, age and tectonic setting of granitoid-hosted, orogenic gold deposits of the Jiaodong Peninsula, eastern North China Craton, China. Mineralium Deposita, 37(3), 283–305. doi: 10.1007/s00126-001-0238-3.

Ratschbacher L, Hacker BR, Webb LE. 2000. Exhumation of the ultra-high pressure continental crust in east central China: Cretaceous and Cenozoic unrooting and the Tanlu Faul. Journal of Geophysical Research, 105, 13303–13338. doi: 10.1029/2000JB900040.

Sai SX, Deng J, Qiu KF, Miggins DP, Zhang L. 2020. Textures of auriferous quartz-sulfide veins and $^{40}$Ar/$^{39}$Ar geochronology of the Rushan gold deposit: Implications for process of ore- fluid infiltration in the eastern Jiaodong gold province, China. Ore Geology Reviews, 117, 103254. doi: 10.1016/j.oregeorev.2019.103254.

Shen BF, Mao DB, Li JJ. 1997. Type and geological Chinese greenstone belts gold deposits. Progress in Precambrian Research, 20(4), 1–12 (in Chinese with English abstract).

Sheppard SMF. 1986. Characterization and isotopic variations in natural waters. Reviews in Mineralogy, 16(1), 165–183. doi: 10.1109/PDMC-HiBi.2010.11.

Song MC, Xun JX, Wang PC. 2009. Tectonic Framework and Tectonic Evolution of Shandong Province. Beijing, Geological Publishing House, 1–274 (in Chinese).

Song MC, Cui SX, Zhou ML, Jiang HL, Yuan WH, Wen XF, Lü GX. 2010a. The deep oversize gold deposit in the Jiaojia field, Shandong Province and its enlightenment for the Jiaojia gold type. Acta Geologica Sinica, 84(9), 1349–1358 (in Chinese with English abstract).

Song MC, Cui SX, Yi PH, Xu JX, Yuan WH, Jiang HL. 2010b. Prospecting and Metallogenic Model of Large- and Super-Large-Scale Deep-Seated Gold Deposits in Northwestern Shandong Peninsula Concentration Region of Gold Deposits. Beijing, Geological Publishing House, 1–339 (in Chinese).

Song MC, Yi PH, Xu JX, Cui SX, Shen K, Jiang HL, Yuan WH, Wang HJ. 2012. A step metallogenetic model for gold deposits in the northwestern Shandong Peninsula, China. Science in China (Ser. D, Earth Sciences), 55(6), 940–948. doi: 10.1007/s11430–012-4366–7.

Song MC, Li SZ, Yi PH, Cui SX, Xu JX, Lü GX, Song YX, Jiang HL, Zhou ML, Zhang PJ, Huang TL, Liu CC, Liu DH. 2014a. Classification and metallogenic theory of the Jiaojia-style gold deposit in Jiaodong Peninsula, China. Journal of Jilin University (Earth Science Edition), 44(1), 87–104 (in Chinese with English abstract). doi: 10.13278/j.cnki.jjuese.201401108.

Song MC, Deng J, Yi PH, Yang LQ, Cun SX, Xu JX, Zhou ML, Huang TL, Song GZ, Song YX. 2014b. The kiloton class Jiaojia gold deposit in eastern Shandong Province and its genesis. Acta Geological Sinica (English Edition), 88(3), 801–824. doi: 10.1111/1755-6724.12239.

Song MC, Zhang JJ, Zhang PJ, Yang LQ, Liu DH, Ding ZJ, Song YX. 2015a. Discovery and tectonic–magmatic background of superlarge gold deposit in offshore of northern Sanshandao, Shandong Peninsula, China. Acta Geological Sinica, 89(2), 365–383 (in Chinese with English abstract).

Song MC, Li SZ, Santosh M, Zhao SJ, Yu S, Yi PH, Cun SX, Lü GX, Xu JX, Song YX, Zhou ML. 2015b. Types, characteristics and metallogenesis of gold deposits in the Jiaodong Peninsula, Eastern North China Craton. Ore Geology Reviews, 65, 612–625. doi: 10.1016/j.oregeorev.2014.06.019.

Song MC, Wang SS, Yang LX, Li J, Li SY, Ding ZJ. 2017. Metallogenic epoch of nonferrous metallic and silver deposits in the Jiaodong Peninsula, China and its geological significance. Acta Geologica Sinica (English Edition), 91(4), 1305–1325. doi: 10.1111/1755-6724.13363.

Song MC, Li J, Li SY, Ding ZJ, Tan XF, Zhang ZL, Wang SJ. 2018. Late Mesozoic thermal upwelling-extension structure and its dynamics background in eastern Shandong Province. Journal of Jilin University (Earth Science Edition), 48(4), 941–964 (in Chinese with English abstract). doi: 10.13278/j.cnki.jjuese.20170145.

Song MC, Song YX, Ding ZJ, Wei XF, Sun SL, Song GZ, Zhang JJ, Zhang PJ, Wang YG. 2019. The discovery of The Jiaojia and the Sanshandao giant gold deposits in Jiaodong Peninsula and discussion on the relevant issues. Geotectonica et Metallogenia, 43(1), 92–110 (in Chinese with English abstract). doi: 10.16539/j.ddgzyckx.2019.01.008.

Song MC, Zhou JB, Song YX, Wang B, Li SY, Li J, Wang SS. 2020a. Mesozoic Weideshan granitoid suite and its relationship to large-scale gold mineralization in the Jiaodong Peninsula, China. Geological Journal, 55, 5703–5724. doi: 10.1002/gj.3607.

Song MC, Lin SY, Yang LQ, Song YX, Ding ZJ, Li J, Li SY, Zhou ML. 2020b. Metallogenic model of Jiaodong Peninsula gold deposits. Mineral Deposits, 39, 215–236 (in Chinese with English abstract).

Song YX, Song MC, Ding ZJ, Wei XF, Xu SH, Li J, Tan XF, Li SY, Zhang ZL, Jiao XM, Hu H, Cao J. 2017. Major advances on deep prospecting in Jiaodong gold ore cluster and its metallogenic characteristics. Gold Science and Technology, 25(3), 4–18 (in Chinese with English abstract). doi: 10.11872/j.issn.1005-2518.2017.03.004.

Song YX, Yu XF, Li DP, Geng K, Wei PF, Zuo XM, Wang XF. 2020. Petrogenesis of the Beijie pluton from the northwestern Jiaodong Peninsula: Constraints from zircon U-Pb age, petrogeochemistry and Sr-Nd-Pb isotopes. Acta Petrologica Sinica, 36(5), 1477–1500 (in Chinese with English abstract). doi: 10.18654/1000-0569/2020.05.10.

Stuart FM, Burnard PG, Taylor RP. 1995. Resolving mantle and crustal contributions to ancient hydrothermal fluids: He-Ar isotopes in fluid inclusions from Dae Hwa W-Mo mineralisation, South Korea. Geochimica et Cosmochimica Acta, 59(22), 4663–4673. doi: 10.1016/0016-7037(95)00300-2.

Tang J, Wu YB, Cha XP, Zhou JB. 2004. Zircon U-Pb ages and oxygen isotopes of metamorphic rocks in the western part of the Shandong Peninsula. Acta Petrologica Sinica, 20(5), 1063–1086 (in Chinese with English abstract). doi: 10.3321/j.issn:1000-0569.2004.05.006.

Taylor HP. 1974. The application of oxygen and hydrogen isotope studies to problems of hydrothermal alteration and ore deposition. Economic Geology, 69, 843–883. doi: 10.2113/gsecongeo.69.6.843.

Wang B, Song MC, Huo G, Zhou ML. Xu ZH, Jiang L, Song YX, Li J. 2021. Source characteristics and tectonic evolution of Late Mesozoic granites in Jiaodong and their implications for gold mineralization. Acta Petrologica et Mineralogica, 40(2), 288–320 (in Chinese with English abstract).

Wang JC, Xia B, Tang JR, 2003. Recognition on some key geological problems of Linglong-Jiaojia ore-concentrated district in Shandong Province. Geotectonica et Metellogenia, 27 (2), 147–151 (in Chinese with English abstract). doi: 10.3969/j.issn.1001–1552.2003.02.007.

Wang JT, Sun ZF, Zhu ZQ. 2005. Minerogenetic Regularity and Prediction of the Xili Gold Deposit in Laizhou City, Shandong

Province. Beijing, Geological Publishing House (in Chinese).

Wang LG, Qiu YM, McNaugmton NJ. 1998. Constraints on crust evolution and gold metallogeny in the northwestern Jiaodong peninsula, China, from SHRIMP U-Pb zircon studies of granitoids. Ore Geology Reviews, 13, 275–291. doi: 10.1016/S0169-1368(97)00022-X.

Wang LG, Zhu DC, Guo RP, Yu XW, Tian JX, Ke CH, Liu HD, Tian RC, Gao HL. 2018. Geochemistry, zircon U-Pb age and Lu-Hf isotopes of the Cangshang and Sanshandao monzogranites in the northwestern Jiaodong Peninsula, China. Acta Geologica Sinica, 92(10), 2081–2095 (in Chinese with English abstract). doi: 10.3969/j.issn.0001-5717.2018.10.009.

Wang SR, Yang LQ, Cheng H, Li DP, Shan W, Yuan JJ. 2020. Effect of basement structure on the spatial distribution of gold deposits: Structure stress transfer modeling of Jiaojia fault. Acta Petrologica Sinica, 36(5), 1529–1546 (in Chinese with English abstract). doi: 10.18654/1000-0569/2020.05.13.

Wang T, Zheng YD, Zhang JJ, Wang XS, Zeng LS, Tong Y. 2007. Some problems in the study of Mesozoic extensional structure in the North China craton and its significance for the study of lithospheric thinning. Geological Bulletin of China, 26(9), 1154–1166 (in Chinese with English abstract). doi: 10.3969/j.issn.1671-2552.2007.09.017.

Wang YW. 1988. Lead isotope composition of gold deposits, northwestern Jiaodong Shandong, and its geological significance. Journal of Changchun University Earth Science, 18(3), 277–286 (in Chinese with English abstract).

Wang YW. 1993. Study on the geochemistry of hydrogen and oxygen isotopes of gold deposits in China. Journal of Precious Metallic Geology, 2(3), 169–180 (in Chinese with English abstract).

Wang ZL, Zhao RX, Zhang Q, Lu HW, Li JL, Cheng W. 2014a. Magma mixing for the high Ba-Sr Guojialing-type granitoids in Northwest Jiaodong Peninsula: Constraints from petrogeochemistry and Sr-Nd isotopes. Acta Petrologica Sinica, 30(9), 2595–2608 (in Chinese with English abstract).

Wang ZL, Yang LQ, Deng J, Santosh M, Zhang HF, Yue L, Li RH, Tao H, Zheng XL, Zhao H. 2014b. Gold-hosting high Ba-Sr granitoids in the Xincheng gold deposit, Jiaodong Peninsula, East China: Petrogenesis and tectonic setting. Journal of Asian Earth Sciences, 95, 274–299. doi: 10.1016/j.jseaes.2014.03.001.

Wen BJ, Fan HR, Hu FF, Liu X, Yang KF, Sun ZF, ZF Sun. 2016. Fluid evolution and ore genesis of the giant Sanshandao gold deposit, Jiaodong gold province, China: Constraints from geology, fluid inclusions and H-O-S-He-Ar isotopic compositions. Journal of Geochemical Exploration, 171, 96–112. doi: 10.1016/j.gexplo.2016.01.007.

Wu FY, Lin JQ, Simon AW, Zhang XO, Yang JH. 2005. Nature and significance of the Early Cretaceous giant igneous event in eastern China. Earth and Planet Science Letters, 233, 103–119. doi: 10.1016/j.epsl.2005.02.019.

Wu FY, Sun DY, Zhang GL, Ren XW. 2000. Deep geodynamics of Yanshain Movement. Geological Journal of China Universities, 6(3), 379–388 (in Chinese with English abstract). doi: 10.3969/j.issn.1006-7493.2000.03.002.

Wu GY. 2006. Cretaceous: A key transition period of the plate tectonic evolution in China and its adjacent areas. Geology in China, 33(1), 64–77 (in Chinese with English abstract).

Wu M, Zhao G, Sun M, Li SZ. 2014. A synthesis of geochemistry and Sm-Nd isotopes of Archean granitoid gneisses in the Jiaodong Terrane: Constraints on petrogenesis and tectonic evolution of the Eastern Block, North China Craton. Precambrian Research, 255(1), 885–899. doi: 10.1016/j.precamres.2014.10.012.

Xie HQ, Wan YS, Wang SJ, Liu DY, Xie SW, Liu SJ, Dong CY, Ma MZ 2013. Geology and zircon dating of trondhjemitic gneiss and amphibolite in the Tangezhuang area, eastern Shandong. Acta Petrological Sinica, 29(2), 619 –629 (in Chinese with English abstract). doi: 10.1016/j.sedgeo.2012.12.001.

Xu WL, Wang DY, Wang QH, Lin JQ. 2003. Petrology and geochemistry of two types of mantle-derived xenoliths in Mesozoic diorite from western Shandong province. Acta Petrologica Sinica, 19(4), 623–636 (in Chinese with English abstract). doi: 10.3969/j.issn.1000-0569.2003.04.004.

Xu ZQ, Qi XX, Yang JS, Zeng LS, Liu FL, Liang FH, Tang ZM, Cai ZH. 2006. Deep subduction erosion model for continent-continent collision of the Sulu HP-UHP metamorphic terrain. Earth Science —Journal of China University of Geosciences, 31(4), 427–436 (in Chinese with English abstract). doi: 10.3321/j.issn:1000-2383.2006.04.001.

Yan J, Chen JF, Xie Z, Gao TS, Foland KA, Zhang XD, Liu MW. 2005. Later Cretaceous basalts and mantle-derived xenoliths from eastern Shandong. Acta Petrologica Sinica, 21(1), 99–112 (in Chinese with English abstract). doi: 10.3321/j.issn:1000-0569.2005.01.010.

Yan QS, Metcalfe I, Shi XF, Zhang PY, Li FC. 2019. Early Cretaceous granitic rocks from the southern Jiaodong Peninsula, eastern China: Implications for lithospheric extension. International Geology Review, 61(7), 821–838. doi: 10.1080/00206814.2018.1474388.

Yang JH, Wu FY, Chung SL, Lo CH, Wilde SA, Davis GA. 2007. Rapid exhumation and cooling of the Liaonan metamorphic core complex: Inferences from $^{40}Ar$ /$^{39}$ Ar thermochronology and implications for Late Mesozoic extension in the eastern North China Craton. Geological Society of America Bulletin, 119(11 –12), 1405 –1414. doi: 10.1130/B26085.1.

Yang JZ, Shen YC, Liu TB. 2000. Gold mineralization associated with Queshan metamorphic core complex. Geology-Geochemistry, 28(1), 15–19 (in Chinese with English abstract). doi: 10.3969/j.issn.1672-9250.2000.01.003.

Yang K, Wang JP, Lin JZ, Zheng JX, Yang GZ, Ji H. 2012. Petrogeochemical characteristics and genetic significance of the Aishan pluton in Jiaodong Peninsula. Geology and Prospecting, 48(4), 693–703 (in Chinese with English abstract).

Yang KF, Fan HR, Santosh M. 2012. Reactivation of the Archean lower crust: Implications for zircon geochronology, elemental and Sr-Nd-Hf isotopic geochemistry of Late Mesozoic granitoids from northwestern Jiaodong Terrane, the North China Craton. Lithos, 146 –147, 112 –127 (in Chinese with English abstract). doi: 10.1016/j.lithos.2012.04.035.

Yang KF, Jiang P, Fan HR, ZuoYB, YangYH. 2018. Tectonic transition from a compressional to extensional metallogenic environment at ~120 Ma revealed in the Hushan gold deposit, Jiaodong, North China Craton. Journal of Asian Earth Sciences, 160, 408–425. doi: 10.1016/j.jseaes.2017.08.014.

Yang L, Zhao R, Wang QF, Liu X, Carranza EJM. 2018. Fault geometry and fluid-rock reaction: Combined controls on mineralization in the Xinli gold deposit, Jiaodong Peninsula, China. Journal of Structural Geology, 111, 14–26. doi: 10.1016/j.jsg.2018.03.009.

Yang LQ, Deng J, Wang ZL, Zhang L, Guo LN, Song MC, Zheng XL. 2014. Mesozoic gold metallogenic system of the Jiaodong gold province, eastern China. Acta Petrological Sinica, 30(9), 2447–2467 (in Chinese with English abstract).

Yang LQ, Deng J, Guo LN, Wang ZL, Li JL. 2016. Origin and evolution of ore fluid, and gold-deposition processes at the giant Taishang gold deposit, Jiaodong Peninsula, eastern China. Ore Geology Reviews, 72, 585–602. doi: 10.1016/j.oregeorev.2015.08.021.

Yang MZ, Lü GX. 1996. The Geochemical Characteristic of Gold Deposits in Jiaodong Greenstone Belt. Beijing, Geological Publishing House, 1–228 (in Chinese).

Yang Q, Shi W, Hou GT. 2019. Late Mesozoic extensional detachment structures in eastern China and adjacent areas: Overview and new insight. Acta Geoscientica Sinica, 40(4), 511–544 (in Chinese with English abstract). doi: 10.3975/cagsb.2019.012301.

Yang QY, Santosh M. 2015. Early Cretaceous magma flare-up and its implications on gold mineralization in the Jiaodong Peninsula, China. Ore Geology Reviews, 65, 626–642. doi: 10.1016/j.oregeorev.2014.01.004.

Yang ZY, Yu XW, Zhang W, Wang LG, Wang QY, Guo RP. 2020. $^{40}Ar/^{39}Ar$ age and its significance of sericite in pyrite sericite in Sanshandao gold deposit in northwest of Shandong Province. Shandong Land and Resources, 36(7), 1–8 (in Chinese with English abstract). doi: 10.12128/j.issn.1672-6979.2020.07.001.

Yu GP, Xu T, Liu JP, Ai YS. 2020. Late Mesozoic extensional structures and gold mineralization in Jiaodong Peninsula, eastern North China Craton: An inspiration from ambient noise tomography on data from a dense seismic array. Chinese Journal of Geophysics, 63(5), 1878–1893 (in Chinese with English abstract). doi: 10.6038/cjg2020N0446.

Zartman RE, Doe BR. 1981. Plumbotectonics—the model. Tectonophysics, 75(1–2), 135–162. doi: 10.1016/0040–1951(81)90213–4.

Zhai MG, Fan HR, Yang JH, Miao LC. 2004. Large-scale cluster of gold deposits in east Shandong: Anorogenic metallogenesis. Earth Science Frontiers, 11(1), 85–98 (in Chinese with English abstract). doi: 10.3321/j.issn:1005-2321.2004.01.005.

Zhai MG, Fan QC, Zhang HF, Sui JL. 2005. Lower crust processes during the lithosphere thinning in eastern China: Magma underplating, replacement and delamination. Acta Petrological Sinica, 21(6), 1509–1526 (in Chinese with English abstract). doi: 10.3321/j.issn:1000-0569.2005.06.001.

Zhang HF, Zhai MG, He ZF, Peng P, Xu BL. 2004. Petrogenesis and implications of the sodium-rich granites from the Kunyushan complex, eastern Shandong Province. Acta Petrologica Sinica, 20(3), 369–380 (in Chinese with English abstract). doi: 10.3321/j.issn:1000-0569.2004.03.001.

Zhang L, Groves DI, Yang LQ, Wang GW, Liu XD, Li DP, Song YX, Shan W, Sun SC, Wang ZK. 2020a. Relative roles of formation and preservation on gold endowment along the Sanshandao gold belt in the Jiaodong gold province, China: Importance for province-to district-scale gold exploration. Mineralium Deposita, 55, 325–344. doi: 10.1007/s00126-019-00908-1.

Zhang L, Weinberg RF, Yang LQ, Groves DI, Deng J. 2020b. Mesozoic orogenic gold mineralization in the Jiaodong Peninsula, China: A focused event at 120±2Ma during cooling of pregold granite intrusions. Economic Geology, 115(2), 415–441. doi: 10.5382/econgeo.4716.

Zhang XO, Cawood PA, Wilde SA, Liu RQ, Song HL, Li Wen, Snee LW. 2003. Geology and timing of mineralization at the Cangshang gold deposit, north-western Jiaodong Peninsula, China. Mineralium Deposit. 38(2), 141–153. doi: 10.1007/s00126-002-0290-7.

Zhang YQ, Zhao Y, Dong SW, Yang N. 2004. Tectonic evolution stages of the Early Cretaceous rift basins in eastern China and adjacent areas and their geodynamic background. Earth Science Frontiers, 11(3), 123–133 (in Chinese with English abstract). doi: 10.3321/j.issn:1005-2321.2004.03.014.

Zhang YQ, Dong SW, Zhao Y, Zhang T. 2007. Jurassic tectonics of North China: A synthetic view. Acta Geologica Sinica, 81(11), 1462–1480 (in Chinese with English abstract). doi: 10.3321/j.issn:0001-5717.2007.11.002.

Zhang YQ, Li JL, Zhang T, Dong SW, Yuan JY. 2008. Cretaceous to Paleocene tectonic-sedimentary evolution of the Jiaolai basin and the contiguous areas of the Shandong Peninsula (North China) and its geodynamic implications. Acta Geologica Sinica, 82(9), 1229–1257 (in Chinese with English abstract). doi: 10.3321/j.issn:0001-5717.2008.09.007.

Zhou TH, Lü GX. 2000. Tectonics, granitoids and Mesozoic gold deposits in East Shandong, China. Ore Geology Reviews, 16(1/2), 71–90. doi: 10.1016/S0169-1368(99)00023-2.

Zhu G, Jiang DZ, Zhang BL, Chen Y. 2011. Destruction of the eastern North China Craton in a backarc setting: Evidence from crustal deformation kinematic. Gondwana Research, 22(1), 86–103. doi: 10.1016/j.gr.2011.08.005.

Zhu RX, Fan HR, Li JW, Meng QR, Li SR, Zeng QD. 2015. Decratonic gold deposits. Science China:Earth Sciences, 58(9), 1523–1537. doi: 10.1007/s11430-015-5139-x.